Utilizing Phylogenetic and Geochemical Techniques to Examine Echinoderms Through Time

A Dissertation Presented for the
Doctor of Philosophy
Degree
The University of Tennessee, Knoxville

Maggie Ryan Limbeck
August 2023

Copyright © 2023 by Maggie Ryan Limbeck
All rights reserved.

DEDICATION

To everyone who has encouraged and supported me through this journey.

ACKNOWLEDGEMENTS

Thank you to my advisor, Dr. Colin Sumrall, for all your guidance, support, and advice throughout this degree. I am so grateful you supported and encouraged my love of weird echinoderms and exploring their chemistry. Thank you to Dr. Linda Kah for the research advice and all the conversations about diagenesis. Thank you to Dr. Brad Deline for your advice through the years, both on research and life overall. Thank you to Dr. Stephanie Drumheller-Horton for the opportunities to develop my teaching skills and ideology and for your help creating Climate Change: The Board Game.

Thank you to the EPS grad students past and present, including the Sumrall lab group throughout the years (Aidan, Nick), CJ, Louisa, Sam, and the grads of the 7th floor who welcomed a senior grad student to hang with them. Thank you to all the EPS office staff for all your help through the years.

Thank you to the Paleo-Fam, there isn't enough room in this document to thank y'all enough. Sarah, thank you for kidnapping me at GSA and roping me into this family. Jen, thank you for all the road trips, hot chocolate, donuts, and Pokémon Go walks. Adriane, thank you for all the sass and support of crazy ideas. Love y'all!

Endless thank-yours to the many others in my non-academic village, without whom this dissertation would not have been possible. Special shout out to the OCAC run club for giving me a scheduled break each week and a place to have fun during the final year of craziness.

Mom and Dad - think big, dream big. I couldn't have done this without your support and encouragement through the years. Thank you for letting me collect rocks wherever we went and encouraging my love of rocks and fossils.

And of course, thank you to my husband, Zack. None of this would have been possible without your support. Thank you for keeping me fed during the last few months, taking me on hikes, music suggestions, all the sports talk all of the time, and all of the candy.

ABSTRACT

Understanding biotic changes through Earth's history has been the goal of paleobiology since the inception of the field. Advances in science and technology have progressed allowing us to reassess old questions and new questions that could have not been addressed without these new methods. Echinoderms (sea stars, sea urchins, etc.) appear in the fossil record during the early Cambrian and are still abundant in marine ecosystems today. This persistence through time has made echinoderms model organisms to answer questions about Earth's past and present. Despite this role as a model organism there are many questions that remain with respect to evolutionary history and biogeochemistry of echinoderms. The research herein therefore focuses on a combination of phylogenetics and geochemistry.

First, I explore the phylogenetics of Paracrinoidea. Paracrinoidea is a clade of Paleozoic echinoderms that exhibit unusual morphologies. These morphologies have hindered our understanding of their phylogenetic relationships and character evolution. This study represents the first rigorous, quantitative phylogenetic analysis of Paracrinoidea. Both a phylogenetic hypothesis and phylomorphospace were generated to inform patterns seen in morphology with an evolutionary perspective.

To explore echinoderm geochemistry, I examined major and minor element inclusion in echinoderm skeletal elements from four genera of modern echinoids from the Gulf of Mexico. These echinoids show measurable variation in skeletal composition which indicates a complex relationship between skeletal element growth rate and geochemical composition. These results help inform the utility of fossil echinoderms in geochemical studies and highlights the need for continued study of elemental incorporation in echinoderm skeletal elements.

Finally, I explore the geochemistry of fossil echinoderms. Fossilization and diagenetic processes can alter the original chemistry of the fossilized skeletal elements and impact their utility as seawater proxies. This study used both petrographic and geochemical techniques to assess the retention of original chemistry of fossil echinoid skeletal elements. Results highlight the need for caution and petrographic work to determine the retention of original chemistry to assess the utility of echinoderms as proxies. This work highlights the utility of echinoderms as case study organisms and the power of combined analyses to elucidate biotic changes during the Phanerozoic.

TABLE OF CONTENTS

LIST OF TABLES

LIST OF FIGURES

INTRODUCTION

Understanding biotic changes through the Phanerozoic has been an important goal of paleobiology since the inception of the field. As new tools and techniques have been developed, we are able to both ask old questions in new ways and address new questions. In this dissertation, I explore how we can use echinoderms to reconstruct our understanding of change through time.

Echinoderms (sea stars, sea urchins, crinoids, etc.) appear in the fossil record during the lowest Cambrian (Ubaghs, 1975; Paul and Smith, 1984; Zamora et al., 2013) and have been common in marine environments since that time. As a result, echinoderms have been model organisms to study in the past, both as a natural laboratory for the studies of group origin and evolutionary innovation and as a geochemical reservoir to sample ocean composition in the past. Echinoderms are ideal organisms to study phylogenetic relationships and morphological disparity as they have an extremely complex bauplan that can be coded and described mathematically. As common animals throughout the Phanerozoic, at times becoming the dominant producers of bioclastic sediment, echinoderms have been targeted as reservoirs for many geochemical studies.

It is important therefore to understand echinoderms from both evolutionary and geochemical perspectives. There are many groups of Paleozoic echinoderms that have yet to be placed into a phylogenetic context using rigorous statistical methods. This limits our understanding of their evolutionary history and their morphological variation and inhibit interpreting their paleoecological and biogeographical patterns. Similarly, the study of the biogeochemistry of echinoderms is important because it can facilitate both our

understanding of biomineralization processes, as well as for our understanding seawater chemistry through time. In order to understand geochemical signals in the geologic past however, the geochemistry of echinoderm skeletons need to be extensively studied in modern taxa to understand incorporation patterns prior to diagenesis.

Part 1: Phylogenetics

Previously, evolutionary relationships among fossil taxa were determined primarily by morphological similarities. However, similarity can result from 1) shared descent representing synapomorphies (if the traits define clades) or plesiomorphy (if the traits are ancestral) or 2) homoplasy if the traits evolved more than once. In modern analyses, the focus is on synapomorphy (heritable characteristics) because it unites taxa based strictly on shared descent. Recently, several Paleozoic echinoderm groups (ex. Diploporita, Blastoidea, Coronoidea, Edrioasteroidea, Stylophora, and Crinoidea) have been examined with rigorous, statistics based phylogenetic methods (Donovan and Paul, 1985; Sumrall, 1993; Guensburg and Sprinkle, 1994; Lefebvre, 2000; Ware and Lefebvre, 2007; Sumrall et al., 2013; Bauer et al., 2017; Sheffield et al., 2017; Wright et al., 2017). However, many small groups, like Paracrinoidea, have yet to be examined using homology and rigorous statistical analyses.

Paracrinoidea is a small group of echinoderms consisting of 13 genera that was both temporally and spatially limited, found only in Middle to Late Ordovician rocks of Laurentia and Baltica. Members of this group exhibit unusual morphologies that have led to confusion and debate over their placement within the larger echinoderm phylogeny and

placement within Paracrinoidea. Through examination of fossil specimens, careful assessment of homologous features, and the evolutionary relationships within Paracrinoidea, the first quantitative phylogenetic analysis was completed for Paracrinoidea. This has implications for the future inclusion of paracrinoids in other paleobiological studies including understanding of the evolution of respiratory structures in early echinoderms, dispersal and biogeography, functional morphology, ecological mode, as well as highlighting remaining taxonomic problems in the group.

Phylogeny, however, only informs about evolutionary relationships, not of how an organism's morphology allows it to interact with its environment. Here we also explore disparity, which quantifies morphological traits for which evolutionary descent is undetermined and separates organisms based on similar morphological features in a multidimensional morphospace. Phylomorphospaces are generated by overlaying a phylogenetic tree on the morphospace. This combined visualization helps interpret the patterns seen in morphospace by adding an evolutionary perspective (Hopkins, 2013 & 2016).

Part 2: Geochemistry

The abundance of echinoderm skeletal elements in the sedimentary record has made them a frequent study organism for geochemical studies (Weber, 1969, 1973; Dickson, 2002, 2004; Ries, 2004; Hermans et al., 2010; Kołbuk et al., 2019; Iglikowska et al., 2020). Specifically, several studies have examined the Mg content of fossil echinoderms to reconstruct paleoseawater temperatures (Dickson, 1995, 2002, 2004;

Ries, 2004) because the incorporation of Mg into calcite is often used to define a temperature sensitive relationship (Weber, 1973; Carpenter and Lohmann, 1992). Additionally, studies examining minor and trace element incorporation into echinoderm skeletal elements have grown in importance as researchers recognize that echinoderm calcite can be used to track changes in seawater chemistry resulting from anthropomorphic influence (i.e., runoff and other pollution) (Hermans et al., 2010; Kołbuk et al. 2019; Iglikowska et al., 2020). However, the results of these studies are hard to compare as they investigate patterns from different species of echinoderm (frequently from different classes as well), and species from different locations. Work presented here focuses on echinoids from the same localities as well as multiple individuals of the same species to ensure the incorporation of major and minor elements is directly comparable.

Modern Echinoids

Echinoderms are known to have significant variation in their skeletal composition (Weber and Raup, 1969a; Weber, 1969, 1973; Hermans et al., 2010; Weiner and Dove, 2013; Kołbuk et al., 2019; Iglikowska et al., 2020) that has often been dismissed as vital effect. However, characterizing this variation among species and within individuals allows for greater use of echinoderms in geochemical studies, which provide insight to ocean chemistry and biomineralization. In this study, we examine four genera of echinoid from the Gulf of Mexico for major and minor element composition. By holding the location of the echinoids constant, we minimize the effects of temperature, salinity, and pH on elemental incorporation into the skeletons of the echinoids. This study helps

elucidate the differences in elemental composition of different echinoids and within individual echinoids as well as highlights the needs for further study to continue characterizing the elemental compositions.

Fossil Echinoids

Echinoderms disarticulate rapidly after death (Brett et al., 1997) and as a result, articulated specimens of echinoderms are somewhat rare in the fossil record. However, these disarticulated skeletal elements are readily preserved and make up a significant proportion of many sedimentary units. This has made echinoderms a desirable study organism for paleoseawater temperature reconstructions (Dickson, 1995, 2001b, 2002, 2004; Ries, 2004; Gorzelak et al., 2016). The retention of original chemistry of these skeletal elements is questionable, however, as fossilization and diagenetic processes potentially alter skeletal elements. This study examines the petrography and geochemical composition of fossilized echinoid skeletal elements from the Late Mississippian Glen Dean Formation of southern Kentucky and highlights the need for caution and extensive petrographic work to determine if echinoderm skeletal elements retain their original chemistry, prior to use as oceanographic proxies.

REFERENCES

Bauer, J.E., Sumrall, C.D., and Waters, J.A., 2017. Hydrospire morphology and implications for Blastoid phylogeny. *Journal of Paleontology*, **91**, 847–857.

Brett, C.E., Moffat, H.A., Taylor, W.L., 1997, Echinoderm taphonomy, taphofacies, and Lagerstätten. The Paleontological Society Papers, **3**, 147–190.

Carpenter, S.J. and Lohmann, K.C., 1992, Sr/Mg ratios of modern marine calcite: Empirical indicators of ocean chemistry and precipitation rate. Geochimica et Cosmochimica Acta, **56**, 1837–1849.

Dickson, J.A.D., 1995, Paleozoic Mg calcite preserved: Implications for the Carboniferous ocean. Geology, **23**, 535–538.

Dickson, J.A.D., 2001a, Diagenesis and crystal caskets: Echinoderm Mg calcite transformation, Dry Canyon, New Mexico, USA. Journal of Sedimentary Research, **71**, 764–777.

Dickson, J.A.D., 2002, Fossil echinoderms as monitor of the Mg/Ca ratio of Phanerozoic Oceans. Science, **298**, 1222–1224.

Dickson, J.A.D., 2004, Echinoderm skeletal preservation: Calcite-Aragonite seas and the Mg/Ca ratio of Phanerozoic oceans. Journal of Sedimentary Research, **74**, 355–365.

Donovan, S.K., and Paul, C.R.C., 1985. Coronate echinoderms from the lower Palaeozoic of Britain. *Palaeontology*, **28**, 527–543.

Gorzelak, P., Kryzkawski, T., Stolarksi, J., 2016, Diagenesis of echinoderm skeletons: Constraints on paleoseawater Mg/Ca reconstructions. Global and Planetary Change, **144**, 142–157.

Guensburg, T.E, and Sprinkle, J., 1994. Revised phylogeny and functional interpretation of the Edrioasteroidea based on new taxa from the Early and Middle Ordovician of western Utah. *Fieldiana (Geology)*, **29**, 1–43.

Hermans, J., Borremans, C., Willenz, P., André, L., Dubois, P., 2010, Temperature, salinity and growth rate dependences of Mg/Ca and Sr/Ca ratios of the skeleton of the sea urchin *Paracentrotus lividus* (Lamarck): an experimental approach. Marine Biology, **157**, 1293–1300.

Hopkins, M.J., 2013. Decoupling of taxonomic diversity and morphological disparity during decline of the Cambrian trilobite family Pterocephaliidae, *Journal of Evolutionary Biology*, **26**, 1665–1676.

Hopkins, M.J., 2016. Magnitude versus direction of change and the contribution of macroevolutionary trends to morphological disparity. *Biological Journal of the Linnean Society*, **118**, 116–130.

Iglikowska, A., Humphreys-Williams, E., Przytarska, J., Chełchowski, M., Kukliński, P., 2020, Minor and trace elements in skeletons of Arctic echinoderms. Marine Pollution Bulletin, **158**, 1–12.

Kołbuk, D., Dubois, P., Stolarski, J., Gorzelak, P., 2019, Effects of seawater chemistry (Mg^{2+}/Ca^{2+} ratio) and diet on the skeletal Mg/Ca ratio in the common sea urchin *Paracentrotus lividus*. Marine Environmental Research, **145**, 22–26.

Lefebvre, B. (2000). A new mitrate (Echinodermata, Stylophora) from the Tremadoc of Shropshire (England) and the origin of the Mitrocystitida. *Journal of Paleontology*, **74**, 890–906.

Paul. C.R.C., and Smith, A.B., 1984, The early radiation and phylogeny of echinoderms. Biological Reviews, **59**, 443–481.

Ries, J.B., 2004, Effect of ambient Mg/Ca ratio on Mg fractionation in calcareous marine invertebrates: A record of the oceanic Mg/Ca ratio over the Phanerozoic. Geology, **32**, 981–984.

Sheffield, S.L. and Sumrall, C.D., 2017. Generic revision of the Holocystitidae of North America (Diploporita, Echinodermata) based on universal elemental homology. *Journal of Paleontology*, **91**, 753–766.

Sumrall, C.D., 1993. Thecal design in isorophinid edrioasteroids. *Lethaia*, **26**, 289–302.

Sumrall, C.D., Heredia, S., Rodríguez, C.M., Mestre, A.I., 2013. The first report of South American edrioasteroids and the paleoecology and ontogeny of rhenopyrgid Echinoderms. *Acta Palaeontologica Polonica*, **58**, 763–776.

Ubaghs, G., 1975, Early Paleozoic echinoderms. Annual Review of Earth and Planetary Sciences, **3**, 79–98.

Ware, D., and Lefebvre, B., 2007. Abnormalities in the Lower Ordovician cornute *Phyllocystis* Thoral, 1935 (Echinodermata: Stylophora) from Montagne Noire (southern France): implications for plate homology and phylogeny. *Journal of Paleontology*, **81**, 779–787.

Weber, J.N. and Raup, D.M., 1968, Comparison of C^{13}/C^{12} and O^{18}/O^{16} in the skeletal calcite of recent and fossil echinoids. Journal of Paleontology, **42**, 37–50.

Weber, J.N., 1969, The incorporation of magnesium into the skeletal calcites of echinoderms. American Journal of Science, **267**, 537–566.

Weber, J.N., 1973, Temperature dependence of magnesium in Echinoid and Asteroid skeletal calcite: A reinterpretation of its significance. Journal of Geology, **81**, 543–556.

Weiner, S. and Dove, P.M., 2003, An overview of biomineralization processes and the problem of the vital effect. Reviews in mineralogy and geochemistry, **54**(1), 1–29.

Wright, D. F., Ausich, W. I., Cole, S. R., Peter, M. E., & Rhenberg, E. C., 2017. Phylogenetic taxonomy and classification of the Crinoidea (Echinodermata). *Journal of Paleontology*, **91**, 829–846.

Zamora, S., Lefebvre, B., Álvaro, J.J., Clausen, S., Elicki, O., Fatka, O., Jell, P., Kouchinsky, A., Lin, J., Nardin, E., Parsley, R., Rozhnov, S., Springle, J., Sumrall, C.D., Vizcaïno, D., Smith, A.B., 2013, Cambrian echinoderm diversity and palaeobiogeography. *In* Early Palaeozoic Biogeography and Palaeogeography, Harper, D.A.T. and Servais, T. (eds), 157–171.

CHAPTER I
INITIAL QUANTITATIVE ASSESSMENT OF THE ENIGMATIC CLADE PARACRINOIDEA (ECHINODERMATA)

A version of this chapter was originally published by Maggie R. Limbeck, Jennifer E. Bauer, Brad Deline, and Colin D. Sumrall

Limbeck, M.R., Bauer, J.E., Deline, B., Sumrall, C.D, 2023, Quantitative assessment of the enigmatic clade Paracrinoidea (Echinodermata): Palaeontology (accepted, with revisions)

My major contributions to this paper include: (1) conducted systematic evaluation of fossil taxa included; (2) initial phylogenetic and phylomorphospace analyses; (3) created figures; (4) writing the manuscript; (5) submitted and revised the manuscript. Jennifer E. Bauer, co-author, conducted additional phylogenetic analyses. Brad Deline and Colin D. Sumrall, co-authors, agreed with interpretations of fossil taxa and helped with revising the manuscript before and during journal revisions.

Abstract

Great strides have been made in understanding the phylogeny of the five extant echinoderm classes, however, many Paleozoic groups have yet to be examined in a rigorous, quantitative framework. The aberrant morphologies of Paracrinoidea, an unusual group of Paleozoic echinoderms, have hindered their inclusion in large-scale phylogenetic and morphologic studies. This study uses a combined approach of phylogenetic analysis and morphological disparity to elucidate species relationships within the clade. Findings from this study suggest that respiratory structures, oral plate arrangement, and ambulacral morphologies are important for defining subclades within Paracrinoidea. Examination of paracrinoids in a quantitative framework, facilitates their inclusion in larger projects examining Paleozoic echinoderm evolution, ecology, and biogeography.

Introduction

One of the great challenges facing paleobiology is understanding aberrant morphologies from the combined perspectives of phylogeny and morphological disparity.

Individually, phylogenetic and morphologic studies can provide insight into the relationships among members of a clade. Using these methods in concert with one another provides a more holistic understanding of fossil organisms (Hopkins and Smith, 2015; Wright, 2017; Deline, 2021). Phylogenetic analysis organizes taxa into a branching cladogram representing shared morphologies that are inferred to reflect shared ancestry. Disparity studies group taxa within a morphospace by gross morphologies that may additionally record ecological tendencies and other information while deemphasizing homology and phylogeny (Foote, 1994; Deline, 2009; Deline and Ausich, 2011; Deline et al., 2012). Valuable information can be learned from each individual study, but combining these analyses into a phylomorphospace facilitates rigorously testing the evolutionary framework of the clade and exploring questions related to biogeography and ecology of these fossil organisms (Sidluaskas, 2008; Brusatte et al., 2011; Benson and Choiniere, 2013; Hopkins, 2015). When these methods are employed for clades that have highly unusual morphologies, we gain a sense of the evolutionary processes that resulted in these aberrant morphologies. Echinoderms provide an ideal model system for these combined methods as they share many homologous elements across clades, but also include many experimental body plans in understudied, morphologically aberrant groups.

Among echinoderms, the evolution of numerous body plans during the late Cambrian and early Ordovician lead to high-level taxonomic diversity (Sumrall, 1997; Zamora et al., 2013). Several early Paleozoic echinoderm groups (e.g. Diploporita, Blastoidea, Coronoidea, Edrioasteroidea, Stylophora, and Crinoidea) have been rigorously examined with phylogenetic methods (Donovan and Paul, 1985; Sumrall,

1993; Guensburg and Sprinkle, 1994; Lefebvre, 2000; Ware and Lefebvre, 2007; Sumrall et al., 2013; Wright et al., 2017; Bauer et al., 2017; Sheffield et al., 2017). However, many groups, such as Paracrinoidea, have yet to be examined using an established homology scheme in concert with phylogenetic methods. Consequently, the evolutionary patterns cannot be quantitatively delineated, including the evolution of complex morphologies, timing of clade origins, and rates of evolution. Only by placing these questions within the context of the echinoderm tree of life can these questions be addressed.

Paracrinoidea, the focus of this study, are a small, temporally restricted echinoderm group. Members of this clade exhibit unusual morphologies such as thecal asymmetry, brachioles born only on the left side of the ambulacra, and reduced ambulacral configurations (Fig. 1.1) that have led to their exclusion in other work. The combined approach of using both phylogeny and morphological disparity analyses improves understanding of this enigmatic group and provides a starting point to use these methods on other highly disparate clades. Herein, we provide a comprehensive analysis of described paracrinoid taxa to better assess their complex morphologies and evolutionary history.

Previous Investigations of Paracrinoidea

Paracrinoidea is a group of early Palaeozoic stemmed echinoderms that bear a unique combination of morphological features. This clade was first recognised as a separate group by Jaekel (1900) and named by Régnell (1945), based on several unusual characters that distinguished it from eocrinoids and other blastozoan groups including

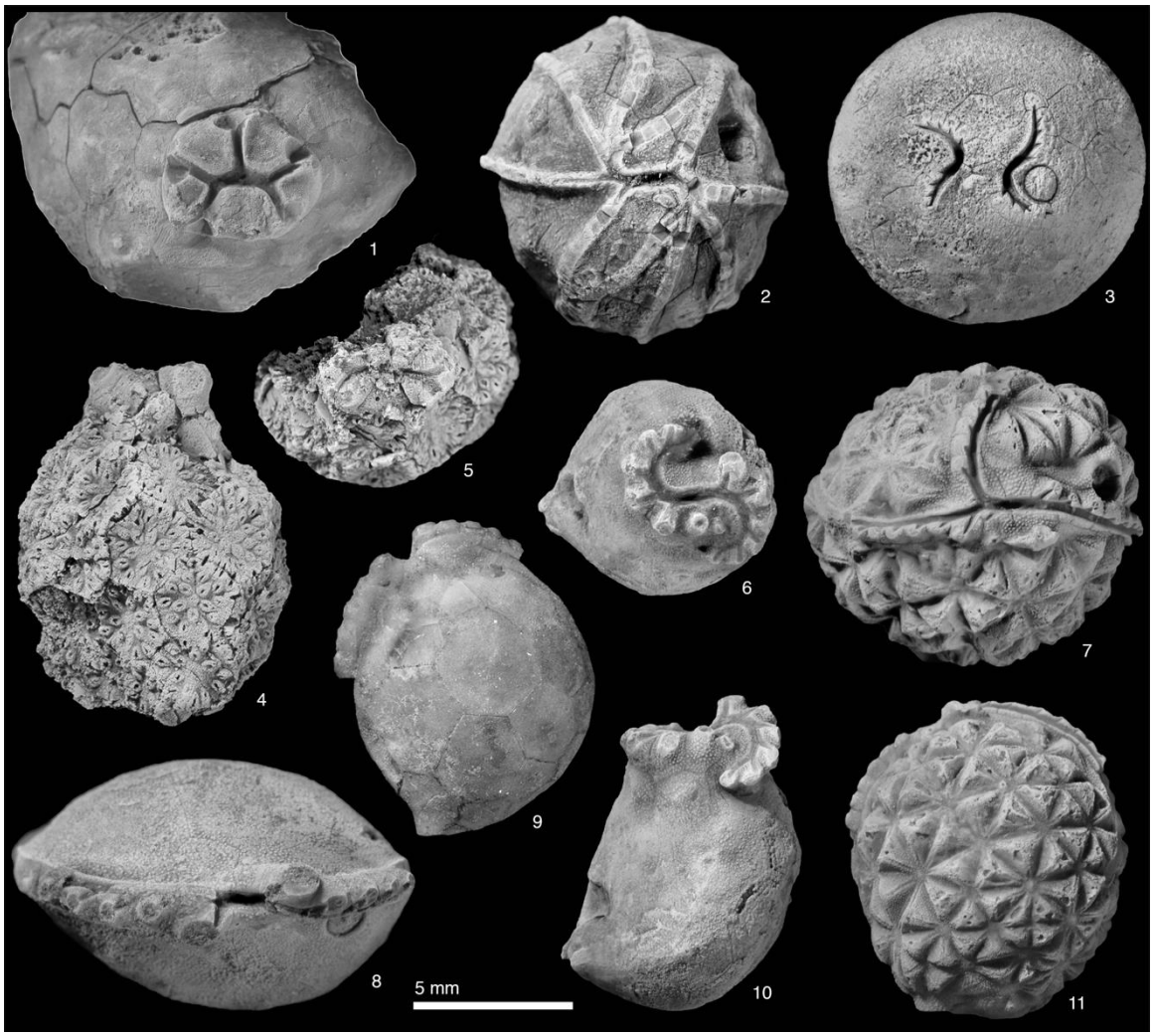

Figure 1.1 Representative specimens from Paracrinoidea. Paracrinoids as a clade exhibit a wide variety of morphologies that make analysis of species relationships challenging. (1) *Columbocystis typica* (Parsley, 1975) characterized by an oral summit with all five ambulacra present (USNM 93407b). (2) *Malocystites murchisoni* (Billings, 1857) characterized by two ambulacra that branch and extend down the theca (CMC-P50436). (3) *Bistomiacystis globosa* (Sprinkle, 1982) characterized by two mouths on the oral surface (OU 8937). (4, 5) *Implicaticystis symmetricus* (Frest, 1982) characterized by four ambulacra on a raised oral surface. (6, 10) *Canadocystis tennesseensis* (Parsley and Mintz, 1975) characterized by two ambulacra with a sinusoidal arrangement and a sickle shaped theca (USNM 241272). (7, 11) *Oklahomacystis tribrachiatus* (Parsley and Mintz, 1975) characterized by three ambulacra and tumid triagonal plate ornamentation (OU8150). (8, 9) *Globulocystites cristatus* (Frest, 1979) characterized by two ambulacra that extend down the theca (OU 8154

rhombiferans and diploporitans. This work was expanded and summarized by Kesling (1967), who described the odd and seemingly contradictory features of paracrinoids as a "Frankenstein", possessing the theca of cystoids, pinnuliferous arms of crinoids, and the stalk of blastoids (Fig. 1.1).

After the identification of Paracrinoidea as a distinct class, there was considerable debate regarding the placement of paracrinoids in the echinoderm tree. Sprinkle (1973) moved several genera from Eocrinoidea to Paracrinoidea but was unable to clarify the relationship with Crinozoa and Blastozoa. Parsley and Mintz (1975) determined that paracrinoid morphology was unusual enough to warrant the erection of the sub-phylum Paracrinozoa. Herein, authors include paracrinoids within Blastozoa. After large-scale faunal studies of the early 1970s, the paracrinoid literature is dominated by species descriptions and re-designations. As such, the taxonomy of Paracrinoidea has formed the background of evolutionary interpretations and is based on conjecture rather than rigorous phylogenetic methods. Major changes in subclade membership occurred with every large-scale re-examination of the group. The orders Varicata and Brachiata were first described by Kesling (1967), divided Paracrinoidea based on the presence of either recumbent or erect ambulacra respectively. Varicata included *Malocystites* Billings, 1857, *Wellerocystis* Foerste, 1920, *Amygdalocystites* Billings, 1854, *Canadocystis* Billings, 1857, and *Sinclairocystis* Bassler, 1950; while Brachiata included *Comarocystites* Billings, 1854. It was later suggested that differences in the ambulacral construction were insufficient for separation of Paracrinoidea and new orders were erected based on the presence or absence of respiratory structures in each member of the

clade (Parsley and Mintz, 1975). This new classification erected the orders Comarocystitida including *Amygdalocystites, Sinclairocystis, Comarocystites, Oklahomacystis* (Parsley and Mintz, 1975), and Platycystitida, including *Platycytites* Miller, 1889, *Canadocystis*, *Wellerocystis,* and *Malocystites*. Later, new genera *Globulocystites* Frest, 1979 and *Bistomiacystis* Sprinkle, 1982 were added to Platycystitida and *Implicatycystis* Frest, 1982 was added to Comarocystitida. These studies followed the classification of Parsley and Mintz (1975) without further revision.

A cladogram was produced for generic relationships (Frest, 1979), but was not the focus of the study nor was it inferred using modern algorithmic methodology. Previous taxonomic studies have identified features in paracrinoid species that suggest close relationships to other groups including blastoids, crinoids, and eocrinoids. These features are often observed in a subset of paracrinoid species, rather than being synapomorphies for Paracrinoidea. There are, however, several identifiable synapomorphies that unite Paracrinoidea, including: asymmetry in the mouth and stem (positioned on the left side of the theca), asymmetrical ambulacra constructed of only one set of floor plates with brachioles arising only from the left side of the food groove, three basals (two zygous and one azygous), uniserial brachioles and unusual placement of the anal opening, generally in the proximal BC interradius (Fig. 1.1) (Régnell, 1945; Kesling, 1967; Sprinkle, 1973; Parsley and Mintz, 1975). This combination of characters is found in no other echinoderm clade. However, even with these synapomorphies, a host of other unusual and highly variable morphologies illustrates a high degree of morphological disparity and plasticity within the group.

These earlier studies proposed classification and evolutionary relationships based solely on qualitative descriptions of morphology (Parsley and Mintz, 1975; Frest, 1979) rather than quantitative phylogenetic methods. The lack of quantitative analysis for this group is understandable considering the unusual nature of the organisms resulted in difficulties reconciling a homology scheme for skeletal elements. This was further exacerbated by the lack of computation power and techniques at a time when phylogenetic methodology was not the norm.

Methods

Paracrinoids (restricted to the Middle to Late Ordovician) have been found exclusively in Laurentia and are limited to North America. There are fourteen genera and 28 species of Paracrinoidea recorded in the literature. Twelve genera and 23 species of Paracrinoidea were used in this analysis. Two species, *Achradocystites schmidti* Hecker, 1958 and *Heckerites multistellatus* Rozhnov, 1987 have been included in Paracrinoidea but are excluded from this analysis. *Achradocystites schmidti* was initially included in Paracrinoidea sensu Parsley and Mintz (1975) based on thecal plating of existing specimens. A more recent specimen found with preserved ambulacra (Rozhnov, 2017) demonstrates that *Achradocystites* had biserally plated ambulacra which is not a synapomorphy for Paracrinoidea and was subsequently excluded from the analysis. *Heckerites multistellatus* was excluded as it was determined by authors to not be a paracrinoid as it has a ring of marginal plates (Rozhnov, 2017) that are not seen in any other species of paracrinoid and does not share any synapomorphies with Paracrinoidea and is therefore excluded from this study. *Canadocystis barrandei* Billings, 1858, was

excluded from the analysis as description of this species did not differentiate it unambiguously from *Canadocystis emmonsi* (Parsley and Mintz, 1975) clearly. A cross section of *Platycystites* and *Globulocystites* species were included in the analysis, however, these two genera are particularly speciose with minimal differentiation among species defined in respective description; therefore, not every species was included in this analysis. The taxonomy of these two genera needs to be re-evaluated but such a revision was outside the scope of this study. Members of *Columbocystis* Bassler, 1950 which as a genus has been suggested to be both a member (Sprinkle, 1973) and not a member of Paracrinoidea (Parsley and Mintz, 1975) was included in this analysis.

Repositories and institutional abbreviations

All studied specimens (Table 1.1) are reposited in museum collections including the National Museum of Natural History (NMNH), Washington, D.C., University of Iowa Paleontology Repository (SUI), Iowa City, IA; Sam Noble Oklahoma Museum of Natural History (OU), Norman, OK; and the Cincinnati Museum Center (CMC), Cincinnati, OH.

Phylogenetic analysis

To ensure a robust phylogenetic hypothesis, a character matrix was executed using maximum parsimony, maximum likelihood, and Bayesian inference. All characters were treated as equally weighted and multistate characters were unordered to ensure that the resulting trees were not skewed by a priori interpretations of character evolutionary sequences. A total of 38 characters were included for all 24 species, with the outgroup

Table 1.1 Table of all taxa examined for this study. Symbols next to each taxon are representative of order as designated by Kesling (1967) or Parsley and Mintz (1975). Those taxa without symbols were either not included in that particular classification scheme or were described after these classification systems and were not added to one or the other, i.e., *Bitsomiacystis*.

Taxa				Specimen Numbers	Sources
Amygdalocystites florealis (Billings, 1854)	●	□		SUI no specimen number; CMC 41584; USNM 241276	
Amygdalocystites radiatus (Billings, 1854)	●	□		CMC 36104, 36214, 36214**	
Bistomiacystis globosa (Sprinkle, 1982)			★	OU 8939, 8937	
Bistomiacystis schrantzi (Sumrall & Deline, 2009)			★	CMC 51985	
Canadocystis emmonsi (Hudson, 1905)	●		★	NYSM 6129*, 6131*, 6130*	Parsley & Mintz, 1975; plate 10, figs. 5-11
Canadocystis tennesseensis (Parsley & Mintz, 1975)	●		★	USNM 241265, 241272, 241273, 241271	
Columbocystis ovata (Parsley, 1975)			★	USNM 25935a	
Columbocystis typica (Bassler, 1950)			★	USNM 97469a, 93402, 934076, 93407a	
Comarocystites punctatus (Billings, 1854)		■	□	CMC 41583, 77956; GSA 33a*	Parsley & Mintz, 1975; plate 1, fig. 3
Comarocystites tribrachius (Parsley & Mintz, 1975)		■	□	USNM 93393	Parsley & Mintz, 1975; plate 1, figs. 4-6
Globulocystites cristatus (Frest, 1979)			★	SUI 91017, 44440; NMNH 112093, 93336; OU 8158, 8156, 8165; CMC 59377	
Globulocystites infundus (Frest, 1979)			★	SUI 39513	
Globulocystites rotundatus (Frest 1979			★	SUI 395358, 44438, 44439	
Implicatycystis shumardi (Frest, 1982)			□	SUI 39513	
Implicatycystis symmetricus (Frest, 1982)			□	SUI 39522, 39524, 39625, 39528	
Malocystites murchisoni (Billings, 1857)			★	CMC 59344, 50436, 26025, 41585**, 59344	
Oklahomacystis bibrachiatus (Sprinkle, 1982)			□	OU 9111	
Oklahomacystis spissus (Frest et. al., 1980)			□	SUI 45073	
Oklahomacystis tribrachiatus (Parsley & Mintz, 1975)			□	OU 7918, 7926, 8150, 8151, 7921	
Oklahomacystis trigonis (Guensburg, 1984)			□	UIX-5922*	Guensburg, 1984; plate 11
Platycystites faberi (Miller, 1889)	●		★	NMNH 112086	
Sinclairocystis praedicta (Bassler, 1950)	●		□	SUI 45072, 45071, 45070; NMNH 116332; OU 7912	
Wellerocystis kimmswickensis (Foerste, 1920)	●		★		
Cheirocystis fultonensis (Sumrall and Schumacher, 2002)					Sumrall and Schumacher, 2002; fig. 2

* specimens viewed only in literature ● Varicata ■ Brachiata □ Comarocystitida ★ Platycystitida

being *Cheirocystis fultonensis* Sumrall and Schumacher, 2002, a glyptocystitid rhombiferan. Characters were generated from all aspects of the theca; characters based on stem, brachiole, and holdfast features were of limited use because of missing data. Many of the thecal characters were focused on the arrangement of the seven oral plates (following the universal elemental homology scheme; Sumrall, 2010; Sumrall and Waters, 2012; Kammer et al., 2013) and how other features in the oral area were related to the oral plates (see Appendices 1 and 2). This was critical in establishing character transformations in paracrinoids as the plating of the theca is unorganised.

Two species included in the analysis (*Canadocystis emmonsi* and *Oklahomacystis trigonis*) were assessed for characters based only on literature sources and images (Parsley and Mintz, 1975; Guensburg, 1984; Rozhnov, 1994, 2017). This was due to species designations based on singular specimens that are either housed in foreign institutions or were at unvisited museums.

Both maximum parsimony and maximum likelihood trees were computed using PAUP*4.0b10 (Swofford, 2003). Heuristic searches were completed for both analyses. In both the parsimony and maximum likelihood analyses, bootstrap support values were generated using the stepwise addition to assess the relative robustness of the nodes within the tree. The Bayesian analysis was executed using RevBayes (Höhna et al., 2016) also following the MkV model with a gamma distribution rate variation for the characters.

Phylomorphospace analysis

To address inter- and intraclade relationships among paracrinoids, both phylogenetically and morphologically, two separate character matrices were assembled. A phylogenetic

character matrix (see Appendix 1) recording alternate states of homologous characters were used to infer evolutionary trees for paracrinoids. In contrast, a disparity matrix (see Appendix 2) recording descriptive morphological traits was used to separate paracrinoids into groups with similar morphological features within a multidimensional morphospace. These morphological characters divide paracrinoids based on rote similarity, rather than along evolutionary lines. Consequently, several important morphological features not found in the phylogenetic matrix were included in the morphological character matrix to capture the complete gross morphology of all analysed taxa irrespective of homology.

To assess morphological disparity with regard to phylogeny, a phylomorphospace was generated where the resulting morphospace was overlain by a phylogenetic tree, integrating the results of the two analyses. This combined analysis helps interpret patterns seen in morphospace by adding an evolutionary perspective (Hopkins, 2013 & 2016). Since two matrices were needed to complete these analyses, special care was taken to ensure that traits were not accidentally differentially weighted, potentially affecting the outcomes of both analyses (Deline and Ausich, 2017). Ultimately, both analyses were used to test whether the phylogenetic hypothesis for Paracrinoidea correlates to the disparity analysis morphospace.

The morphological character suite used in the phylomorphospace analysis was coded based on the protocol outlined by Deline (2009) and Deline and Ausich (2011). A total of 46 characters were identified for this analysis (Appendix 2), ranging from description of the ambulacral shape and curvature and thecal shape, to ornamentation of the plates themselves; many were developed in concert with those characters used in the

phylogenetic analysis and modified to assess gross morphology. Others recorded generalised morphologies that, while similar among taxa, were excluded from the phylogenetic analysis. Similar to the phylogenetic analysis, each paracrinoid species used in the analysis was coded using multiple specimens to provide the most complete morphological picture possible.

Prior to creating a phylomorphospace, a morphospace needed to be calculated from the morphological character data. Characters were coded according to the protocol outlined in Deline and Ausich (2011). Using this protocol, missing data was coded numerically and not-applicable data was coded as non-applicable. This coding protocol allows Gower's coefficient of similarity and a principle coordinate analysis (PCO) to differentiate between missing and non-applicable data and a greater flexibility in character types. Gower's coefficient of similarity has been shown to be appropriate for handling both numeric and alphanumeric character coding, allowing a dataset to retain missing data which is an inherent feature of datasets containing fossil organisms (Gower, 1971). Data were analyzed using PCO and the Cailliez correction factor to eliminate negative eigenvalues (Cailliez, 1983).

A phylomorphospace was created by overlaying a Bayesian inference consensus tree over the previously calculated morphospace. The phylomorphospace and supporting morphospace were executed in R, using the packages: phytools, paleotree, geiger, and cluster (see Appendix 3) (Revell, 2012; Bapst, 2012; Pennell et al., 2014; Maecheler et al., 2017).

Results

Phylogenetic Analysis

The parsimony analysis returned 22,852 equally parsimonious trees with lengths of 85 steps (Fig. 1.2). Out of the 38 characters used in the analysis, two were determined constant, seven were variable, and 27 were used to infer trees in this analysis. The strict consensus tree is largely unresolved but has stable groupings within the ingroup taxa.The most parsimonious trees were tested for statistical support using bootstrap analysis. The bootstrap analysis shows six clades with bootstrap scores greater than 50%. Parsimony tree scores: consistency index = 0.576471, retention index = 0.739130, rescaled consistency index = 0.426087, homoplasy index = 0.423529. The maximum likelihood analysis retained six trees, with the best fit tree (Fig. 1.2) having a -lnL score of 335.9417 and used all 38 characters that were included in the analysis. All six trees had -lnL scores within 0.1 of one another. The results of this analysis depict a largely resolved phylogenetic hypothesis compared to largely congruent with the results of the maximum parsimony analysis. For the relationships inferred by the maximum likelihood analysis, the confidence scores provided by the bootstrap analysis are similar to those relationships inferred by parsimony.

The Bayesian inference analysis resulted in 15,000 trees and we produced the consensus trees from reading in the tree trace from the analysis output to produce a maximum clade credibility (MCC), majority rule consensus (MRC) tree, and maximum posteriori (MAP) tree (Fig. 1.2). Both the MAP and MCC tree topologies are largely resolved and return similar groups as seen in the maximum parsimony and maximum likelihood trees, though they depict quite different relationships among taxa within those

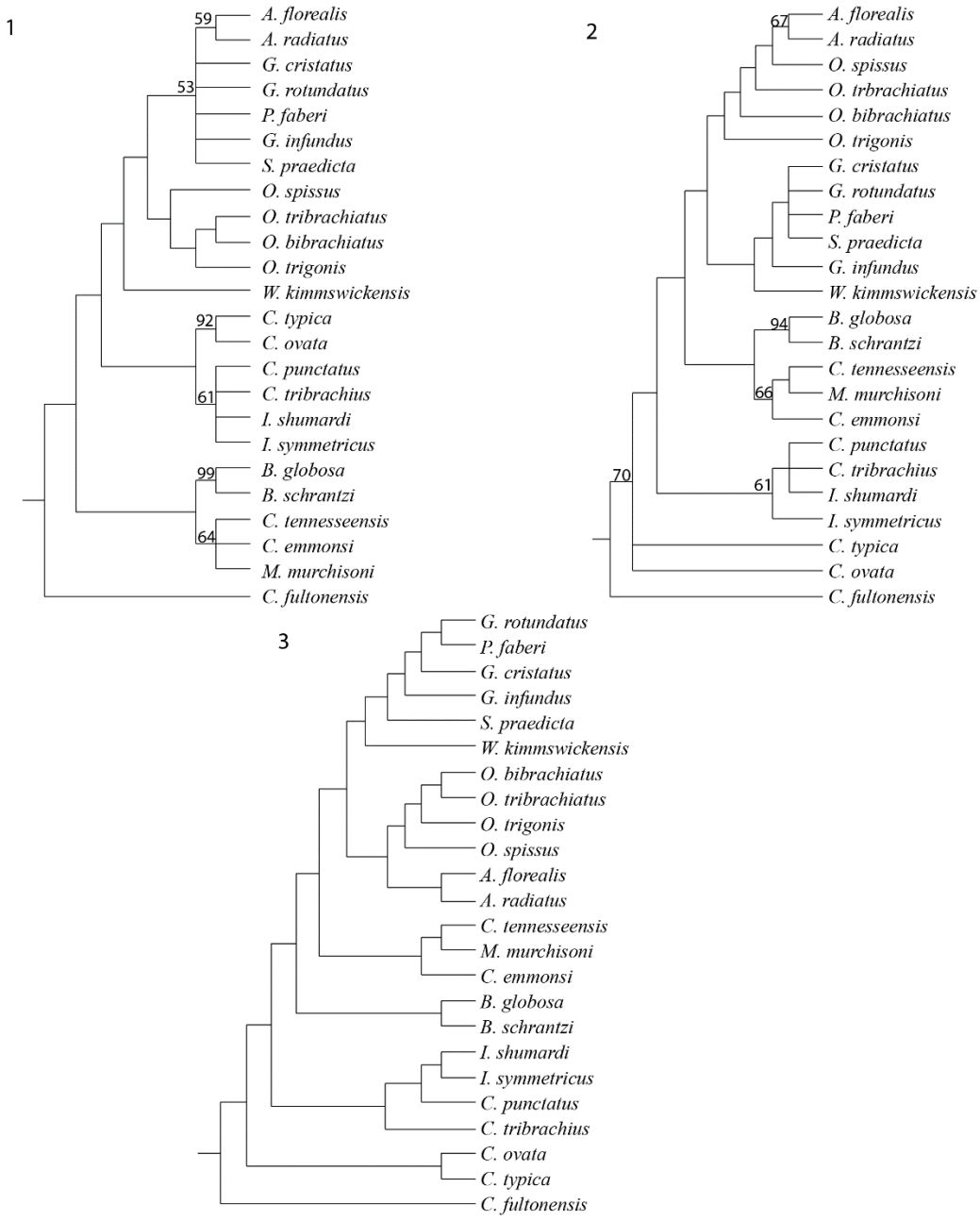

Figure 1.2 Phylogenetic hypotheses calculated using (1) maximum parsimony, (2) maximum likelihood, and (3) Bayesian methods. Numbers included on the parsimony and likelihood trees are recorded bootstrap scores greater than 50. Here we report the MCC tree as calculated using Bayesian methods. While species relationships are varied among the three trees, the major group relationships are retained across the tree trees.

larger groups. The MRC tree returns a tree topology dominated by polytomies among the majority of taxa, with only a few defined groups.

We focus herein on the relationships supported across the maximum parsimony, maximum likelihood and MCC trees, as those are likely to be the most stable. *Bistomiacystis* is consistently found at the base of the trees and the two species in this genus are returned as sister taxa 100% of the time. The unusual condition of two peristomes and the resulting ambulacral system are the determining factors in the consistency of this group. *Canadocystis* and *Malocystites* appear as a group in all trees, though the resolution of the included species varies among the trees. In the parsimony tree, *Canadocystis* and *Malocystites* are a polytomy while in the maximum likelihood and Bayesian trees, the relationships are resolved. The sigmoidal shape of the oral system and resulting ambulacral system is consistent within these taxa, though there is a lot of missing data from *M. murchisoni* and *C. emmonsi* that is playing a role in the polytomy seen in the parsimony tree. *Comarocystites* and *Implicaticystis* are returned as a group in all of the trees, though the arrangement and resolution of the species in these two genera can vary among the trees. These two genera are united by characters related to the shape of the ambulacral system and the presence of respiratory structures. The majority of paracrinoid species are in the genera *Amgydalocystites*, *Oklahomacystis*, *Platycystites*, and *Globulocystites* and these genera are arranged within two large sister groups that are deeply nested in all three trees. The parsimony tree places *Amygdalocystites* species in a polytomy with *Platycystites* and *Globulocystites* species; the ambulacral arrangement and overall thecal morphology of these three genera is very similar. Species of

Oklahomacystis form a sister group to *Amygdalocystites*, *Platycystites*, and *Globulocystites* and have well resolved relationships. In the likelihood and Bayesian analyses, however, *Amygdalocystites* and *Oklahomacystis* form one of the sister groups, while *Platycstites* and *Globulocystites* form the other. Species relationships within *Amygdalocystites* and *Oklahomacystis* are completely resolved while within the group that has *Platycystites* and *Globulocystites* forming a polytomy and resolved relationships in the likelihood and Bayesian trees respectively. The placement of *Wellerocystis* and *Sinclairocystis* at the top of the tree is consistent among the trees and are both more closely related to *Platycystites* and *Globulocystites* than to *Amygdalocystites* and *Oklahomacystis*. However, because of the discrepancies in relationships among these genera, the placement of *Wellerocystis* and *Sinclairocystis* differs on each of the five trees.

Phylomorphospace

The phylomorphospaces (Fig. 1.3) were created by joining a morphospace of paracrinoids with the maximum parsimony, maximum likelihood, MCC, and MRC trees that were estimated (Fig. 1.2). There are five major groups that are recognised in the phylomorphospace that correspond to the five major groups that are retained in all iterations of the phylogenetic analysis. Among the phylomorphospaces estimated from the parsimony, likelihood, and MCC trees all demonstrate relatively short branch lengths within each of the five groups, indicating close phylogenetic relationships and similar morphologies, while the branches joining the five groups are relatively long, indicating greater differences in morphology among these major evolutionary groups. In contrast,

the phylomorphospace estimated from the MRC tree has relatively long branches joining all of the taxa, reflecting the ambiguous evolutionary relationships that were estimated in the MRC tree.

Group one includes both species of *Columbocystis*. This grouping has short branch lengths and is largely defined by the presence of five ambulacra arranged in ideal 2-1-2 symmetry (Sprinkle, 1973) and exhibits clear oral plating in accordance with UEH (Sumrall, 2010).

Group two includes species of *Comarocystites* and *Implicaticystis*. This group has short branch lengths joining the four species and is morphologically constrained. Members of this group have a generally tumid theca, four ambulacra, and respiratory structures. Two of the species plot on top of each other in the phylomorphospace indicating very minimal disparity between the species.

Group three consists of both species of *Bistomiacystis* with relatively short branch lengths joining the two species. While the branch lengths are short, each species is clearly in its own region of the morphospace, indicating clear morphological differences between the two species.

Group four includes both species of *Canadocystis* and *Malocystites* with longer branch lengths among the included species than in either group one or two. This group is largely united by a sigmoidal ambulacral ambulacral system that is not seen in any of the other paracrinoid taxa included in this study. *Malocystites* is separated from both species of *Canadocystis* by a longer branch because its overall thecal morphology is a different shape and has a significant amount of missing data due to incomplete preservation.

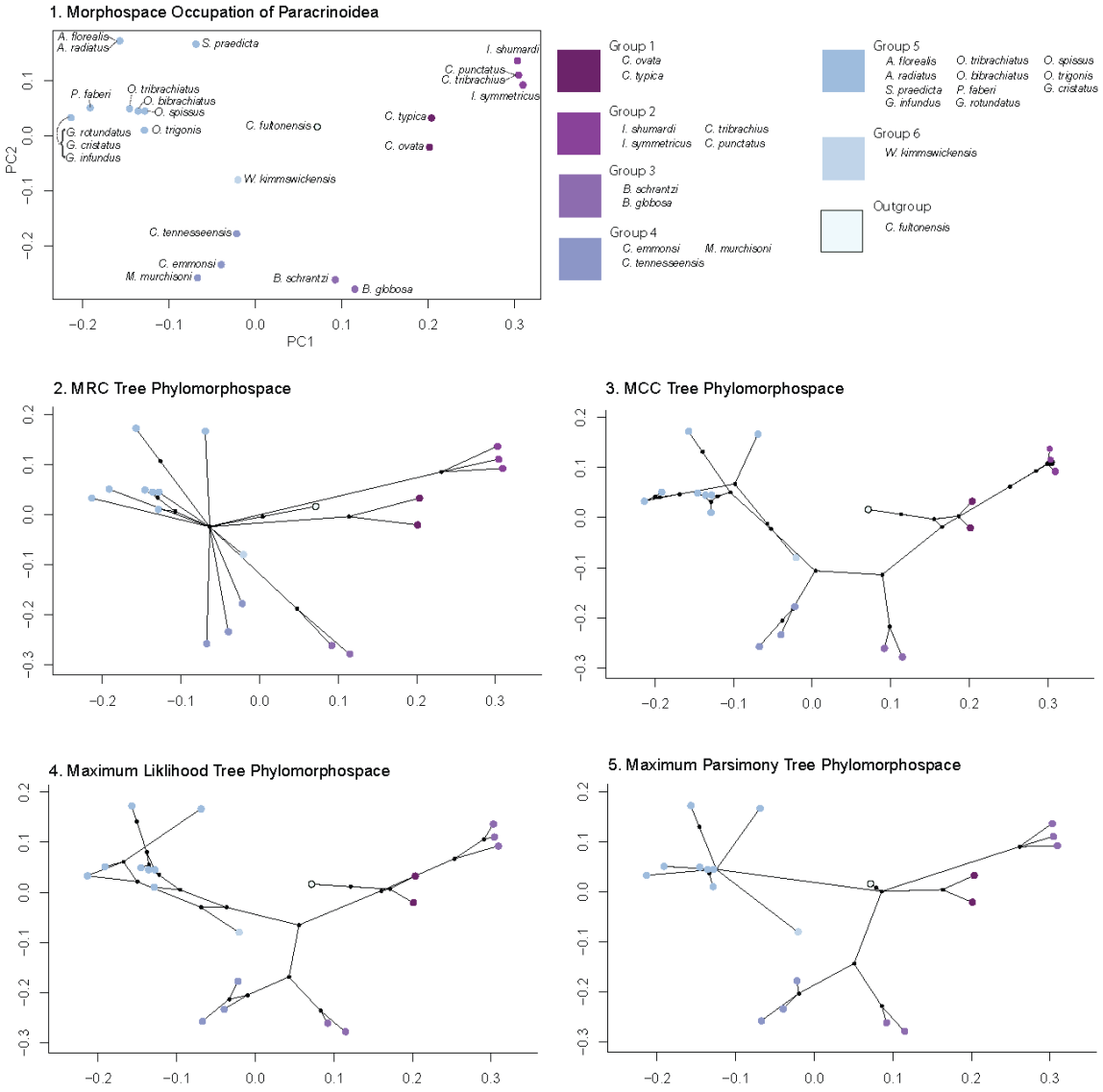

Figure 1.3 Paracrinoid morphospace and resulting phylomorphospaces for the maximum parsimony, maximum likelihood, Bayesian MCC and Bayesian MRC trees. In the morphospace, the five main groups that are returned by the parsimony, maximum likelihood, and MCC analyses are also estimated in the morphospace. The individuals in each group are relatively close to each other, demonstrating similarities in morphology, though there are individuals and groups that have more distance between them indicative of morphological differences.

Group five includes species of *Amygdalocystites, Platycystites, Globulocystites, Sinclairocystis,* and *Oklahomacystis*. This grouping is representative of the largest group seen in the phylogenetic analysis. Members of this group have generally almond-shaped thecae and two ambulacra that extend from the oral surface down the theca. There are longer branches joining the genera included in this group as there are significant morphological differences with respect to thecal plate size and shape and the presence and absence of respiratory structures.

Wellerocystis lies outside any of the major groups and has long branches joining to the rest of the phylomorphospace. Specimens of *Wellerocystis* show morphological plasticity within the ambulacral system that led to incomplete datasets for both the phylogenetic and morphological character suites.

Discussion

Phylogenetic Analysis

The results of all three phylogenetic analyses (maximum parsimony, maximum likelihood, and Bayesian) are congruent, with the MCC Bayesian tree being the most resolved. Five small groups have been inferred in these analyses, with specific synapomorphies that diagnose each group (Figure 1.2). Bootstrap analyses were performed for both the maximum parsimony and maximum likelihood trees, suggesting strong nodal support for the inferred trees (Fig 1.2). Similarly, *a posteriori* support was estimated in the Bayesian estimation and is represented by the maximum a posteriori (MAP) tree. Herein, discussion is focused on the relationships as shown in the MCC Bayesian tree as that tree has the most resolved and congruent relationships among the included species.

The taxa *Columbocystis typica* and *Columbocystis ovata* show the most discrepancy among the three different analyses. In the maximum parsimony analysis *Columbocystis* is more deeply nested in the tree and is included as a sister group to the clade that includes *Comarocystites* and *Implicaticystis.* In contrast, in the maximum likelihood and three Bayesian tree analyses, *Columbocystis* is located at the base of the tree as a sister group to the rest of Paracrinoidea, sensu Parsley and Mintz (1975). The genus *Columbocystis* has been proposed to be both a part of Paracrinoidea (Sprinkle, 1973) and not a part of Paracrinoidea (Parsley and Mintz, 1975). While sharing the synapomorphy of strong asymmetry and periproct offset in the BC interambulacrum, the clade Paracrinoidea is here diagnosed by the absence of the A ambulacrum and brachioles arising from the left side of the ambulacrum only. *Columbocystis* possesses the A ambulacrum and has complete 2-1-2 symmetry (Sprinkle, 1973), but it is unknown how the erect ambulacra are plated. *Columbocystis* on the inferred tree is a sister taxon to Paracrinoidea, and current exclusion from the clade, is still subjective based on how Paracrinoidea is phylogenetically defined.

Respiratory structures have been historically used to diagnose clades of echinoderms (Paul, 1968; Sprinkle, 1973) and paracrinoids are no exception. Parsley and Mintz (1975) diagnosed two orders of paracrinoids based on the presence or absence of respiratory structures. The phylogenetic relationships inferred herein suggest that respiratory structures have evolved at least three times independently (Fig. 1.4): once in the group with *Comarocystites* and *Implicatycystis,* once with *Sinclairocystis,* and once in the group with *Amygdalocystites* and *Oklahomacystis*. These structures have evolved

different water flow mechanics as well. The group including *Amygdalocystites* and *Oklahomacystis* has covered epispires, which are exothecal respiratory structures that bring coelomic fluid into proximity with ambient seawater (Parsley and Mintz, 1975; Sheffield et al., 2022). The group including *Comarocystites* and *Implicatycystis* has endothecal structures that bring ambient seawater into proximity to coelomic fluid through internal canals (Parsley and Mintz, 1975; Frest and Strimple, 1982; Sheffield et al., 2022). *Sinclairocystis* has endothecal respiratory structures that are similar in structure to those seen in *Comarocystites*, however, *Sinclairocystis* does not group with *Comarocystites* or *Implicaticystis* in any of the phylogenetic analyses. While the presence of respiratory structures and in particular, the difference in type of respiratory structure, do help to diagnose groups in this analysis (Fig. 1.4), the divisions are not as simple as presence and absence as they are non-homologous through the test of similarity (Patterson, 1988). This study along with recent others focused on echinoderm respiratory structures (Bauer et al., 2017, Sheffield et al., 2022) demonstrate that while these structures are important for understanding evolutionary relationships, they are often oversimplified for classification purposes.

Paracrinoid ambulacra evolve through paedomorphic ambulacral reduction (PAR) in which the plesiomorphic state for echinoderms is the presence of five ambulacra with 2-1-2 symmetry (Sumrall and Wray, 2007) and numerous subclades lose ambulacra in a predictable manner based on developmental patterning. The ambulacra present in each species in the analysis can be mapped onto the phylogeny (Figure 1.5). It is observed that

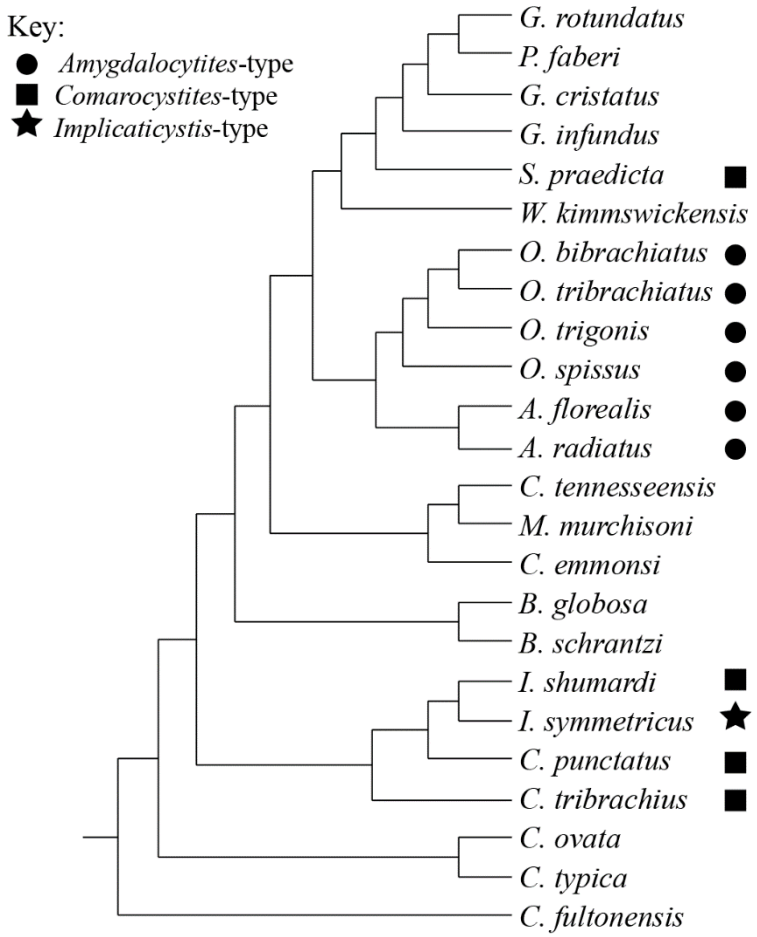

Figure 1.4 Bayesian MCC tree with respiratory structures mapped onto the tree. The distribution of respiratory structures across the tree topology indicates that respiratory structures evolved more than once within the group and are not defining characteristics for larger groups within Paracrinoidea.

the outgroup (*C. fultonensis*) and *Columbocystis* are the only members of the tree that have five ambulacra arranged with 2-1-2 symmetry (Sprinkle, 1973). The next group, that includes *Comarocystites* and *Implicaticystis* all have four ambulacra in which A fails to form but BC and DE both bifurcate. The position of the failed A ambulacrum is marked by the suture of O3 and O4 which are present in all paracrinoid taxa. The remaining group, that includes *Canadocystis, Bistomiacystis, Malocystites, Wellerocystis, Sinclairocystis, Globulocystites, Platycystites, Oklahomacystis,* and *Amygdalocystites,* all have two ambulacra in which A fails to form and BC DE fail to bifurcate.

Paedomorphic ambulacral reduction suggests that the reduction of ambulacral number is a derived state and it can be predicted which ambulacra are present, based on typical echinoderm development. Typically, where three ambulacra are present, they include the A ambulacrum, and the two shared ambulacra, BC and DE, which fail to bifurcate. Interestingly, the two species included in this study that have three ambulacra, *Oklahomacystis tribrachiatus,* and *Comarocystites tribrachius,* evolved tri-radial symmetry in a different manner. In *Oklahomacystis tribrachiatus* the A ambulacrum failed to develop, DE shared ambulacrum bifurcated, and the BC shared ambulacrum failed to bifurcate. Furthermore, it seems likely that only *Oklahomacystis tribrachiatus* is a valid taxon diagnosed by this unusual ambulacral arrangement. Unlike *Oklahomacystis tribrachiatus*, where the vast majority of specimens have three ambulacra, *Comarocystites tribrachius* is uncommon in populations of the otherwise identical *Comarocystites punctatus* and it is likely these specimens result from teratology.

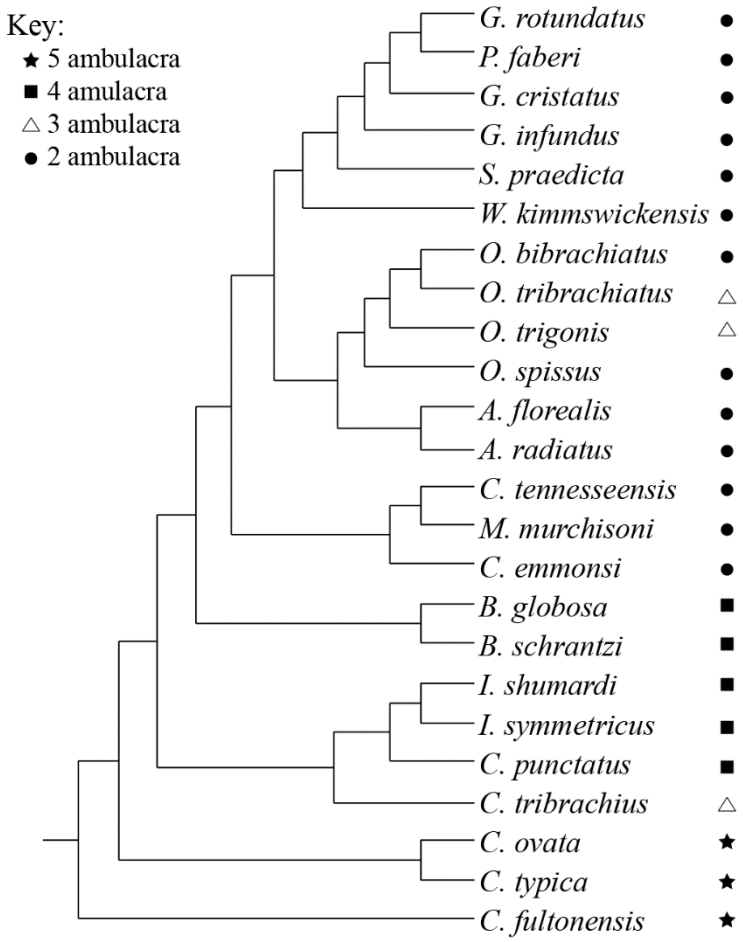

Figure 1.5 Bayesian MCC tree with number of ambulacra present in each species mapped onto the tree topology. There is a reduction in ambulacra as you move up the tree with the majority of paracrinoids having only two ambulacra present. There are several species that have three ambulacra present, but only one of those species can be confirmed in this study to always have three ambulacra.

Phylomorphospace

The relationships depicted in the phylomorphospace shed light on the evolutionary basis for the morphologies seen in paracrinoids. Of the five groups shown in the phylomorphospace, each correspond to clades inferred in all of the phylogenetic analyses and largely, each group has short branch lengths joining included species relative to branches between groups (Fig. 1.3).

The defining characters for these groups correspond to the shape of the ambulacrum; *Comarocystites* and *Implicatycystis* have bifurcating ambulacra, *Canadocystis, Malocystites,* and *Bistomiacystis* have sinusoidal ambulacra and *Platycystites, Globulocystites, Oklahomacystis, Sinclairocystis,* and *Amygdalocystites* have two ambulacra that do not bifurcate. While differences in the construction of respiratory structures have also been suggested to be of importance in establishing relationships among Paracrinoidea (Parsley and Mintz, 1975), there is only one group present where all taxa included have respiratory structures, *Comarocystites* and *Implicaticystis*. However, *Implicaticystis symmetricus* has differently constructed respiratory structures. In addition, within the large group containing *Platycystites, Globulocystites, Oklahomacystis, Sinclairocystis, Wellerocystis* and *Amygdalocystites*, only three of the six genera have respiratory structures and one has the same type of respiratory structures found in *Comarocystites* and *Implicatycystis*. This suggests that ecologically, the type of respiratory structures was not as important as the shape of the ambulacrum and gross thecal morphologies. These groups, supported by the ambulacral structure, are reminiscent of the original orders suggested for Paracrinoidea by Kesling (1967).

The largest grouping of paracrinoids (Fig. 1.3) represents a group and its member species are, consequently, close morphologically and evolutionarily. This clade is relatively unresolved when comparing the three phylogenetic analyses because of their evolutionary similarity. However, the phylomorphospace demonstrates here that this general morphology was a "Goldilocks Zone" for paracrinoid body plans. There is variation in these genera, *Sinclairocystis* has concave thecal plates and *Comarocystites*-like respiratory structures, *Oklahomacystis* and *Amygdalocystites* share the same type of respiratory structures, and *Oklahomacystis tribrachiatus* has three ambulacra. Despite this variation, this area of morphospace was accessed and modified by several paracrinoid genera. Alternatively, it is suggested that the close relationships defined by the phylogenetic analysis and morphological disparity result from paedomorphic reduction of ambulacra commonly seen in this group. It is possible that the reduction of five ambulacra to two ambulacra significantly constrains the morphologies seen in this clade and that morphological plasticity within the clade is limited by the reduction of ambulacra.

Phylomorphospace provides insight to the relationships found by the phylogeny and suggested by general morphology. We see that the same large groups present in the phylogenetic analyses (Fig. 1.2) are present in the phylomorphospace as expected and the included species in each group are joined by relatively short branches (Fig. 1.3), indicating morphological similarity in closely related taxa. The longer branch lengths that join each of the five groups in phylomorphospace suggest that paracrinoids evolved their unusual characteristics to be successful in different ecological niches and were able to

access a large area in morphospace, demonstrating a high degree of morphological plasticity. Future work will examine the role of paracrinoid morphology with respect to success in ecological niches in more detail.

Limitations of the analyses

Paracrinoidea is a small and temporally restricted group which leads to challenges in correctly assessing a phylogenetic analysis. Paracrinoids evolved rapidly in a short geologic time frame, effectively leaving the fossil record to only capture the basal taxa of a group that did not persist long enough for traits to stabilise within the population. Therefore, the fossils themselves possess a wide array of morphologies that are challenging to reconcile with existing homology schemes (i.e., UEH). In order to better estimate change through time and reconcile the differences in phylogenetic hypothesis, more substantial work is required in understanding the homologous elements of paracrinoids to better capture their aberrant morphologies.

Taxonomy and taxonomic revisions have featured prominently in the study of Paracrinoidea, though, because the majority of these descriptions were completed in the absence of UEH or other homology schemes, defining features of each genus (and in some cases, species) are dubious. This has led to the erection of several novel taxa that are difficult to differentiate from existing species. This leads to inconsistencies in museum labelling, publications, and in this case, discrepancies in character coding and resulting tree topology. Additionally, because of the prior emphasis on taxonomy within the field of palaeontology, there are several taxa within Paracrinoidea that are likely invalid taxa and are rather the result of anomalous ambulacral development. The absence

of regular thecal plating and homology schemes (outside of UEH) have resulted in the erection of novel taxa based on major differences in ambulacral arrangement. Two taxa included in this study, *Comarocystites tribrachius* and *Oklahomacystis bibrachiatus*, are considered invalid taxa by the authors. Apart from the ambulacra they show no substantial differences from their counterparts, *Comarocystites punctatus* and *Oklahomacystis tribrachiatus* are here considered to be teratological.

Multiple methods for examining the evolutionary relationships among paracrinoids were employed to determine the extent of their influence on topology within a small, temporally restricted clade. While there were several groups of paracrinoids that were consistently inferred via maximum parsimony, maximum likelihood, and Bayesian analyses, the overall tree topology was not consistent. The effects of these challenges in Paracrinoidea are seen in the resulting MCC, MAP, and MRC trees (Fig. 1.2). It has been demonstrated that MCC and MAP trees estimated using morphological data produce resolved trees, but also introduce groups with low posterior probabilities. Therefore, the MRC tree is considered to infer a tree with fewer erroneous groups (O'Reilly and Donoghue, 2018). In the case of Paracrinoidea, the MRC tree estimation results in a highly conservative tree that is largely a polytomy of all included taxa with only a few groups returned. This is unsurprising given that resolved taxa have very distinct morphologies and possess the least amount of missing character data. The polytomies across this tree are indicative of missing character data because of fossil preservation, a lack of a comprehensive homology scheme for paracrinoids, and other taxonomic challenges. In contrast, the MCC and MAP trees do return resolved trees, though with

differing topologies, and inferred clades are consistent with the groups that are inferred using maximum parsimony and maximum likelihood.

Additionally, it has been demonstrated that groups branching from the base of a clade that underwent both rapid evolution and morphological change, are hard to accurately infer evolutionary relationships (Novack-Gottshall et al., 2022). Paracrinoids are an example of this scenario because they are a temporally restricted group (Late Ordovician) that exhibit a wide range of aberrant and diverse morphologies. Based on the results of the phylogenetic analyses in combination with the estimated phylomorphospace, it appears that these basal taxa with a short temporal range, complicate our ability to clearly understand the evolutionary relationships in the clade.

Conclusions

Phylogenetic analyses largely agree with the proposed evolutionary relationships based on general morphology in previous studies (Parsley and Mintz, 1975; Frest el al., 1979). Relationships within Paracrinoidea are moderately resolved, while the contested genus, *Columbocystis*, sits as a sister taxon to Paracrinoidea. The relationships of taxa within the tree topology suggest that the orders, based on the presence of respiratory structures found in certain species (Parsley and Mintz, 1975), are paraphyletic, and therefore the previous taxonomy was unable to fully capture the complexity of these organisms. The phylogenetic analysis suggests the type of respiratory structure and arrangement of the ambulacral system are the major clade defining characters within Paracrinoidea. Furthermore, the resulting phylomorphospace suggests that Paracrinoidea was able to access several areas of morphospace during its evolution. The temporal restriction of this

group, however, makes it challenging to accurately assess this evolutionary history because Paracrinoidea did not persist long enough to converge and stabilise within a smaller morphospace.

These methods, (phylogenetic analysis and phylomorphospace) when used in conjunction with each other, provide a distinct and quantitative way to examine a clade. In this study, the phylogenetic analysis inferred several robust relationships within Paracrinoidea and the phylomorphospace recognises patterns that may be overlooked if only one method is used. Such studies can inform other questions with regard to paleoecology, biogeography, and rates of evolution.

Paracrinoidea has long been an enigmatic clade, with little consensus concerning characters that define the clade, taxonomy, and clade membership. While taxa have been assigned or moved around within the clade since its classification (Régnell, 1945), no rigorous, quantitative analysis has been completed prior to this study. This comprehensive study has provided a basis of homology through UEH for Paracrinoidea, inferred a phylogenetic hypothesis for the group and calculated a phylomorphospace that was used to assess and compare the results of the phylogenetic and morphological analyses. Beyond elucidating evolutionary relationships for Paracrinoidea, these methods are easily transferable to other invertebrate groups and can be used to address questions of biogeography and paleoecology.

ACKNOWLEDGEMENTS

We are grateful to the following for their assistance with museum specimens: T. Adrain, The University of Iowa; R. Burkhalter, Sam Noble Museum; K. Hollis, U.S. National

Museum of Natural History; B. Hunda, Cincinnati Museum Center. We would like to thank S. Sheffield for comments on earlier drafts of this study and discussion of figures. This work was supported by grants awarded to MRL from The Geological Society of America and The Dry Dredgers.

REFERENCES

Adams, E.N., 1972. Consensus techniques and the comparison of taxonomic trees *Systematic Biology*, **21**, 390–397.

Bapst, D.W., 2012. paleotree: An R package for paleontological and phylogenetic analyses of Evolution. *Methods in Ecology and Evolution*, **3**, 803–807.

Bassler, R.S., 1943. New Ordovician cystidean echinoderms of Oklahoma. *American Journal of Science*, **241**, 694–703.

Bassler, R.S., 1950. New genera of Middle Ordovician "Cystidae". *Journal of the Washington Academy of Sciences*, **40**, 273–277.

Bauer, J.E., Sumrall, C.D., and Waters, J.A., 2017. Hydrospire morphology and implications for Blastoid phylogeny. *Journal of Paleontology*, **91**, 847–857.

Benson, R.B.J. and Choiniere, J.N., 2013. Rates of dinosaur limb evolution provide evidence for exceptional radiation in Mesozoic birds. *Proceedings of the Royal Society B*, **280**, 1–7.

Billings, E., 1854. On some new genera and species of Cystidea from the Trenton Limestone. *Canadian Journa*l, **2**, 215–219, 250–253, 268–274.

Billings, E., 1857. New species of fossils from Silurian rocks of Canada: Report for the years 1853–1856. *Geological Survey of Canada*, 245–345.

Billings, E., 1858. On the Cystidae of the lower Silurian rocks of Canada. *Geological Survey of Canada Decade* **3**, 9–74.

Bremer, K., 1994. Branch support and tree stability. *Cladistics*, **10**, 295–304.

Brusatte, S.L., Montanari, S., Yi, H., and Norell, A., 2011. Phylogenetic corrections for morphological disparity analysis: new methodology and case studies. *Paleobiology*, **37**, 1–22.

Cailliez, F., 1983. The analytical solution of the additive constant problem. *Psychometrika*, **48**, 305–308.

Deline, B., 2009. The effects of rarity and abundance distribution on measurements of local and morphological disparity. *Paleobiology*, **35**, 175–189.

Deline, B. and Ausich, W.I., 2011. Testing the plateau: a reexamination of disparity and morphological disparity. *Paleobiology*, **37**, 214–236.

Deline, B., Ausich, W.I., and Brett, C.E., 2012. Comparing taxonomic and geographic scales in the morphological disparity of Ordovician through Early Silurian Laurentian crinoids. *Paleobiology*, **38**, 538–553.

Deline, B. and Ausich, W.I., 2017. Character selection and the quantification of morphological disparity. *Paleobiology*, **43**, 68–84.

Deline, B., 2021. Echinoderm morphological disparity: Methods, patterns, and possibilities. Cambridge University Press, 41pp.

Donovan, S.K., and Paul, C.R.C., 1985. Coronate echinoderms from the lower Palaeozoic of Britain. *Palaeontology*, **28**, 527–543.

Frest, T.J., and Strimple, H.L., 1982. A new comarocystitid (Echinodermata: Paracrinoidea) from the Kimmswick Limestone (Middle Ordovician), Missouri, *Journal of Paleontology*, **56**, 358–370.

Frest, T.J., Strimple, H.L., and Coney, C.C., 1979. Paracrinoids (Platycystitidae) from the Benbolt Formation (Blackriverian) of Virginia. *Journal of Paleontology*, **53**, 380–398.

Frest, T.J., Strimple, H.L., and Witzke, B.J., 1980. New Comarocystitida (Echinodermata: Paracrinoidea) from the Silurian of Iowa and Ordovocian of Oklahoma. *Journal of Paleontology*, **54**, 217–228.

Foerste, A.F., 1920. Racine and Cedarville cystids and blastoids with notes on other echinoderms. *The Ohio Journal of Science*, **21**, 33–78.

Foote, M., 1994. Morphological disparity in Ordovician-Devonian crinoids and the early saturation of morphological space. *Paleobiology*, **20**, 320–344.

Gower, J.C., 1971. A general coefficient of similarity and some of its properties. *Biometrics*, **27**, 857–871.

Guensburg, T.E., 1984. Echinodermata of the Middle Ordovician Lebanon Limestone, Central Tennessee. *Bulletins of American Paleontology*, **86**, 126.

Guensburg, T.E., 1991. The stem and holdfast of *Amygdalocystites florealis* Billings. *Journal of Paleontology*, **65**, 696–695.

Guensburg, T.E, and Sprinkle, J., 1994. Revised phylogeny and functional interpretation of the Edrioasteroidea based on new taxa from the Early and Middle Ordovician of western Utah. *Fieldiana (Geology)*, **29**, 1–43.

Hecker, R.P., 1958. New data on genus *Achradocystites* (Echinodermata, Paracrinoidea). *Proceedings of the Institute of Geology of the Estonian Academy of Sciences*, **3**, 145–162.

Höhna, S., Landis, M.J., Heath, T.A., Bissau, B., Lartillot, N., Moore, B.R., Huelsenbeck, J.P., and Ronquist, F., 2016. RevBayes: Bayesian phylogenetic inference using graphical models and an interactive model-specification language. *Systematic biology*, **65**, 726–736.

Hopkins, M.J., 2013. Decoupling of taxonomic diversity and morphological disparity during decline of the Cambrian trilobite family Pterocephaliidae, *Journal of Evolutionary Biology*, **26**, 1665–1676.

Hopkins, M.J. and Smith, A.B., 2015. Dynamic evolutionary change in post-Paleozoic echinoids and the importance of scale when interpreting changes in rates of evolution. *Proceedings of the National Academy of Science*, **112**, 3758–3763.

Hopkins, M.J., 2016. Magnitude versus direction of change and the contribution of macroevolutionary trends to morphological disparity. *Biological Journal of the Linnean Society*, **118**, 116–130.

Hudson, G.H., 1905. Contributions to the fauna of the Chazy Limestone on Valcour Island, Lake Champlain. *N.Y. State Museum Bulletin*, **80**, 270–295.

Kammer, T.W., Sumrall, C.D., Zamora, S., Ausich, W.I., and Deline, B., 2013. Oral region homologies in Palaeozoic crinoids and other plesiomorphic pentaradial echinoderms. *PLOS One*, **8**, 1–16.

Kesling, R.V., 1967. Cystoidea. *In* Moore, R.C. (ed.) *Treatise on Invertebrate Paleontology, Part S, Echinodermata 1*. Geological Society of America, & University of Kansas Press, S85–S262.

Lefebvre, B. (2000). A new mitrate (Echinodermata, Stylophora) from the Tremadoc of Shropshire (England) and the origin of the Mitrocystitida. *Journal of Paleontology*, **74**, 890–906.

Lefebvre, B., Eble, G.J., Navarro, N. and David, B., 2006. Diversification of atypical Palaeozoic echinoderms: a quantitative survey of patterns of stylophoran disparity, diversity, and geography. *Paleobiology*, **32**, 483–510.

Maechler, M., Struyf, A., and Maechler, M.M., 2008. The cluster package.

Miller, S.A., 1889. *North American Geology and Paleontology*. Western Methodist Books, 664 p.

Novack-Gottshall, P.M., Sultan, A., Smith, N.S., Purcell, J., Hanson, K.E., Lively, R., Ranjha, I., Collins, C., Parker, R., Sumrall, C.D., Deline, B., 2022. Morphological Volatility precedes ecological innovation in early echinoderms. *Nature Ecology and Evolution*, **6** 63–272.

O'Reilly, J.E., and Donoghue, P.C.J., 2018. The efficacy of consensus tree methods for summarising phylogenetic relationships from a posterior sample of trees estimated from morphological data. *Systematic Biology*, **62**, 354–362.

Paradis, E., Claude, J., and Strimmer, K., 2004. APE: Analyses of phylogenetics and evolution in R language. *Bioinformatics*, **20**, 289–290.

Parsley, R.L., 1975. Systematics and functional morphology of *Columbocystis*, a Middle Ordovician "cystidean" (Echinodermata) of uncertain affinities. *Bulletins of American Paleontology*, **67**, 349–360.

Parsley, R.L., and Mintz, L.W., 1975. North American Paracrinoidea: (Ordovician: Paracrinozoa, new, Echinodermata). *Bulletins of American Paleontology*, **68**, p. 1–113.

Patterson, C., 1988. Homology in classical and molecular biology. *Molecular Biology and Evolution*, **5**, 603–625.

Paul, C.R.C., 1968. Morphology and function of dichoporite pore-structures in cystoids. *Palaeontology*, **11**, 697–730.

Pennell, M.W., Eastman, J.M., Slater, G.J., Brown, J.W., Uyeda, J.C., Fitzjohn, R.G., Alfaro,M.E., Harmon, L.J., 2014. geiger v2.0: An expanded suite of methods for fitting macroevolutionary models to phylogenetic trees. *Bioinformatics*, **15**, 2216–2218.

R Core Team, 2013, R: A language and environment for statistical computing: R Foundation for Statistical Computing, Vienna, Austria. URL http://www.Rproject.org/.

Régnell, G., 1945. Non-crinoid Pelmatozoa from the Palaeozoic of Sweden: a taxonomic study. Lunds Geologisk-Mineralogiska Institution, 225 p.

Revell, L.J., 2012. phytools: an R package for phylogenetic comparative biology (and other things). *Methods in Ecology and Evolution*, **3**, 217–223.

Rozhnov, S.V., 1987. New data on eocrinoids with flattened theca. *Doklady Earth Science Section*, **295**, 965–968.

Rozhnov, S.V., 2012. Reinterpretation of Baltic Ordovican *Heckerites multistellatus* Rozhnov 1987 as a possible paracrinoid based on new material. *Zoosymposia*, **7**, 307–316.

Rozhnov, S.V., 2017. Ordovician Paracrinoids from the Baltic: key problems in comparative morphology of Pelmatozoan echinoderms. *Paleontological Journal*, **51**, 643–662.

Sheffield, S.L. and Sumrall, C.D., 2017. Generic revision of the Holocystitidae of North America (Diploporita, Echinodermata) based on universal elemental homology. *Journal of Paleontology*, **91**, 753–766.

Sprinkle, J., 1973. *Morphology and evolution of blastozoan echinoderms*. Harvard University, 284 pp.

Sprinkle, J. and Parsley, R.L., 1982. “Golf-Ball” Paracrinoid. 224–230. *In* Sprinkle, J. (ed.) *Echinoderm faunas from the Bromide Formation (Middle Ordovician) of Oklahoma*, 370 pp.

Sumrall, C.D., 1993. Thecal design in isorophinid edrioasteroids. *Lethaia*, **26**, 289–302.

Sumrall, C.D., 1997. The role of fossils in the phylogenetic reconstruction of Echinodermata. *Paleontological Society Papers*, **3**, 267–288.

Sumrall, C.D., and Schumacher, G.A., 2002. *Cheirocystis fultonensis*, a new glyptocystitoid rhombiferan from the Upper Ordovician of the Cincinnati Arch — comments on cheirocrinid ontogeny. *Journal of Paleontology*, **76**, 843–851.

Sumrall, C.D., and Wray, G.A., 2007.Ontogeny in the fossil record: diversification of body plans and the evolution of "aberrant" symmetry in Palaeozoic echinoderms. *Paleobiology*, **33**, 149–163.

Sumrall, C.D., and Deline, B., 2009. A new species of the dual-mouthed paracrinoid *Bistomiacystis* and a redescription of the edrioasteroid *Edrioaster priscus* from the upper Ordovician Curdsville member of the Lexington limestone. *Journal of Paleontology*, **83**, 135–139.

Sumrall, C.D., 2010. A model for elemental homology for the peristome and ambulacra in blastozoan echinoderms. 269–276. *In* Harris, L.G., Böttger, S.A., Walker, C.W., and Lesser, M.P. (eds.). *Echinoderms*.

Sumrall, C.D., and Waters, J.A., 2012.Universal elemental homology in glyptocystitoids, hemicosmitoids, coronoids, and blastoids: steps toward echinoderm phylogenetic reconstruction in derived blastozoa. *Journal of Paleontology*, **86**, 956–972.

Sumrall, C.D., Heredia, S., Rodríguez, C.M., Mestre, A.I., 2013. The first report of South American edrioasteroids and the paleoecology and ontogeny of rhenopyrgid Echinoderms. *Acta Palaeontologica Polonica*, **58**, 763–776.

Swofford, D., 2003, PAUP*. Phylogenetic Analysis Using Parsimony (*and other methods). Version 4b10. Sinauer Associates, Sunderland, MA.

Ware, D., and Lefebvre, B., 2007. Abnormalities in the Lower Ordovician cornute *Phyllocystis* Thoral, 1935 (Echinodermata: Stylophora) from Montagne Noire (southern France): implications for plate homology and phylogeny. *Journal of Paleontology*, **81**, 779–787.

Wright, D.F., 2017. Bayesian estimation of fossil phylogenies and the evolution of early to middle Paleozoic crinoids (Echinodermata). *Journal of Paleontology*, **91**, 799–814.

Wright, D. F., Ausich, W. I., Cole, S. R., Peter, M. E., & Rhenberg, E. C., 2017. Phylogenetic taxonomy and classification of the Crinoidea (Echinodermata). *Journal of Paleontology*, **91**, 829–846.

APPENDIX 1

Phylogenetic Character list

1. 0: O7 absent. 1: O7 present
2. 0: O6 absent. 1: O6 present
3. 0: Orals do not touch periproct. 1: O7 touches periproct. 2: O5 touches periproct.
4. 0: O6 does not touch peristome. 1: O6 touches peristome.
5. 0: O2 & O5 equal in size to other orals. 1: O2 &O5 different sizes than other orals
6. 0: O2 is not first facetal plate. 1: O2 is the first facetal plate.
7. 0: O5 is not first facetal plate. 1: O5 is the first facetal plate.
8. 0: Hydropore present on O1, O6. 1: Hydropore present on O1, O6, O7. 2: Hydropore present on O1/O7.
9. 0: Gonopore is present in a plate. 1: Gonopore crosses sutures.
10. 0: Gonopore on O1. 1: Gonopore on other oral plate. 2: Gonopore crosses O1/O7 suture.
11. 0: Hydropore and gonopore are not paired. 1: Hydropore and gonopore paired.
12. 0: Periproct in CD interray. 1: Periproct in AB interray. 2: Periproct in BC interray.
13. 0: One peristome. 1: Two peristomes.
14. 0: A ambulacrum present. 1: A ambulacrum absent.
15. 0: BC ambulacrum split. 1: BC ambulacra not split.
16. 0: DE ambulacrum split. 1: DE ambulacrum not split.
17. 0: Brachioles are erect. 1: Brachioles are recumbent.

18. 0: Ambulacrum flush with theca. 1: Ambulacrum raised above theca.
19. 0: Floor plates form thecal walls (ex. *Canadocystis*). 1: Floor plates are epithecally positioned (ex. *Amygdalocystites*).
20. 0: Floor plates recumbent. 1: Floor plates erect.
21. 0: Ambulacra are restricted to summit (ex. *Canadocystis*). 1: Ambulacra extend down theca (ex. *Globulocystites*).
22. 0: Ambulacra are linear (ex. *Comarocystites*). 1: Ambulacra curve clockwise (ex. *Canadocystis*).
23. 0: Floor plates wide. 1: Floor plates narrow.
24. 0: Terminal floor plate is not enlarged. 1: Terminal floor plate is enlarged.
25. 0: Brachioles biserial. 1: Brachioles uniserial.
26. 0: Floor plates attach in center of thecal plates. 1: Floor plates attach on thecal plate sutures. 2: Floor plates attach on both center of thecal plates and plate sutures.
27. 0: Brachioles are the same size. 1: First brachioles are larger. 2: Last brachioles are larger.
28. 0: No respiratory structures 1: *Comarocystites*-type 2: *Amygdalocystites*-type 3: *Implicatycystis*-type 4: pectinirhombs
29. 0: Mouth and stem at poles. 1: Mouth and stem offset.
30. 0: Small basal plate in BC interray. 1: Small basal plate in DE interray. 2: Four basals one large in BC others small.
31. 0: Plates are convex. 1: Plates are concave.
32. 0: Theca is tumid. 1: Theca is anterior-posteriorly flattened.

33. 0: Plates are unornamented. 1: Plates are stellate. 2: Plates ornamented with triangles.
34. 0: Lumen is elliptical. 1: Lumen is circular.
35. 0: Plate sizes are equivalent. 1: Plate sizes are unequal.
36. 0: Plating of theca is irregular. 1: Plating of theca is consistent with *Platycystites.* 2: Plating of theca is consistent with *Comarocystites.* 3. Plating of theca follows the *Glyptocystitoid* pattern.
37. 0: Periproctal membrane is present. 1: Periproctal membrane is absent.
38. 0: Floor plates are biserially plated. 1: Floor plates are not biserially plated.

Phylogenetic Character Matrix

A. florealis	??????????00111001010101?121?011??011
A. radiatus	??????????00111001010101??21?011?0011
B. globosa	11211001???2110000000101?020??000?1011
B. schrantzi	11211001???2110000000?1?020??001?1011
C. tennesseensis	11010111001101110000001?0?0001100000011
C. emmonsi	1101011100120111000001?0??101?000?0011
C. typica	11010001???2000001110?0?1001200001011
C. ovata	11??000????0000011100?0?100??000?1011
C. punctatus	??????????????0100011100101001?100?1211
C. tribrachius	?1???11????2010001110?0?0010?100?0211
G. cristatus	11111111001001110010101?2001001001111
G. rotundatus	1?1010010010011100101?0???01201001111
I. shumardi	?1???11?????0100011100?0?001?310001211
I. symmetricus	11??1111001?0100011100?0?003??10001?11
M. murchisoni	1101?111??100111100001?0???01100000011
O. spissus	1111011????0011000101?0?1021?00200011
O. tribrachiatus	1120011100110110001010?0??121100200011
O. bibrachiatus	?1200111???1011100101?0??121?00201011
O. trigonis	1121011100120110001010?0???21?00201011
P. faberi	11111??1?0100111001010?0???0??01001111
G. infundus	11111??1???0011100101?0???01101001111
S. praedicta	11111111001001110010101?0?2111010000211
W. kimmswickensis	1111011????0010000101?0?2101100001011
C. fultonensis	1100011212020000001000000104040011030 0

APPENDIX 2

Morphological Disparity Character List and Matrix

1. 0: Oral surface is flat. 1: Oral surface is a curved summit.

2. 0: Oral surface is raised. 1: Oral surface is flush with theca.

3. 0: Oral surface is narrower than the theca. 1: Oral surface is the same width as the theca.

4. 0: Oral surface is not reduced to edge because of lateral flattening. 1: Oral surface is reduced to edge because of lateral flattening.

5. 0: Oral area is centered. 1: Oral area is offset.

6. 0: One peristome present. 1: Two peristomes present.

7. 0: 7 oral plates present. 1: 6 oral plates present.

8. 0: Oral plates are equal in size. 1: O2 and O5 are larger. 2: All oral plates are different sizes. 3: O6 and O7 are smaller. 2 could also be true

9. 0: Oral plates are the same shape. 1: O3 and O6 are elongated. 2: O2 and O5 are elongated. 3: Oral plates are all different shapes.

10. 0: Hydropore is on O1, O6, O7. 1: Hydropore is on O1, O6. Its on O1/O7

11. 0: Hydropore and gonopore are not paired. 1: Hydropore and gonopore are paired.

12. 0: A ambulacrum is present. 1: A ambulacrum is absent.

13. 0: Ambulacra are not branching. 1: Ambulacra are branching.

14. 0: BC DE ambulacra split. 1: BC DE ambulacra not split. 2: DE ambulacra split. 3: BC ambulacra split.

15. 0: BC DE ambulacra are the same length. 1: D ambulacrum is longer.

16. 0: Ambulacra not curved. 1: Ambulacra curve clockwise. 2: Ambulacra curve counterclockwise.

17. 0: Ambulacra curve the same direction. 1: Ambulacra curve different directions. NA they are straight

18. 0: Branches off ambulacra do not curve. 1: Branches off ambulacra curve. NA not branched

19. 0: Branches curve clockwise. 1: Branches curve counterclockwise. 2: Branches curve different directions. NA not branched

20: 0: B ambulacrum curves clockwise. 1: B ambulacrum curves counterclockwise. 2: B ambulacrum does not curve.

21. 0: C ambulacrum curves clockwise. 1: C ambulacrum curves counterclockwise. 2: C ambulacrum does not curve.

22. 0: D ambulacrum curves clockwise. 1: D ambulacrum curves counterclockwise. 2: D ambulacrum does not curve.

23. 0: E ambulacrum curves clockwise. 1: E ambulacrum curves counterclockwise. 2: E ambulacrum does not curve.

24. 0: DE ambulacrum curves clockwise. 1: DE ambulacrum curves counterclockwise. 2: DE ambulacrum does not curve.

25. 0: BC ambulacrum curves clockwise. 1: BC ambulacrum curves counterclockwise. 2: BC ambulacrum does not curve.

26. 0: Ambulacrum are straight. 1: Ambulacrum are sinusoidal. 2: Ambulacrum bent.

27. 0: Ambulacra are recumbent. 1: Ambulacra are erect.

28. 0: Ambulacra are restricted to the oral area. 1: Ambulacra extend down the theca.

29. 0: Brachioles are the same size. 1: First brachiole is larger. 2. Brachioles are all different sizes. 3. Last brachiole is larger.

30. 0: Brachioles are attached on plates. 1: Brachioles are attached on plate sutures.

31. 0: Brachioles are on floor plates. 1: Brachioles are on oral plates. 2: Brachioles are on both floor and oral plates.

32. 0: Respiratory openings are absent. 1: Respiratory openings are present.

33. 0: *Comarocystites* respiratory structures present. 1: *Amygdalocystites* respiratory structures present. 2: *Implicatycystis* respiratory structures present. Pectinirhombs so NA

34. 0: Periproct located in BC interray. 1: Periproct located in CD interray.

35. 0: Oral plates do not touch the periproct. 1: Oral plates do touch the periproct.

36. 0: O7 touches the periproct. 1: O5 touches the periproct. NA

37. 0: Small basal plate is in the BC interray. 1: Small basal plate is in the DE interray. 2: Small basal plate is in EA interray. 3. Small basal plate is in CD interray. NA three small one big in these.

38. 0: Plates are concave. 1: Plates are convex.

39. 0: Plating of theca is irregular. 1: Plating of theca is consistent with *Platycystites*. 2: Plating of theca is consistent with *Comarocystites*. NA glyptocystitoid 3: Plating is consistent with Glyptocystitids.

40. 0: Plates are not ornamented. 1: Plates are ornamented.

41. 0: Plates stellate. 1: Plates ornamented with triangles.

42. 0: Plates are equal in size. 1: Plates are unequal in size.

43. 0: Small plates located in BC interray. 1: Small plates located at stem. 2: Small plates located in both locations. 3: small plates distributed at random. NA

44. 0: Pustules are absent. 1: Pustules are present.

45. 0: Theca is spherical. 1: Theca is half-moon in shape. 2: Theca is oval. 3: Theca is strawberry shaped. Barrel shaped

46. 0: Theca is not flattened laterally. 1: Theca is flattened laterally.

	1	2	3	4	5	6
A._florealis	2	2	2	2	2	1
A._radiatus	2	2	2	2	2	1
B._globosa	1	2	1	1	1	2
B._schrantzi	1	2	1	1	1	2
C._tennesseensis	1	1	2	1	2	1
C._emmonsi	1	1	2	1	2	1
C._typica	1	1	1	1	2	1
C._ovata	1	1	1	1	2	1
C._punctatus	1	1	1	1	1	1
C._tribrachius	1	1	1	1	1	1
G._infundus	2	2	2	2	2	1
G._cristatus	2	2	2	2	2	1
G._rotundatus	2	2	2	2	2	1
I._shumardi	1	1	1	1	1	1
I._symmetricus	1	1	1	1	1	1
M._murchisoni	1	2	2	1	1	1
O._spissus	2	2	2	1	2	1
O._tribrachiatus	2	2	2	1	2	1
O._bibrachiatus	2	2	2	1	2	1
O._trigonis	2	2	2	1	2	1
P._faberi	2	2	2	2	2	1
S._praedicta	2	2	2	1	2	1
W._kimmswickensis	2	2	2	1	1	1
C._fultonensis	1	2	2	1	1	1

	7	8	9	10	11	12
A._florealis	0	0	0	0	0	2
A._radiatus	0	0	0	0	0	2
B._globosa	1	2	3	1	0	2
B._schrantzi	1	2	3	1	0	2
C._tennesseensis	1	1	1	1	0	2
C._emmonsi	1	1	1	1	0	2
C._typica	2	1	1	2	0	1
C._ovata	2	1	1	2	0	1
C._punctatus	0	2	4	1	0	2
C._tribrachius	0	2	4	1	0	2
G._infundus	1	2	1	0	0	2
G._cristatus	1	2	1	0	0	2
G._rotundatus	1	2	1	0	0	2
I._shumardi	0	2	4	0	0	2
I._symmetricus	0	2	4	1	2	2
M._murchisoni	1	0	0	1	0	2
O._spissus	1	1	2	0	0	2
O._tribrachiatus	1	1	2	1	2	2
O._bibrachiatus	1	1	2	1	2	2
O._trigonis	1	1	2	1	0	2
P._faberi	1	1	1	0	0	2
S._praedicta	1	1	1	1	0	2
W._kimmswickensis	1	1	2	0	0	0
C._fultonensis	1	4	4	3	1	1

	13	14		15	16	26	27
A._florealis	1	2		1	1	1	1
A._radiatus	1	2		1	1	1	1
B._globosa	2	1		1	2	2	1
B._schrantzi	2	1		1	2	2	1
C._tennesseensis	1	2		1	2	2	1
C._emmonsi	1	2		1	2	2	1
C._typica	2	1	NA		1	1	2
C._ovata	2	1	NA		1	1	2
C._punctatus	2	1		1	1	1	2
C._tribrachius	2	1		1	1	1	2
G._infundus	1	2		2	1	1	1
G._cristatus	1	2		2	1	1	1
G._rotundatus	1	2		2	1	1	1
I._shumardi	2	1	NA		1	1	2
I._symmetricus	2	1	NA		1	1	2
M._murchisoni	1	2		1	2	2	1
O._spissus	1	3		1	1	1	1
O._tribrachiatus	1	3		1	1	1	1
O._bibrachiatus	1	2		1	1	1	1
O._trigonis	1	3		1	1	1	1
P._faberi	1	2		2	1	1	1
S._praedicta	1	2		2	1	1	1
W._kimmswickensis	2	1		0	1	1	1
C._fultonensis	1	1		1	1	1	1

	28	29	30	31	32	33
A._florealis	2	1	2	2	2	2
A._radiatus	2	1	2	2	2	2
B._globosa	1	4	1	3	1	NA
B._schrantzi	1	4	1	3	1	NA
C._tennesseensis	1	2	1	3	1	NA
C._emmonsi	1	2	0	3	1	NA
C._typica	1	1	2	2	1	NA
C._ovata	1	1	2	2	1	NA
C._punctatus	1	1	2	1	2	1
C._tribrachius	1	1	2	1	2	1
G._infundus	2	2	1	NA	1	NA
G._cristatus	2	2	1	NA	1	NA
G._rotundatus	2	2	1	NA	1	NA
I._shumardi	1	1	2	1	2	1
I._symmetricus	1	1	2	3	2	3
M._murchisoni	0	0	1	NA	1	NA
O._spissus	2	2	2	2	2	2
O._tribrachiatus	2	2	2	2	2	2
O._bibrachiatus	2	2	2	2	2	2
O._trigonis	2	2	2	2	2	2
P._faberi	2	2	1	NA	1	NA
S._praedicta	2	2	2	1	2	1
W._kimmswickensis	2	0	0	3	1	NA
C._fultonensis	1	1	2	3	2	4

	34	35	36	37	38	39
A._florealis	0	0	2	0	2	1
A._radiatus	0	0	2	0	2	1
B._globosa	1	2	2	1	2	1
B._schrantzi	1	1	2	0	2	1
C._tennesseensis	1	2	2	1	2	1
C._emmonsi	1	2	2	NA	2	0
C._typica	0	0	0	2	2	1
C._ovata	0	0	0	0	2	0
C._punctatus	0	0	1	3	1	3
C._tribrachius	0	0	1	3	1	3
G._infundus	2	1	2	2	2	2
G._cristatus	2	1	2	2	2	2
G._rotundatus	2	1	2	2	2	2
I._shumardi	0	0	1	3	1	3
I._symmetricus	0	0	1	3	1	3
M._murchisoni	1	2	2	1	2	0
O._spissus	1	1	2	2	2	1
O._tribrachiatus	1	1	2	2	2	1
O._bibrachiatus	1	1	2	2	2	1
O._trigonis	1	1	2	2	2	1
P._faberi	0	1	2	2	2	2
S._praedicta	2	1	1	2	1	3
W._kimmswickensis	2	2	1	0	2	1
C._fultonensis	1	1	NA	NA	2	4

	40		41	42	43	44	45
A._florealis	2		1	1	4	2	3
A._radiatus	2		1	1	4	2	3
B._globosa	1	NA		2	2	1	1
B._schrantzi	2		1	2	0	1	1
C._tennesseensis	1	NA		2	4	1	2
C._emmonsi	1	NA		2	0	0	2
C._typica	1	NA		0	4	1	2
C._ovata	1	NA		0	0	1	2
C._punctatus	1	NA		2	4	1	4
C._tribrachius	1	NA		2	4	1	4
G._infundus	1	NA		1	1	2	3
G._cristatus	1	NA		1	1	2	3
G._rotundatus	1	NA		1	1	2	3
I._shumardi	1	NA		2	4	1	4
I._symmetricus	1	NA		1	0	1	4
M._murchisoni	1	NA		0	0	0	1
O._spissus	2		2	1	4	0	1
O._tribrachiatus	2		2	1	1	2	1
O._bibrachiatus	2		2	1	1	2	1
O._trigonis	2		2	1	0	0	1
P._faberi	1	NA		1	1	2	3
S._praedicta	1	NA		1	4	2	3
W._kimmswickensis	1	NA		1	4	1	1
C._fultonensis	2		1	1	NA	1	5

A._florealis	2
A._radiatus	2
B._globosa	1
B._schrantzi	1
C._tennesseensis	1
C._emmonsi	1
C._typica	1
C._ovata	1
C._punctatus	1
C._tribrachius	1
G._infundus	2
G._cristatus	2
G._rotundatus	2
I._shumardi	1
I._symmetricus	1
M._murchisoni	1
O._spissus	1
O._tribrachiatus	1
O._bibrachiatus	1
O._trigonis	1
P._faberi	2
S._praedicta	1
W._kimmswickensis	1
C._fultonensis	1

APPENDIX 3

Phylomorphospace R Code

Libraries used:

Phytools
Paleotree
Geiger
Cluster
Ape

Code:

```
data <- read.csv("phylospace_6.22_b.csv", row.names = 1)


x1 <- daisy(data, metric=c("gower"))
x2 <- pcoa(x1, correction="cailliez")
x2$vectors
write.csv(x2$vectors, file="points.csv")


mcc <- read.nexus("mcc.tree")
rootmcc <- root(mcc, 'C._fultonensis',resolve.root=TRUE)
equalmcc <- compute.brlen(rootmcc, 1)


paradata <- read.csv("points.csv")
rownames(paradata) <- paradata$X


PCO1 <- paradata$Axis.1
names(PCO1) <- row.names(paradata)
PCO2 <- paradata$Axis.2
names(PCO2) <- row.names(paradata)

phylomorphospace(equalmcc, paradata[,1:2])
```

CHAPTER II
MAJOR AND MINOR ELEMENT DISTRIBUTION IN FOUR ECHINOID GENERA FROM THE GULF OF MEXICO

Abstract

Echinoids are a globally abundant group of organisms that have a distinct skeletal structure (stereom) composed of hundreds to thousands of skeletal elements. These skeletal elements are specialized for different functions and grow at different rates. Such rate variation is often accompanied by differences in the isotopic and elemental composition of skeletal elements. Differences, often termed vital effects, that occur both within single organisms and between species (Weber and Raup, 1969; Weber, 1969, 1973; Weiner and Dove, 2013; Kołbuk et al., 2019; Iglikowska et al., 2020). Studies recording vital effects, however, are often difficult to compare directly, because the organisms in question frequently are from different locations or the study focuses on several classes of echinoderm rather than genera from the same class and location. In this study we examine four echinoid genera from the Florida coast in the Gulf of Mexico to test the hypotheses that 1) major and minor element composition is related to growth rate of skeletal elements and 2) there is a phylogenetic signal that can be seen in skeletal element composition. Data suggest that spines have statistically significant incorporation of Mg and Sr when compared to other skeletal elements. The remaining skeletal elements, however, are not able to be distinguished based on chemical composition. The composition of the skeletal elements does reflect growth rate dependent incorporation of major and minor elements, though the relationships are more complex than originally hypothesized This study highlights the need for more in-depth studies of elemental composition across genera of echinoids and mineralization pathways to further understand the incorporation of major and minor elements into echinoid skeletal elements.

Introduction

Echinoids are a diverse and globally abundant group of organisms that include sea urchins, sea biscuits, and sand dollars. Echinoid skeletal elements are recognized by their unique formation as a single crystal of calcite and the ubiquitous presence of stereom (Weber, 1959; Melville and Durham, 1967), which reflects soft tissue attachments (i.e., pores infilled with soft tissues, notches for muscle attachments) and structural features (i.e., denser stereom for strength versus a laminated structure in the tooth) (Smith, 1992). Echinoids have been demonstrated to exhibit strong biological control over the skeletonization process, with a marked vital effect present in both isotopic and elemental composition (Weber and Raup, 1969a; Weber, 1969, 1973; Weiner and Dove, 2013).

At present, investigation into the chemistry of echinoderm skeletons has focused predominantly on biologically driven variation in isotopic composition (Weber and Raup, 1969a; Limbeck et al., 2017); there has been less investigation into elemental composition (Weber, 1973; Kołbuk et al., 2019; Iglikowska et al., 2020). All members of this group have a test (skeleton) composed of multiple skeletal elements made of biologically precipitated high-magnesium calcite (Melville and Durham, 1967), regardless of the chemical state of their marine habitats. Incorporation of non-Ca cations, on the other hand, are believed to be controlled largely by water temperature, pH, pCO_2, salinity, and crystallization rate and are described by standard partition coefficients (Morse and Bender, 1990; Burton and Walter, 1991; Carpenter and Lohmann, 1992; Borremans et al., 2009; Hermans et al., 2010). Biologic influence on the elemental composition of echinoderm calcite, however, cannot be discounted, and may play a role in the incorporation of both major and minor cations (cf. Mg, Sr, Fe, and Mn). For

example, it has been hypothesized that skeletal elements with a faster rate of growth incorporate higher levels of minor and trace elements than those with slower rates of growth (Weber, 1973; Hermans et al., 2010). Previous work has also suggested that trace metal incorporation into the echinoid skeleton has a genetic component as well as a growth rate component (Weber, 1969; Carpenter and Lohmann, 1992; Borremans et al., 2009; Iglikowska et al., 2020). These studies suggest that differences in biomineralization and trace metal incorporation between species may reflect echinoid phylogeny. Metal incorporation can also vary among individuals of the same species and among skeletal elements of the same species (Weber, 1973; Kołbuk et al., 2019; Iglikowska et al., 2020) indicating biological control that has yet to be fully understood. This study examines the incorporation of elements in the major skeletal elements (test plates, spines, and ossicles of the Aristotle's Lantern) from four species of echinoid to explore potential mechanisms driving metal incorporation.

Echinoids

Echinoids evolved during the Ordovician, however, they did not diversify until the Jurassic (Melville and Durham, 1967; Kroh and Smith, 2010). In the modern, approximately 70 families can be found globally and many are keystone species within their environments (Kroh and Smith, 2010). Echinoids are characterized by a test that is subspherical (as in sea urchins) to flattened (as in sand dollars), have spines, tube feet, and commonly a jaw apparatus known as the Aristotle's Lantern (Melville and Durham, 1957). The test is divided into ambulacral and interambulacral plates which are found in organized columns down the test (Figure 2.1) and the entire test is covered in spines.

Spines are used for defense against predation and to hold the animal in place against rocks and corals. The jaw apparatus is made of five different skeletal elements (dipyramid, epiphysis, rotula, compass, and tooth) that each appear five times (Figure 2.1) in the apparatus.

Echinoids are broadly split into two groups, the Regularia (sea urchins) and Irregularia (sea biscuits, sand dollars). Regular echinoids exhibit predominantly pentaradial symmetry and are epifaunal. Notably, they have very long and stout spines and fully developed Aristotle's Lanterns. In contrast, irregular echinoids exhibit bilateral symmetry and are semi-infaunal to infaunal (Melville and Durham, 1957). Notably, they have very short and gracile spines and have underdeveloped Aristotle's Lanterns, and in several groups the lantern is phylogenetically lost.

Echinoid Biomineralization

Echinoderms exhibit what has classically been referred to as biologically controlled mineralization. Mineralization of their skeletal elements is mediated by proteins and proteinaceous structures that are templated by the organism's genetic make-up (Marin et al., 2013). Most metazoans that mineralize use similar mineralization pathways (as opposed to microbially induced mineralization) and there is evidence that skeletal mineralization with a variety of minerals beginning approximately 550–540 million years ago (Marin et al., 2013; Wood, 2018).

Much of the research on biomineralization processes has used echinoids as a study organism because of the availability of the complete genome of *Strongylocentrotus purpuratus* (Sodergren et al., 2006).

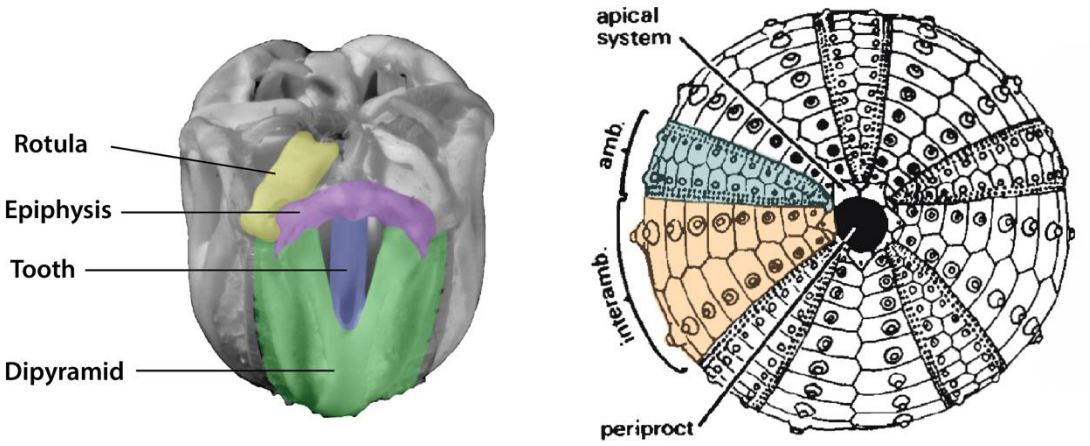

Figure 2.1 Anatomical description of echinoids. Left image is the Aristotle's Lantern (jaw apparatus). Elements in the lantern that are color-coded were included in the analysis. To the right is the test of an echinoid with the ambulacral and interambulacral columns color-coded.

In echinoids, the initial mineralization process begins in the larval stage, where, during gastrulation, the primary mesenchyme cells (PMCs) form a multicellular syncytium (Gilbert and Wilt, 2011). The PMCs fuse and calcite spicules (rods) that support the larval body plan develop and are then resorbed prior to mineralization of the adult skeleton (Gorzelak, 2020). The majority of studies examining chemical composition of echinoid skeletal elements measure the composition of adult echinoids, not the larval stage. When investigating echinoid biomineralization, it is also important to consider how plating of the non-larval echinoderms varies with growth. During the juvenile life-stage, new skeletal elements of the test are added biserially, immediately distal from the apical system following the ocular plate rule (OPR) in which plates are added to the ambulacral and interambulacral columns starting from the ocular plate within the apical system (Mooi and David, 1993b; Mooi et al., 1994). Consequently, plates near the oral region are older than those near the anus. In some echinoids, test plates are added throughout the individual's lifespan. However, many echinoids reach a stable plating pattern and after the juvenile stage, the plates themselves grow via holoperipheral growth (Pearse and Pearse, 1975). As the individual ages, plates increase in size and the older plates incorporate skeletal material throughout the lifespan of the organisms, whereas younger plates only incorporate skeletal material since their formation. In echinoids, the mineralization of the spine and tooth elements differ, rather, spines can regenerate (Albéric et al., 2019) and teeth grow continuously (Ma et al., 2007).

In contrast to holoperipheral growth, echinoid spines are able to regenerate when broken. Spines grow through a process wherein longitudinal micro-spines develop at the

distal tip which connect via a series of lateral bridges. The bridges thicken as the spine grows to create wedges that thicken the spine overall (Alberic et al., 2019). Spines have been determined to incorporate amorphous calcium carbonate (ACC) (hydrated and anhydrous depending on location) within their structure at all times to facilitate the regeneration process. The ability to regenerate also leads to possession of different proteins than other regions of the skeleton that relate to the maintenance of ACC to repair broken spines (Gilbert and Wilt, 2011; Alberic et al., 2019; Gorzelak, 2020). Consequently, it is important to determine if there is evidence of spine repair when utilizing spines in geochemical studies as repaired portions of spines may have a different composition than the base of the spine.

Echinoid teeth have continuous growth at the distal end to compensate for tooth wear at the proximal end (Lowenstam and Weiner, 1989, Ma et al., 2007), also differ from other ossicles in the echinoid skeleton. Teeth mineralize in a similar way to spines via a series of spicules (thin rods) and bridges that connect the spicules (Gilbert and Wilt, 2011) in two specialized tissues that create a laminated, T shaped tooth (Ma et al., 2007). The teeth have porous stereom in the horizontally laminated structures and develop a protodolomite core (Lowenstam and Weiner, 1989; Reich and Smith, 2009). The tooth also incorporates ACC within its structure to facilitate continuous tooth growth. Because of the different growth mechanisms seen in teeth and spines, sampling of these skeletal elements for geochemical studies can be biased based on sampling protocol. However, the differences in mineralization may also reflect in different incorporation patterns.

Our understanding of echinoid biomineralization has been greatly enhanced by advances in documenting gene regulatory networks (GRNs). Evolution of these networks results in the expression of different functions and timing that controls skeletal development at different taxonomic levels (Bottjer, 2017). Echinoderms have extensive GRNs that are just now beginning to be understood (Kohr and Ettensohn, 2017; Morgulis et al., 2019; Thompson 2022), although early data suggests these transcription factors are not present across the whole of echinoderms. For example, the Alx1 transcription factor, which is linked to the PMCs that initiate skeletal growth, is present in echinoderms, but has a larger role in echinoderms with larval skeletons (echinoids, holothurians, ophiuroids) than those that lack a larval skeleton (asteroids) (Khor and Ettensohn, 2017). Vascular endothelial growth factor (VEGF) signaling is important to skeletogenesis as it initiates spicule formation in larval echinoderms. VEGF is not present in asterozoa (sea stars) which do not produce larval skeletons (Morgulis et al., 2019). It is also important to note that there are differences in spine development between cidaroids and euechinoids. Cidaroid echinoids do not have an epidermis covering on their spines whereas euechinoid echinoids have an epidermal covering on their spines (Lawrence and Jangoux, 2013). This indicates that in cidaroids, spines are in direct contact with seawater while euechinoid spines have tissues that control contact with seawater. These subtle differences in GRNs among echinoderms suggests that details of biomineralization, such as variation in elemental chemistry, may highlight phylogenetic differences.

Methods

Sample Selection

Samples were collected as part of the Southeast Area Monitoring and Assessment Program (SEAMAP) data collection cruise from a region in the Gulf of Mexico (Figure 2.2) with average seawater temperatures ranging from 20–28°C and salinity ranging from 35–36‰ (see Table 2.1 for relevant ambient water chemistry, i.e., water temperature, sampling depth, salinity, etc.). Samples used in this study were collected during cruises in Summer 2018, Fall 2018, and Summer 2019 from 8 different locations in the Gulf of Mexico. Specimens were collected live, via seabed trawling and stored in 70% ethanol, then cataloged into the Florida Fish and Wildlife Biodiversity Collections. When extra specimens of the same species from the same locations are collected, they are made available to researchers. A total of 12 individuals of the four taxa (*L. variegatus, E. tribuloides, A. punctulata,* and *C. chesheri*) were examined in this study, chosen according to the number of samples that were donated and the number of samples that were collected at the same location.

Echinoids for this study were collected within a single marine environment. Echinoids include *Lytechinus variegatus, Eucidaris tribuloides, Arbacia punctulata,* and *Clypeaster chesheri*. It was important for this study to examine species across Echinoidea to assess how elemental composition varies across echinoid groups. These four species represent a cross-section of the established phylogeny of echinoids (Kroh and Smith, 2010) (Figure 2.3). *Eucidaris* is a member of Cidaroidea, which is the most ancestral group of echinoids, *Lytechinus* and *Arbacia* are more derived regular echinoids. *Clypeaster* is an irregular echinoid representing a highly derived echinoid clade.

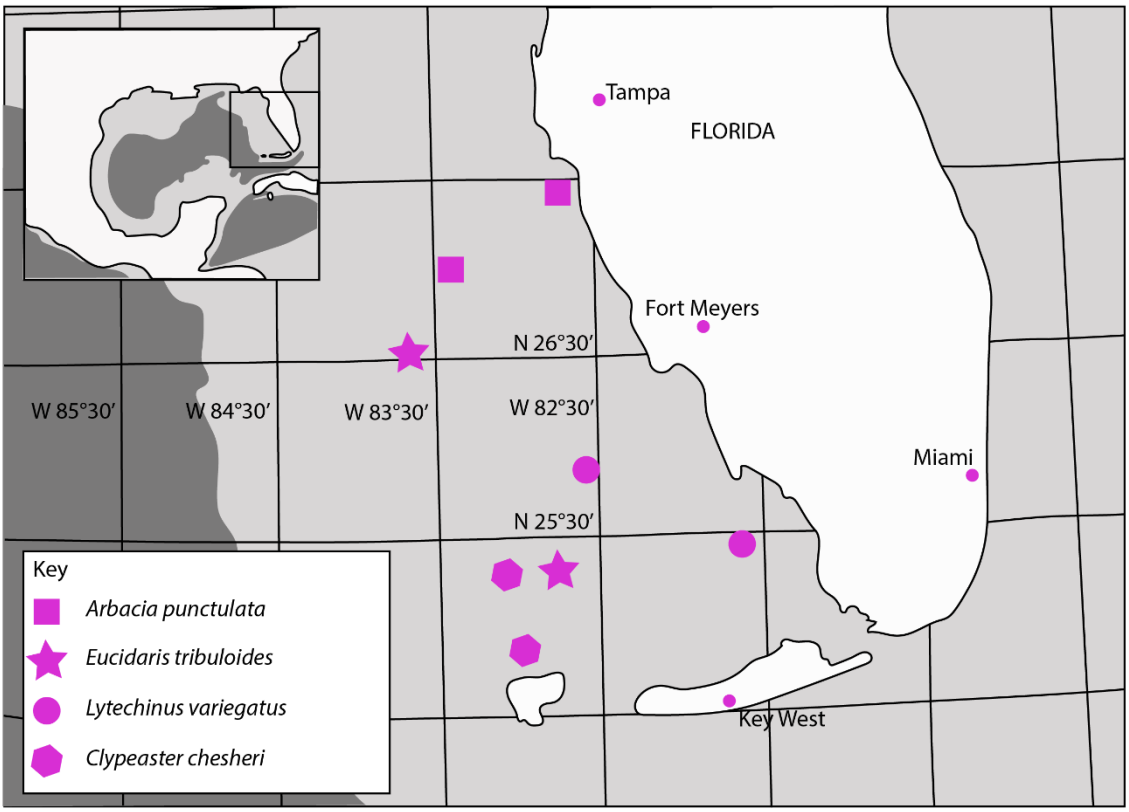

Figure 2.2 Echinoid collection locations in the Gulf of Mexico. Yellow inset box shows the whole Gulf of Mexico and the rest of the map is just the region the samples were collected from. Colors correspond to the taxa that were sampled in the specific locations.

Table 2.1 Summary of specimens included in the study and relevant ecological information about where they were collected.

Species	Cruise	Latitude N	Longitude W	Depth (m)	Temperature (°C)	Salinity (%)
A. punctulata	Summer 18	27°20'50"	82°44'38"	11.3	30.3	35.6
A. punctulata	Summer 18	28°53'74"	83°27'08"	17.6	29.3	34.2
C. chesheri	Fall 18	25°12'26"	83°25'86"	59	27.9	36.2
C. chesheri	Summer 19	25°48'27"	83°00'00"	26.7	29	35.2
E. tribuloides	Fall 18	26°28'60"	83°25'86"	56	23	36.6
E. tribuloides	Fall 18	25°14'05"	82°49'09"	46	25	36.2
L. variegatus	Summer 19	25°47'26"	82°37'09"	19	29.1	36.6
L. variegatus	Summer 19	25°21'54"	81°39'47"	6	30.2	35.6

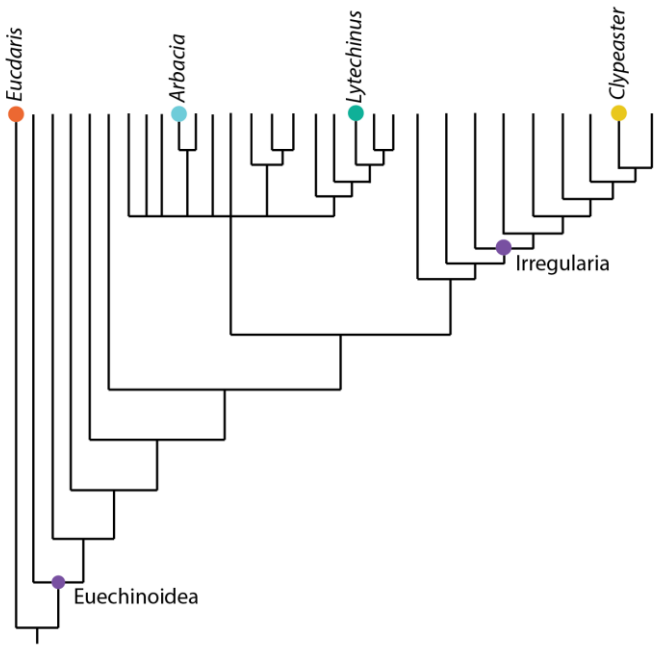

Figure 2.3 Simplified phylogeny of echinoids with the studied genera included in their appropriate relationships on the tree. The node for Euechinoidea is included to demonstrate that *Eucidaris* is a part of Cidaroidea and therefore has a sister taxa relationship to the rest of the studied species. The node for Irregularia is included as well indicating that *Clypeaster* is a more derived echinoid.

Three of these species, *L. variegatus*, *E. tribuloides,* and *A. punctulata*, are epifaunal and feed mainly on algae. By contrast, *C. chesheri* is epifaunal to partly embedded into the sediment and feeds on detritus. *C. chesheri* was used to represent irregular echinoids rather than consistently or deeply infaunal groups to avoid complications that may be associated with pore water fluids, which may differ in composition from overlying seawater (Smrzka et al., 2019).

Dissection and removal of organic matter

Specimens were dissected to separate skeletal elements for analysis of discrete plates from different regions of the echinoid skeleton. The methods for this process differed between the regular and irregular echinoids because specimens of *C. chesheri* are flat compared to the subspherical tests of the regular echinoids and have much thinner skeletal elements that were easily damaged in initial dissection methods.

Regular echinoids were dissected and organic material removed from the skeleton. Spine samples from the oral surface, aboral surface, and from the ambitus (peripheral edge) of the test were removed by hand and collected for analysis. Remaining large spines were removed with suture scissors to make dissection easier. Small spines (such as those found on *L. variegatus* and *A. punctulata*) were removed as needed for analysis and all others were left on the test from which they rapidly disarticulated during organic material removal. After spine removal, suture scissors were inserted into the anus and were used to cut halfway down the echinoid test. At the ambitus of the echinoid, the dissection scissors were used to separate the echinoid oral and aboral halves. After the

echinoid was in two halves, large pieces of organic tissue were removed using a scalpel. The goal of this process was to leave both hemispheres intact before being separately cleaned and disarticulated. In some instances, a scalpel was used to dissect the muscular tissues attaching the lantern to the test, allowing intact removal of the Aristotle's Lantern. The lantern was left articulated until the cleaning and disarticulation process.

The oral and aboral hemispheres and Aristotle's Lantern were placed in separate containers and soaked in 30% reagent grade hydrogen peroxide for 48 hours. This removed the remaining organic material and allowed the skeletal elements of the ambulacral and interambulacral columns to easily separate along suture boundaries. Those that remained intact were able to be broken along suture boundaries manually or with the assistance of a scalpel. The Aristotle's lantern was fully disarticulated after 48 hours and morphologically distinct skeletal elements were separated by type.

The irregular echinoid specimens were soaked in 30% reagent grade hydrogen peroxide for 24–36 hours prior to dissection to remove organic matter and make disarticulation of individual skeletal elements easier. A scalpel was used to make incisions along plate sutures to remove desired skeletal elements from the test. Collecting individual spines was not possible because of their small size (~0.4–2mm long). Lantern elements (dipyramids and teeth) disarticulated during the hydrogen peroxide soak and were easily removed either by hand or with tweezers as needed.

ICP-MS

Organic free samples were then prepared for ICP-MS analysis. Samples were weighed and digested using 2% trace metal grade HNO_3 mixed with an internal standard

prepared by Inorganic Ventures. Samples were agitated on a shaker plate for approximately 30 seconds, then samples were left overnight to assure complete digestion. Samples were then measured for Ca, Mg, Sr, Mn, Fe, V, Cr, Cu, Zn, Rb, Mo, Ba, Pb on an Agilent 7700 Quadrupole ICP-MS. Error is within ± 5% for all elements.

Data Analysis

To test for phylogenetic signal and growth rate significance in the resulting dataset, Analysis of Similarities (ANOSIM) and t-Tests were performed. ANOSIM was conducted on both the complete data set organized by genus and on just the lantern skeletal elements from all included species. t-Tests were conducted on each species to test significance between spines and all other skeletal elements.

Results

A total of 117 elemental measurements were made on discrete ossicles from 12 individuals representing four genera. These data are summarized in Table 2.2, for full data and detection limits, see Appendices 1 and 2 at the end of full text. Of the minor and trace elements that were analyzed, only major and minor elements Mg, Sr, Mn, and Fe were able to be compared among all four taxa. Strontium incorporation ranges from 0.3–0.2 wt% (Figure 2.4). All included species, except *L. variegatus* have a Sr range of approximately 1,000 ppm, while *L. variegatus* has a Sr range of approximately 1,500 ppm. Magnesium incorporation ranges from 1.0–4.5 weight % (4.35–18.9 mol%) in the four included species (Figure 2.5). *C. chesheri* and *A. punctulata* have restricted ranges of Mg incorporation, ranging from 2.5–4.0 weight % and 1.0–2.5 weight % respectively. In contrast, *L. variegatus* and *E. tribuloides* exhibit large ranges in Mg incorporation across

Table 2.2 Summary of major and minor trace metals in modern echinoid specimens.

		Average Composition (ppm)					
Specimen	**n**	**Mg**	**Sr**	**Fe**	**Mn**	**Ba**	**Zn**
E. tribuloides							
Tooth	3	30501	2564	10	18	19	2492
Rotula	3	34379	2328	11	18	25	78
Epiphysis	3	37904	2582	9	14	12	3
Dipyramid	3	41565	2726	13	23	13	149
Ambulacra	6	36085	2524	4	14	9	33
Interambulacra	6	33083	2646	4	15	12	44
Spines	8	14100	2363	2	18	13	74
A. punctulata							
Tooth	2	23773	1989	16	17	556	408
Rotula	2	22496	2295	13	19	1026	402
Epiphysis	2	24325	2398	13	15	323	280
Dipyramid	2	19840	2355	16	27	613	266
Ambulacra	4	22159	2295	7	13	217	116
Interambulacra	4	20631	2440	7	14	60	75
Spines	6	12902	2077	3	21	438	232
L. variegatus							
Tooth	4	28277	2601	9	8	29	19
Rotula	4	27185	2899	7	7	12	3
Epiphysis	4	30340	2804	11	7	13	6
Dipyramid	4	29169	3180	7	7	16	6
Ambulacra	8	32466	2934	4	8	10	6
Interambulacra	8	29870	3021	5	7	11	6
Spines	16	19174	2508	1	8	1	2
C. chesheri							
Tooth	3	34057	2593	35	11	8	ND
Dipyramid	3	25982	2513	65	13	13	ND
Ambulacra	6	28923	2401	32	15	3	ND
Interambulacra	6	29602	2445	25	16	3	ND

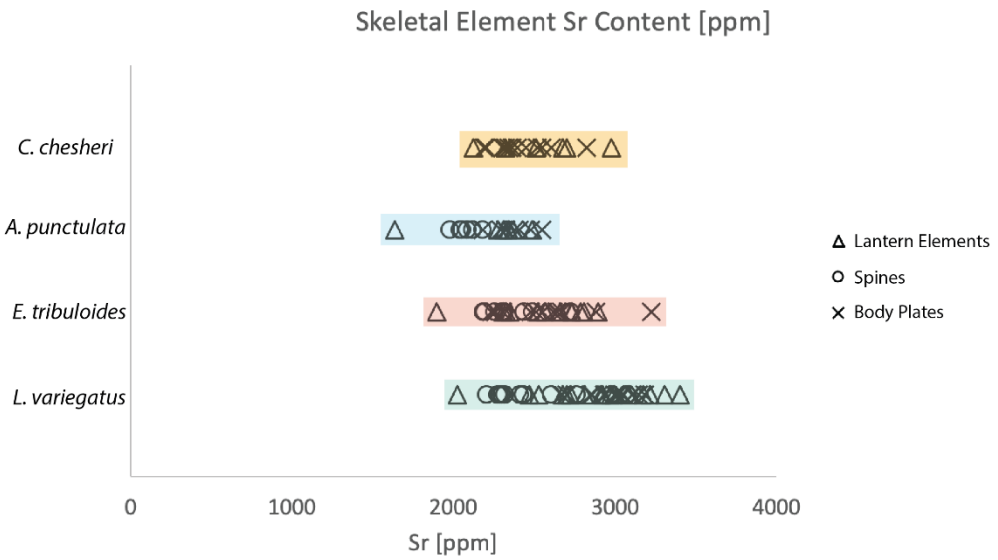

Figure 2.4 Strontium incorporation in the four genera organized by skeletal element type. The range of incorporated Sr is relatively narrow for all the genera and there is no separation of specific skeletal elements based on Sr incorporation.

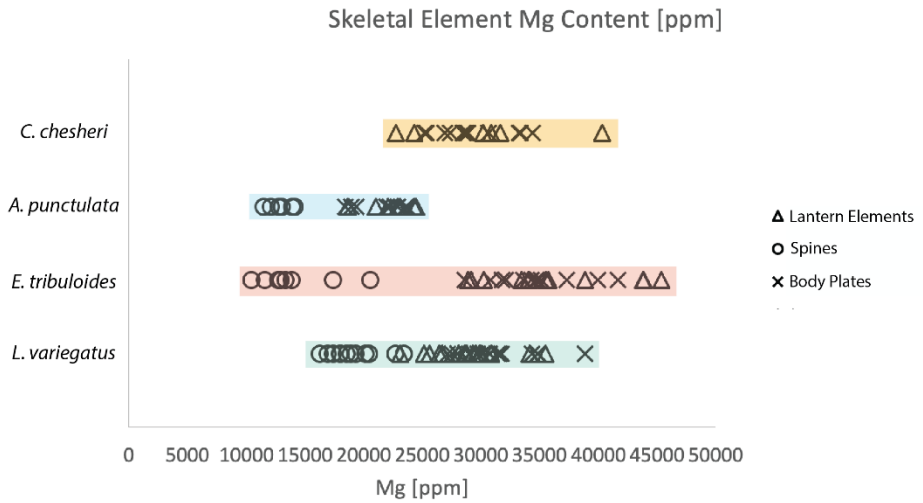

Figure 2.5 Magnesium incorporation in the four genera organized by skeletal element type. The range of incorporated Mg is wider than that of Sr and does separate the four genera. Additionally, spines all have less Mg incorporated than the other skeletal elements.

the examined skeletal elements. This leads to the four genera appearing distinct when visualized graphically (Figures 2.4 and 2.5).

Statistical Significance

Graphical recognition of potentially distinct elemental compositions among the four included species and the hypothesis of skeletal element growth rate playing a role in skeletal element composition, ANOSIM and t-Tests were completed to test for statistical significance. ANOSIM is a non-parametric significance test to assess differences between two or more groups based on a distance measure (Clarke, 1983). Testing of data grouped by genus and skeletal elements returns R values of $R = 0.217$ and $R = 0.297$ respectively. These R values indicate that the data are too similar to be separated based on genus or skeletal element type. Code for ANOSIM testing can be found in Appendix 3.

t-Tests were completed to test for significant compositional differences between spines and all other skeletal elements for each examined species. With respect to Mg, $p = 7.22 \times 10^{-11}$ and the spines are statistically different than the other skeletal elements. Strontium $p = 0.001$, indicating again that the spines are statistically different than the other skeletal elements.

Iron and manganese were recorded in almost every skeletal element of the four genera examined, albeit in low amounts (Figure 2.6). Iron was incorporated between 10–20 ppm in *E. tribuloides*, *A. punctulata* and *C. chesheri*, while it was present in much lower concentrations (<10 ppm) in all skeletal elements of *L. variegatus*. Manganese was incorporated at low levels (0–20 ppm) in all skeletal elements of *L. variegatus*,

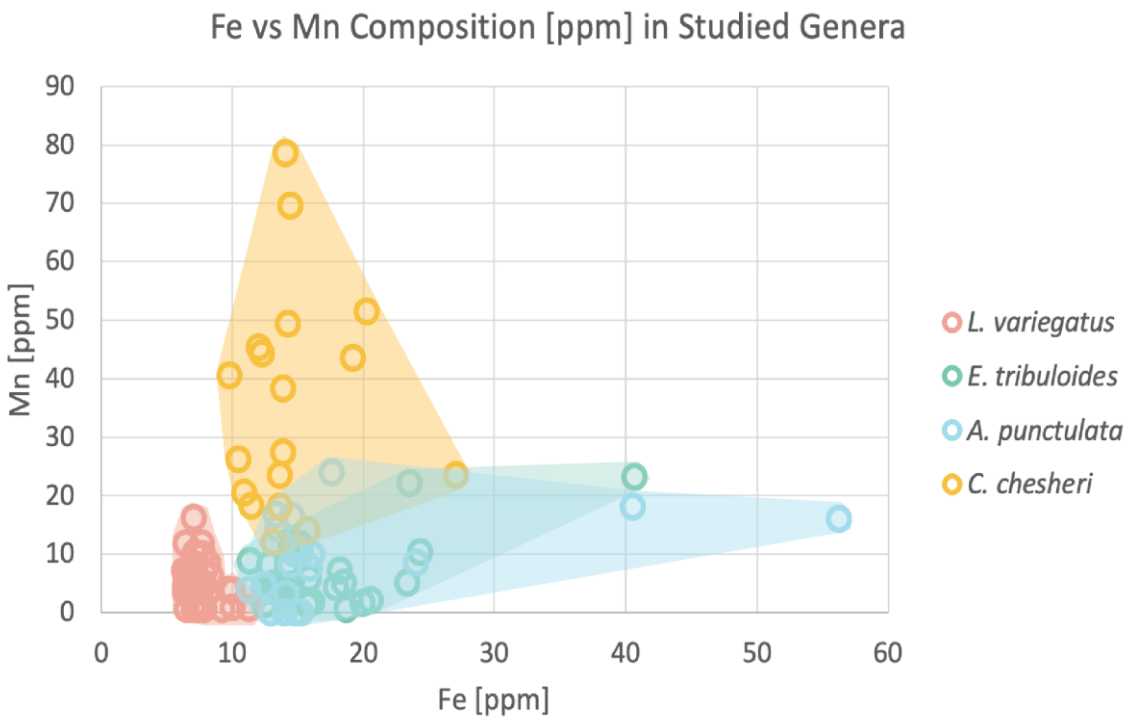

Figure 2.6 Iron and manganese incorporation in the four genera of modern echinoid. All regular echinoids (*L. variegatus*, *A. punctulata*, and *E. tribuloides*) have minor amounts of Mn and Fe incorporated in their skeletal elements. The irregular echinoid *C. chesheri* has greater amounts of Mn incorporated than the other echinoids. *C. chesheri* is a semi-infaunal species; elevated Mn is interpreted to result from greater interaction with pore fluids potentially enriched in Mn.

E. tribuloides, and *A. punctulata*. However, it was incorporated at higher concentrations (20–50 ppm) in all skeletal elements of *C. chesheri.*

Discussion

Results of this study demonstrate variability in major and minor trace element composition among different species, among individuals of the same species, and among the type of skeletal element analyzed. These findings broadly agree with previous investigations of trace metals in other classes of echinoderms, as well as in different echinoids species (Weber, 1969; Kołbuk et al., 2019; Iglikowska et al., 2020); direct comparison with other species, however, remains challenging because of studies using different species, different classes of echinoderms, or echinoderms from drastically different environmental conditions, i.e., arctic waters. We had initially hypothesized that skeletal element growth rates would influence major and minor element incorporation such that spines and teeth would have distinctly different compositions from body plates and other Aristotle's Lantern skeletal elements. The geochemical data and t-tests both demonstrate this original hypothesis is half-supported, spines do have distinct geochemical compositions compared to other skeletal elements, however, the relationship between teeth and incorporation rate is not readily apparent. Our data suggest that growth rate does affect major and minor element incorporation, though the relationship is not as straightforward as was originally hypothesized by authors or previous work (Weber, 1969). Additionally, we hypothesized that there is a phylogenetic signal within major and minor element incorporation. The geochemical data and ANOSIM analyses suggest that there is too much compositional overlap among the included species to determine

compositional differences by species. Discrepancies between this study and previous work likely results from several factors, including: environmental conditions, growth rate and mineralization pathways, as well as relationships among the studied species and are explored below.

Environmental Conditions

This study utilized epifaunal regular echinoids as well as a mostly epifaunal irregular echinoid from a well constrained study area to minimize the need to explore pore fluid chemistry and changes in seawater conditions. Temperature in the Gulf of Mexico ranges from 14–18°C (NOAA). The SEAMAP cruises that collected the specimens used in this study recorded temperature averages of 25.9°C (June 2018), 27.1°C (October 2018), and 25.5°C (June 2019). Salinity averaged between 36.0 and 36.2 on the same cruises (SEAMAP). pH data were not collected by SEAMAP at any of the stages of these three cruises, however, the average pH of the Gulf of Mexico is 8–8.1.

Previous work has suggested that Mg incorporation into echinoderm calcite is dependent on temperature of the surrounding water (Weber, 1969; Burton and Walker, 1991; Carpenter and Lohmann, 1992; Hermans et al., 2010; Kołbuk et al., 2019). This is a function of mineralization thermodynamics and the ability for Mg to substitute for Ca within the calcite crystal lattice (Hermans et al., 2010). Strontium incorporation into calcite is also commonly affected by temperature, crystallization rate, and salinity (Carpenter and Lohmann, 1992; Hermans et al., 2010). In this study, however, the variation across these well-mixed environments is unlikely to play a significant role in influencing Sr geochemistry. We tested the hypothesis that crystallization rate plays a

role in Sr incorporation, but the overlap in Sr incorporation (Figure 2.5), had a narrow range 0.15-0.35 weight %, and showed no significant separation among ossicles suggesting that echinoid growth rate is not a factor.

Iron and manganese incorporation was expected to be low because Fe^{3+} and Mn^{3+} are not soluble in oxygenated seawater (Tribovillard et al., 2006; Smrzka et al., 2019). This supposition held true for *L. variegatus, E. tribuloides,* and *A. punctulata*; ossicles from these three genera show only minor incorporation of Fe and Mn. By contrast, *C. chesheri* has minor amounts of Fe incorporated into its skeletal elements, but has a substantially larger amount of Mn incorporated into its ossicles. The major difference between *C. chesheri* and the other studied species is that *C. chesheri* is partially infaunal (Serafy, 1975). We hypothesize that enhanced Mn incorporation may reflect interaction with pore fluids during infaunal growth. Microbial activity at the oxic-anoxic interface reduces manganese to Mn^{2+}, which is then soluble in seawater and can diffuse across the sediment-water interface (Tribovillard et al., 2006). Additionally, in the top 20 cm of sediment (where we would expect to find *C. chesheri)* Mn^{2+} is more common than Fe^{2+} (James et al., 2021). Although there is a paucity of research into whether Mn and Fe are biologically favored during mineralization of irregular echinoid skeletal elements, results here indicate the potential importance of local environment. Future work will include: 1) examining more specimens of *C. chesheri* from different locations in the Gulf of Mexico to determine if this pattern holds in other localities while holding temperature and salinity relatively constant, 2) looking at other species of *Clypeaster* that exhibit similar hybrid epifaunal/infaunal lifestyles to determine if this characteristic Mn and Fe incorporation is

a feature of *Clypeaster* or unique to *C. chesheri*, and 3) looking at other irregular echinoids that are exclusively infaunal to test the hypothesis that infaunal species have even larger amounts of incorporated Mn and Fe because of pore water chemistry.

Skeletal Element Growth Rate

Mineralization rate of the different skeletal elements has long been hypothesized to play a role in the incorporation of minor and trace elements into the skeleton (Weber, 1969; 1973; Carpenter and Lohmann, 1992). Weber (1969) suggested there should be the highest Mg incorporation within the epiphyses, followed by dipyramids, test, and rotulae, with the least amount of Mg in the teeth and spines. Experimental evidence suggests spines mineralize the fastest (~106–183µm per day) (Gorzelak et al, 2017), teeth mineralize at a rate of ~10µm per day (Gorzelak et al., 2017; Albéric et al., 2019), and body plates grow the slowest at ~1.9–2.1 µm per day (Johnson et al., 2013). It is clear in our dataset that spines have the least amount of Mg incorporation (Figure 2.5), however, the lantern elements (the tooth in particular) are not separated by Mg incorporation and test plates have Mg concentrations that overlap with the lantern elements (Figure 2.5). The separation of spines based on Mg incorporation is statistically significant in each species according to t-tests ($p < 0.005$). Sr incorporation is affected by incorporation of Mg in the skeletal element and is affected by crystallization rate (Carpenter and Lohmann, 1992; Hermans et al., 2010). Unlike Mg, Sr incorporation by skeletal element isn't as graphically distinct, however, spines reflect statistically significant Sr incorporation according to t-tests ($p < 0.005$).

The different methods of mineralization known to occur between different ossicles of the same individuals may also affect the inclusion of major and minor elements into the echinoid skeleton. Incorporation of Mg and Sr in calcite is affected by pH, temperature, salinity and precipitation rate (Carpenter and Lohmann, 1992). Additionally, D_{Sr} increases with increased precipitation rate and the amount of incorporated Mg (Lorens, 1981; Mucci, 1986; Carpenter and Lohmann, 1992). In echinoids that live in tropical to subtropical environments, temperature has less of an effect on Mg and Sr distribution coefficients, however, precipitation rate (in this case, a proxy for growth rate) does affect the Sr distribution coefficient (Carpenter and Lohmann, 1992).

Documenting the effect of growth rate on the rate of inclusion of major and minor metals into the echinoderm calcite lattice and growth rate has been challenging. In particular, a faster growth rate is assumed to be less discriminatory with respect to what ions are included in the lattice (Hermans et al., 2010) suggesting a positive correlation with metal incorporation and growth rate. However, this relationship with growth rate is hard to quantify as each study focuses on different echinoid species (or other classes of echinoderms) (Weber, 1969, 1973; Hermans et al., 2010; Iglikowska et al., 2020) and Mg weight % varies among studied echinoids and even within the same individual (Weber, 1969, 1973.) In our dataset, spines, which are inferred to have the most rapid growth rate of the skeletal elements based on other experiments (Gorzelak et al., 2013), have lower to equivalent concentrations of minor element incorporation when compared to other ossicles on the same individual.

The results of our study somewhat support our initial hypothesis that growth rate of skeletal elements plays a role in metal incorporation in that spines have a statistically significant compositional difference compared to other skeletal elements. However, as only spines were able to be compositionally separated, the affect growth rate has on metal incorporation in other skeletal elements is not as straight forward as initially hypothesized. Additionally, it is also difficult to compare the results of this study with previous work as some researchers use lab grown echinoids (Hermans et al., 2010; Kołbuk et al., 2019) versus wild caught echinoids (this study, Weber, 1969; 1973; Iglikowska et al., 2020). The differences in wild caught versus lab raised individuals are numerous because of the ability to control variables for lab individuals (Hermans et al., 2010; pers. communication with P. Gorzelak).

Effect of Mineralization Pathways

It has been well-documented that these skeletal elements do not all mineralize in the same manner (Livingston et al., 1991; Ma et al., 2007; Gilbert and Wilt, 2011; Alberic et al., 2019; Gorzelak, 2020). Spines are the only ossicles that show a consistent geochemical distinction from the other ossicles in every genus examined (Figures 2.4 and 2.5). This compositional distinction mostly results from lower concentrations of Mg present in the spines, however, across all examined elements, spines have equal to or lower concentrations than the rest of the skeletal elements. The compositional differences seen in spines is consistent with the idea that continuous presence of ACC for regeneration and spine growth may slow or prevent the inclusion of other metals into the calcite crystal lattice (Alberic et al., 2019; Gorzelak, 2020).

In contrast, the tooth most often plots with non-spine ossicles (Figure 2.5). Like spines, teeth also contain reserves of ACC within the skeletal structure, however, the microstructure of teeth is very different from that of spines and body plates (Ma et al., 2007). Additionally, the tooth core is known to be high in Mg (28-29% $MgCO_3$) even though the rest of the tooth structure has Mg levels that are similar to that of the rest of the skeletal elements (Lowenstam and Weiner, 1989). This again highlights that the two fastest growing skeletal elements (Gorzelak et al., 2013) that were hypothesized to have similar compositions based on growth rate, are not incorporating metals in the same way. As previously discussed, the presence of ACC in both the teeth and spines may be slowing or preventing the inclusion of other metals in these skeletal elements (Albéric et al., 2019; Gorzelak, 2020). It is also possible that the GRN responsible for tooth growth allows more Mg incorporation into the tooth crystal lattice for added strength, however, future analyses of echinoid skeletal element strength are needed to test this hypothesis.

It is important to remember that mineralization pathways are controlled by a combination of genes and proteins present in the organism and the source ions present in the environment. However, it has proved difficult to determine the exact roles that each of the genes and proteins play in mineralization as they differ genus to genus (Livingston et al., 1991; Khor and Ettensohn, 2017; Thompson, 2021). More work needs to be done examining the role of specific genes, transcription factors, and proteins on biomineralization, and where and when these are expressed in echinoid development. Because little is understood about Mg pathways in echinoderm mineralization (Hermans et al., 2010), studies should be done examining how Mg is utilized in the mineralization

process of both larval and juvenile stage echinoderms and how that differs in skeletal elements. Additionally, more work needs to be done examining the role Mg plays in strengthening skeletal elements. Previous work has measured the strength of skeletal elements (Weber et al., 1969; Su et al., 2000) and commented that the skeletal elements are remarkably strong given their porosity. This area of research may shed light on the incorporation of Mg within the echinoid tooth.

Phylogenetic Relationships

Finally, we test whether elemental incorporation is congruent with echinoid phylogenetic relationships. Most of the prior work done examining trace metal incorporation and Mg/Ca ratios in echinoderms has been conducted on either several classes of echinoderms (Iglikowska et al., 2020) or a single, specific species (Asnaghi et al., 2014; Kołbuk et al., 2019) In this study, we included a range of species from the same general location (Figure 2.3) to better understand major and minor element incorporation from a cross section of echinoids phylogeny. The inclusion of *E. tribuloides* (Cidaroidea) captures a sister taxon relationship to Euechinoidea which encompasses the remaining three genera that were included in the study. Cidaroid echinoids have both morphological and physiological characteristics that differentiate them from Euechinoids (Collard et al., 2014; Kołbuk et al., 2019); specifically, they have been demonstrated to be able to buffer the pH of their coelomic fluid in a different manner than Euechinoids (Collard et al., 2014; Dery et al., 2014). Euechinoids use both bicarbonate and non-bicarbonate buffers to alter the pH of their coelomic fluid while cidaroids coelomic fluid has a buffering capacity similar to seawater (Collard et al., 2014). These differences in buffering capacity

and therefore coelomic fluid pH Cidaroids is currently attributed differences in gas exchange and skeletal permeability between cidaroids and euechinoids (Collard et al., 2014).

However, in this study, there is considerable overlap in the skeletal element composition between *E. tribuloides* (cidaroid) and *L. variegatus* (euechinoid). When comparing the compositions of skeletal elements, particularly with respect to Mg incorporation, there are different ranges of composition that graphically separate the included genera (Figures 2.4 and 2.5). However, ANOSIM analysis demonstrates that there is enough overlap among the genera that signal from ossicle composition does not clearly discriminate between genera in the study.

The relationship between genus and major and minor element incorporation is currently difficult to determine, namely because the mineralization process in all echinoderms is challenging to elucidate. More work needs to be done examining the role of proteins in the echinoderm mineralization process as well as the role pH differences in coelomic fluid may play in metal incorporation. The first step to determining the role of these factors is including more genera in studies like this one to solidify the differences between cidaroids and euechinoids as well as among the different taxonomic groups within euechinoidea.

Conclusions

The major and minor element composition of echinoid skeletal elements is affected by environment, mineralization physiology, and phylogenetics. The temperature of the Gulf of Mexico does exhibit variability, however, the source regions for specimens in this

study does not vary significantly and Mg incorporation does not change significantly at temperatures over 24°C (Carpenter and Lohmann, 1992; Hermans et al., 2010; Kołbuk et al., 2019). Therefore, it seems likely that there is no significant difference in incorporation rate in the included specimens' ossicles based on temperature. The hypothesis that growth rates of the different ossicles impact the composition is not supported by this dataset, as only spines consistently have different compositions, and that is only seen in Mg incorporation which is counter to expectations of growth rate. On the other hand, mineralization physiology seems to account for observed compositional variation. The role of genetic signaling is seen in the compositional differences between spines and the rest of the skeletal elements that were examined and these differences by genera are weakly supported by this dataset. However, further examination of these species with an extended dataset could change this finding.

While the data do not support the initial hypothesis that genera would have distinct and diagnosable minor and trace element compositions, this study highlights the complexities of using wild caught specimens and future work to be done. In the future, a comparison study should be conducted examining trends in wild caught genera against the same genera raised in a lab setting. This will allow direct comparison of the results rather than applying data from different genera raised in labs to wild caught specimens. In addition, tagging experiments (such as the introduction of a high concentration of a specific element like Mn or an isotope of Mg to seawater in which organisms are grown) should be conducted to examine growth rates and the inclusion of minor and trace elements in the various skeletal elements. These kinds of experiments are typically

conducted on spines alone because of their fast growth rate, however, the mineralization pathway that spines follow is not consistent across the animal. There is also the assumption that a faster growth rate leads to less discrimination in ion inclusion in skeletal elements (Weber, 1969; Hermans et al., 2010) that has not been rigorously tested and does not appear to be necessarily true with this dataset.

The minor and trace element composition of echinoid ossicles remains a challenge to elucidate and characterize. The variation in composition likely results from several factors including environmental conditions and the mineralization pathways utilized by any particular genus. Variation recorded in individuals of the same genus and species is likely location and diet dependent as the variation is still within a range of other individuals. The vital effect in echinoderms (Weiner and Dove, 2013) is not to be discounted as this could be a source of the variation as well. However, as more research is done, this vital effect may be able to be quantified. Additional work needs to be done in this area though, as baseline characterization of major and minor trace element incorporation in ossicles will be important moving forward to understand the impact of human impact on our oceans including climate change and warming oceans.

ACKNOWLEDGEMENTS

We are grateful to Julie Bartley and Jeff La Frenierre at Gustavus Adolphus College for the use of lab space and materials, ICP-MS facilities, and assistance in collecting the geochemical data for this study. We would like to thank Janessa Fletcher and the collections teams at SEAMAP and the Florida Biodiversity Collections for the donation

of echinoids. This work was supported by grants awarded to MRL from The Geological Society of America and the University of Tennessee Graduate Student Senate.

REFERENCES

Alberic, M., Stifler, C.A., Zou, A., Sun, C., Killian, C.E., Valencia, S., Mawass, M., Bertinetti, L., Gilbert, P.U.P.A., Politi, Y., 2019, Growth and regrowth of adult sea urchin spines involve hydrated and anhydrous amorphous calcium carbonate precursors. Journal of Structural Biology: X, **1**, 1–9.

Asnaghi, V., Mangialajo, L., Gattuso, J.P., Francour, P., Privitera, D., Chiantore, M., 2014, Effects of ocean acidification and diet on thickness and carbonate elemental composition oof the test of juvenile sea urchins. Marine Environmental Research, **93**, 78–84.

Borremans, C., Hermans, J., Baillon, S., André L., Dubois, P., 2009, Salinity effects on the Mg/Ca and Sr/Ca in starfish skeletons and the echinoderm relevance for paleoenvironmental reconstructions. Geology, **37** (4) 351–354.

Bottjer, D.J., 2017, Geobiology and palaeogenomics. Earth-Science Reviews, **164**, 182–192.

Burton, E.A., and Walter, L.M., 1987. Relative precipitation rates of aragonite and Mg calcite from seawater: Temperature or carbonate ion control? Geology, **15**, 111–114.

Carpenter, S.J. and Lohmann, K.C., 1992, Sr/Mg ratios of modern marine calcite: Empirical indicators of ocean chemistry and precipitation rate. Geochimica et Cosmochimica Acta, **56**, 1837–1849.

Collard, M., Dery, A., Dehairs, F., Dubois, P., 2014, Euechinoidea and Cidaroiodea respond differently to ocean acidification. Comparative Biochemistry and Physiology, Part A, **174**, 45–55.

Dery, A., Guibourt, V., Catarino, A.I., Compere, P., Dubois, P., 2014, Properties, morphogenesis, and effect of acidification on spines of the cidaroid sea urchin *Phyllacanthus imperialis*. Invertebrate Biology, **133**, 188–199.

Durham, J.W., Fell, H.B., Fischer, A.G., Kier, P.M., Melville, R.V., Pawson, D.L., Wager, C.D., 1966. Echinoidea. *In* Moore, R.C. (ed.) *Treatise on Invertebrate Paleontology, Part U, Echinodermata 3*. Geological Society of America & University of Kansas Press, U211–640.

Gilbert, P.U.P.A. and Wilt, F.H., 2011, Molecular aspects of biomineralization of the echinoderm endoskeleton. *In* Müller, W.E.G. (ed.) *Molecular Biomineralization*. Progress in Molecular and Subcellular Biology **52**, 199–223.

Gorzelak, P., Stolarski, J., Dery, A., Dubois, P., Escrig, S., Meibom, A., 2014, Ultrascale and microscale growth dynamics of the cidaroid spine of *Phyllacanthus imperialis* revealed by ^{26}Mg labeling and NanoSIMS isotopic imaging. Journal of Morphology, **275**, 788–796.

Gorzelak, P., Dery, A., Dubois, P., Stolarski, J., 2017, Sea urchin growth dynamics at microstructural length scale revealed by Mn-labeling and cathodoluminescence imaging. Frontiers in Zoology, **14**, 1–17.

Gorzelak, P., 2020, Functional micromorphology of the echinoderm skeleton. *In* Sumrall, C.D., (ed.) *Elements of Paleontology*, 1–44.

Hermans, J., Borremans, C., Willenz, P., André, L., Dubois, P., 2010, Temperature, salinity and growth rate dependences of Mg/Ca and Sr/Ca ratios of the skeleton of the sea urchin *Paracentrotus lividus* (Lamarck): an experimental approach. Marine Biology, **157**, 1293–1300.

Iglikowska, A., Humphreys-Williams, E., Przytarska, J., Chełchowski, M., Kukliński, P., 2020, Minor and trace elements in skeletons of Arctic echinoderms. Marine Pollution Bulletin, **158**, 1–12.

James, D.H., Bradbury, H.J., Antler, G., Steiner, Z., Hutchings, A.M., Sun, X., Saar, R., Greaves, M., Turchyn, A.V., 2021, Assessing sedimentary boundary layers calcium carbonate precipitation and dissolution using the calcium isotopic composition of pore fluids. Frontiers in Earth Science, **9**, 1–16.

Johnson, A.S., Salyers, J.M., Alcorn, N.J., Ellers, O., Allen, J.D., 2013, Externally visible fluorochrome marks and allometries of growing sea urchins. Invertebrate Biology, **113**, 251–269.

Khor, J.M. and Ettensohn, C.A., 2020, Transcription factors of the Alx family: Evolutionarily conserved regulators of deuterostome skeletogenesis. Frontiers in Genetics, **11**, 1–15.

Killian, C.E., and Wilt, F.H., 2008, Molecular aspects of biomineralization of the echinoderm endoskeleton. Chemical Reviews, **108**, 4463–4474.

Kołbuk, D., Dubois, P., Stolarski, J., Gorzelak, P., 2019, Effects of seawater chemistry (Mg^{2+}/Ca^{2+} ratio) and diet on the skeletal Mg/Ca ratio in the common sea urchin *Paracentrotus lividus*. Marine Environmental Research, **145**, 22–26.

Kroh, A., and Smith, A.B., 2010, The phylogeny and classification of post-Palaeozoic echinoids. Journal of Systematic Palaeontology, **8** (2), 147–212.

Lawrence, J.M., and Jangoux, M., 2013, Cidaroids. *In* J.M. Lawrence (ed.) Sea Urchins: Biology and Ecology, 225–242.

Livingston, B., Shaw, R., Bailey, A., Wilt, F., 1991, Characterization of a cDNA encoding protein involved in formation of the skeleton during development of the sea urchin *Lytechinus pictus*. Developmental Biology, **148**, 473–480.

Lorens, R.B., 1981, Sr, Cd, Mn, and Co distribution coefficients in calcite as a function of calcite precipitation rate. Geochimica et Cosmochimica Acta, **45**, 553–561.

Lowenstam, H.A. and Weiner, S., 1989, Echinodermata. *In* On biomineralization, Oxford University Press on Demand, 123–134.

Ma, Y.R., Weiner, S., Addadi, L., 2007, Mineral deposition and crystal growth in the continuously forming teeth of sea urchins. Advanced Functional Materials, **17**(15), 2693–2700.

Marin, F., Marie, B., Hamada, S.B., Silva, P., LeRoy, N., Guichard, N., Wolf, S., Montgnani, C., Joubert, C., Piquemal, D., Saulnier, D., Gueguen, Y., 2013, "Shellome": Proteins involved in mollusc shell biomineralization—diversity, functions. Recent Advances in Pearl Research, **149**, 1–18.

Mooi, R., and David, B., 1993b, Ontogeny and origin of the brooding system in Antarctic urechinid sea urchins (Echinodermata, Holasteroidea). Zoomorphology, **113**, 69–78.

Mooi, R., David, B., Marchand, D., 1994, Echinoderm skeletal homologies: Classical morphology meets modern phylogenetics. *In* Echinoderms through Time, Balkema, Rotterdam, 87–95.

Morgulis, M., Gildor, T., Roopin, M., Sher, N., Malik, A., Lalzar, M., Dines, M., de-Leon, S.B., Khalaily, L., de-Leon, S.B., 2019, Possible cooption of a VEGF-driven tubulogenesis program for biomineralization in echinoderms. PNAS, **116**(25), 12353–12362.

Morse, J.W. and Bender, M.L., 1990, Partition coefficients in calcite: Examination of factors influencing the validity of experimental results and their application to natural systems. Chemical Geology, **82**, 265–277.

Mucci, A., 1986, Growth kinetics and composition of magnesian calcite overgrowths precipitated from seawater: Quantitative influence of orthophosphate ions. Geochimica et Cosmochimica Acta, **50**, 2255–2265.

Pearse, J.S. and Pearse, V.B., 1975, Growth Zones in the Echinoid Skeleton. American Zoology, **15**, 731–753.

Reich, M., and Smith, A.B., 2009, Origins and biomechanical evolution of teeth in echinoids and their relatives. Palaeontology **52**, 1149–1168.

Serafy, D. K., 1975, A new species of *Clypeaster* from the Gulf and Caribbean and a key to the species in the tropical northwestern Atlantic (Echinodermata: Echinoidea). Biological Results of the University of Miami Deep-Sea Expeditions, **58**, 662–677.

Smith, A.B., 1980. Stereom microstructure of the echinoid test.

Smrzka, D., Zwicker, J., Bach, W., Feng, D., Himmler, T., Chen, D., Peckmann, J., 2019, The behavior of trace elements in seawater, sedimentary pore water, and their incorporation into carbonate minerals: a review. Facies, **2019**, 1–47.

Sodergren, E., Weinstock, G.M., Davidson, E.H., Cameron, R.A., Gibbs, R.A., Angerer, R.C., Angerer, M.I., Wright, R., 2006, The genome of the sea urchin *Strongylocentrotus purpuratus*. Science, **314**(5801), 941–952.

Su, X., Kamat, S., Heuer, A.H., 2000, The structure of sea urchin spines, large biogenic single crystals of calcite. Journal of Materials Science, **35**, 5545–5551.

Thompson, J.R., 2022, Molecular paleobiology of the echinoderm skeleton. *In* Sumrall, C.D. (ed.), Elements of Paleontology, 1–70.

Tribovillard, N., Algeo, T.J., Lyons, T., Riboulleau, A., 2006, Trace metals as paleoredox and paleoproductivity proxies: An update. Chemical geology, **232**, 12–32.

Weber, J.N., 1969, The incorporation of magnesium into the skeletal calcites of echinoderms. American Journal of Science, **267**, 537–566.

Weber, J.N., 1973, Temperature dependence of magnesium in Echinoid and Asteroid skeletal calcite: A reinterpretation of its significance. Journal of Geology, **81**, 543–556.

Weiner, S. and Dove, P.M., 2003, An overview of biomineralization processes and the problem of the vital effect. Reviews in mineralogy and geochemistry, **54**(1), 1–29.

Wood, R. 2018, Exploring the drivers of early biomineralization. Emerging Topics in Life Sciences, **2**, 201–212.

APPENDIX 1

Sample	Genus	24 Mg [He]	43 Ca [He]	55 Mn [He]	56 Fe [He]	88 Sr [He]
171902056AT	Lytechinus	29291.35	361169.92	10.15	7.13	2974.47
171902070BT	Lytechinus	25599.38	366742.43	8.39	8.16	2024.69
171902070CT	Lytechinus	28653.31	362236.27	10.09	7.66	2727.26
171902070AT	Lytechinus	29562.86	361158.49	6.43	8.35	2676.02
171902056AR	Lytechinus	26701.64	364978.07	9.87	7.77	2471.17
171902070BR	Lytechinus	28118.52	362747.48	7.24	6.93	2914.56
171902070CR	Lytechinus	25126.87	366422.22	7.00	7.05	2993.43
171902070AR	Lytechinus	28793.71	361592.06	4.28	6.68	3217.50
171902056AE	Lytechinus	26448.00	365045.82	11.89	6.42	2701.19
171902070BE	Lytechinus	29889.77	360607.24	16.20	7.07	2813.77
171902070CE	Lytechinus	30860.25	359678.20	11.81	7.69	2527.95
171902070AE	Lytechinus	34161.45	354839.94	5.25	7.66	3174.61
171902056AD	Lytechinus	23107.35	369001.96	9.90	7.20	2922.78
171902070BD	Lytechinus	28091.69	362375.61	5.60	6.42	3309.53
171902070CD	Lytechinus	29978.38	360224.54	7.21	6.30	3085.59
171902070AD	Lytechinus	35499.03	352905.78	4.43	6.39	3402.04
171902056ASPM	Lytechinus	17396.93	376664.59	0.58	6.51	2413.95
171902070BSPM	Lytechinus	17963.51	376089.08	0.92	10.04	2277.40
171902070CSPM	Lytechinus	16270.63	378260.08	0.80	11.29	2204.81

171902070ASPM	Lytechinus	22696.34	369393.93	0.73	7.32	3077.97
171902056ASPD	Lytechinus	18045.91	375975.37	0.86	7.13	2301.59
171902070BSPD	Lytechinus	18911.85	374766.33	0.58	7.08	2433.00
171902070CSPD	Lytechinus	20487.94	372923.60	1.13	7.45	2317.95
171902070ASPD	Lytechinus	23408.15	368609.43	0.63	7.89	2976.50
171902056ASPP	Lytechinus	16907.71	377393.37	0.88	7.64	2290.31
171902070BSPP	Lytechinus	20144.64	373233.47	1.17	7.04	2432.22
171902070CSPP	Lytechinus	19297.73	373947.50	0.69	7.26	2765.65
171902070ASPP	Lytechinus	18552.51	375031.14	0.60	9.25	2607.36
171902056AAMD	Lytechinus	27998.21	362703.99	3.48	6.38	3104.99
171902070BAMD	Lytechinus	30106.50	360228.27	3.15	6.58	2933.15
171902070CAMD	Lytechinus	34863.34	354277.06	4.07	6.37	2858.68
171902070AAMD	Lytechinus	34353.68	355112.75	4.00	9.65	2668.82

Sample	**Genus**	**24 Mg [He]**	**43 Ca [He]**	**55 Mn [He]**	**56 Fe [He]**	**88 Sr [He]**
171902056AIAD	Lytechinus	27192.09	363668.18	5.20	6.83	3147.13
171902070BIAD	Lytechinus	29008.86	361696.12	4.04	7.01	2848.62
171902070CIAD	Lytechinus	30759.62	359315.54	4.64	6.53	3015.05
171902070AIAD	Lytechinus	31433.19	358463.26	3.73	8.20	3014.95
171902056AIAP	Lytechinus	27531.11	363286.10	5.25	6.85	3109.10
171902070BIAP	Lytechinus	31569.75	358260.96	3.90	7.67	3042.46
171902070CIAP	Lytechinus	31759.97	358127.47	6.65	6.35	2942.33

171902070AIAP	Lytechinus	29708.62	360601.49	3.54	7.52	3050.78
171902056AAMP	Lytechinus	27996.13	362792.76	4.90	6.98	3019.32
171902070BAMP	Lytechinus	30719.90	359684.37	6.85	7.87	2702.44
171902070CAMP	Lytechinus	34835.79	353972.71	5.02	7.16	3185.78
171902070AAMP	Lytechinus	38858.01	349025.33	3.76	10.03	3000.30
171805033BT	Eucidaris	29154.39	353796.35	22.14	23.50	2311.21
171805033CT	Eucidaris	28881.10	362137.53	3.28	13.74	2571.51
171805014AT	Eucidaris	33468.16	356086.00	5.95	15.85	2809.13
171805033BR	Eucidaris	30229.65	360367.70	10.89	14.95	2351.40
171805033CR	Eucidaris	34055.84	356250.80	10.45	24.32	1896.85
171805014AR	Eucidaris	38851.63	349293.69	12.21	14.43	2734.82
171805033BE	Eucidaris	34068.26	355805.84	8.34	14.15	2326.28
171805033CE	Eucidaris	35774.24	353444.43	8.24	12.78	2523.87
171805014AE	Eucidaris	43868.39	342682.40	11.79	15.15	2896.62
171805033BD	Eucidaris	43794.08	342482.08	7.24	18.19	2730.26
171805033CD	Eucidaris	35538.46	353474.29	8.90	11.36	2790.31
171805014AD	Eucidaris	45363.75	340949.29	23.25	40.68	2658.88
171805033BSPM	Eucidaris	17411.11	375860.49	2.12	20.54	2727.34
171805033CSPM	Eucidaris	12947.09	382253.31	1.35	15.70	2312.68
171805014ASPM	Eucidaris	13321.21	381601.72	1.92	16.11	2492.23
171805033BSPD	Eucidaris	20554.51	372767.35	1.38	12.42	2303.99
171805033CSPD	Eucidaris	13862.26	381245.77	0.71	18.71	2183.84
171805014ASPD	Eucidaris	11557.73	383828.00	2.58	14.11	2436.43
171805033BSPP	Eucidaris	10449.55	385246.05	5.08	23.34	2195.03
171805014ASPP	Eucidaris	12696.77	382605.73	1.74	19.91	2256.39

Sample	Genus	24 Mg [He]	43 Ca [He]	55 Mn [He]	56 Fe [He]	88 Sr [He]
171805033BAMD	Eucidaris	34321.17	355483.22	4.26	13.98	2234.08
171805033CAMD	Eucidaris	34838.45	354656.67	4.27	12.56	2510.52
171805014AAMD	Eucidaris	41676.96	345535.50	4.80	14.55	2881.48
171805033BIAD	Eucidaris	28629.38	362192.23	4.98	13.53	2645.31

171805033CIAD	Eucidaris	31807.07	358691.89	4.37	17.90	2307.21
171805014AIAD	Eucidaris	35134.57	353552.98	2.30	14.11	3224.50
171805033BIAP	Eucidaris	30799.48	359632.06	5.17	13.52	2553.90
171805033CIAP	Eucidaris	32140.84	358108.89	4.68	13.47	2479.54
171805014AIAP	Eucidaris	39985.31	347917.28	5.18	18.50	2667.75
171805033BAMP	Eucidaris	34712.04	354971.06	3.63	13.84	2259.16
171805033CAMP	Eucidaris	37329.50	351371.05	3.77	13.01	2620.98
171805014AAMP	Eucidaris	33629.11	356064.31	4.96	13.11	2638.14
171802073AT	Arbacia	24445.06	367767.67	23.99	17.57	1635.80
171802131AT	Arbacia	23100.43	368265.70	7.69	15.88	2343.11
171802073AR	Arbacia	22061.22	370441.17	16.74	13.31	2275.99
171802131AR	Arbacia	22930.79	367107.35	8.54	23.99	2314.82
171802073AE	Arbacia	24295.20	367839.94	16.49	14.52	2310.55
171802131AE	Arbacia	24354.08	366928.35	9.94	16.08	2485.46
171802073AD	Arbacia	21041.35	371803.72	14.47	13.42	2338.42
171802131AD	Arbacia	18639.40	373436.95	18.11	40.52	2370.67
171802073ASPM	Arbacia	13936.64	380782.19	0.00	14.81	2086.30
171802131ASPM	Arbacia	12120.52	380667.63	16.07	56.27	1979.71
171802073ASPD	Arbacia	13017.31	381781.43	0.00	15.03	2051.70
171802131ASPD	Arbacia	14123.86	381089.38	0.00	13.98	2039.92
171802073ASPP	Arbacia	12753.59	381954.17	0.00	15.23	2181.04
171802131ASPP	Arbacia	11461.50	384289.90	0.00	12.95	2121.35
171802073AAMD	Arbacia	23689.21	368340.93	10.17	15.24	2180.26
171802131AAMD	Arbacia	23575.99	369087.17	4.56	12.41	2295.02
171802073AIAD	Arbacia	18414.49	375148.10	8.22	14.44	2321.56
171802131AIAD	Arbacia	22935.40	369627.93	3.19	14.12	2549.58
171802073AIAP	Arbacia	22223.88	370295.48	11.00	14.88	2479.38
171802131AIAP	Arbacia	18949.74	374736.80	4.89	12.44	2407.50
171802131AAMP	Arbacia	22000.18	370154.16	10.29	14.68	2326.90
171802073AAMP	Arbacia	19370.67	374245.50	3.96	11.28	2378.31
171805029BT	Clypeaster	40305.52	347474.25	44.32	12.23	2675.85
171902100AT	Clypeaster	30212.02	360885.56	40.66	9.75	2125.48

Sample	Genus	24 Mg [He]	43 Ca [He]	55 Mn [He]	56 Fe [He]	88 Sr [He]

171902100BT	Clypeaster	31654.77	358206.68	20.62	10.89	2976.86
171805029BD	Clypeaster	22758.94	369606.93	69.65	14.41	2703.46
171902100AD	Clypeaster	30851.48	359631.74	78.54	14.02	2512.99
171902100BD	Clypeaster	24334.47	368058.60	45.43	12.03	2322.15
171805029BAAM	Clypeaster	28452.08	362921.27	23.56	13.64	2323.42
171902100AAAM	Clypeaster	28911.71	362255.17	51.51	20.27	2363.14
171902100BAAM	Clypeaster	33276.28	356310.82	18.18	13.59	2827.58
171805029BAIA	Clypeaster	25174.83	366889.01	23.60	27.04	2450.42
171902100AAIA	Clypeaster	28713.09	362383.77	27.48	13.85	2518.67
171902100BAIA	Clypeaster	34402.83	355120.64	12.09	13.15	2605.77
171805029BOIA	Clypeaster	28551.01	362920.79	26.31	10.44	2202.12
171902100AOIA	Clypeaster	27405.30	364182.86	49.41	14.26	2340.85
171902100BOIA	Clypeaster	33366.87	356486.96	14.05	15.74	2550.92
171805029BOAM	Clypeaster	26901.42	364875.92	38.40	13.85	2303.55
171902100AOAM	Clypeaster	25338.51	366929.97	43.66	19.20	2190.40
171902100BOAM	Clypeaster	30657.72	360072.93	18.26	11.44	2397.04

APPENDIX 2

ANOSIM R Code

Libraries used:

Vegan

Code:

```
install.packages("vegan")
library(vegan)
lantern <- read.csv("lantern_elements.csv", header=TRUE)
com <- lantern[,4:ncol(lantern)]
lantern_com <-as.matrix(com)
ano <-anosim(lantern_com,lantern$Type, distance="bray", permutations=9999)
summary(ano)
```

CHAPTER III
A COMBINED APPROACH TO CHARACTERIZING THE GEOCHEMICAL COMPOSITION OF FOSSIL ECHINOID SKELETAL ELEMENTS

Abstract

Echinoderms have a long evolutionary history and are abundant in the fossil record as both articulated and disarticulated specimens. This abundance lends them to use in paleobiological studies to address questions on evolution, biogeography, and as geochemical archives to reconstruct physical and chemical ocean conditions throughout the Phanerozoic. This has been attempted by several researchers (Dickson, 2002, 2004; Ries, 2004; Gorzelak et al., 2016) however, the process of diagenesis impacts the preservation of the original geochemical signatures of the echinoderm skeletal elements. In this study, we examine fossil echinoid skeletal elements from the Late Mississippian Glen Dean Formation of southern Kentucky using a combination of petrographic and geochemical techniques to understand how diagenesis impacts the reliability of echinoderms as geochemical proxies. Data indicate a loss in Mg when compared to measurements taken from modern echinoids as well as almost complete infilling of the pores from the original stereom microstructure with abiotic, syntaxial calcite. These changes to the original geochemical signatures and porous stereom seen in life make it challenging for researchers to identify primary versus secondary calcite in echinoids. These results indicate that prior to use as geochemical proxies, echinoderms must undergo petrographic analysis to determine the amount of diagenesis that has occurred and that echinoderms are not commonly reliable reservoirs of original skeletal chemistry. This study highlights significant avenues for future research in understanding microscale diagenesis in echinoderm skeletal elements.

Introduction

As biomineralizing organisms with a long evolutionary history (middle Cambrian to Recent) (Sumrall, 1997), echinoderm skeletal material has been used as a geochemical archive for past ocean physical and chemical conditions throughout the Phanerozoic (Dickson, 1995, 2001b, 2002, 2004; Ries, 2004). These organisms construct their skeleton from hundreds to thousands of individual elements (ossicles) that are characterized by a porous microstructure, known as stereom, and are formed from a single crystal of high-Mg calcite (Weber, 1959; Durham et al., 1967; Smith, 1980). Ossicles are abundant in the fossil record (at times comprising the majority of grains in sedimentary rocks) and are an obvious target for geochemical analysis to determine seawater composition throughout the Phanerozoic. Indeed, previous work establishing Mg/Ca ratios of seawater was done in part utilizing echinoderm skeletal elements (Dickson, 1995, 2001b, 2002, 2004, Ries, 2004). Such work included a combination of traditional optical microscopy, scanning electron microscopy (SEM), electron microprobe analysis (EMPA), and x-ray diffraction (XRD) to determine Mg/Ca (Dickson, 1995, 2001b, 2002, 2004). However, more recent work (Gorzelak et al., 2016), using similar comparative analysis, suggested that there may be considerable preservational variation in fossil echinoderm ossicles that may compromise the potential for reliable geochemical results unless the preservation is pristine. Here we examine the preservation of Mississippian echinoid ossicle stereom microstructure and major and minor elemental composition to test the effects of diagenesis on echinoid geochemistry and the utility of echinoderm skeletal elements as proxies.

Growth of echinoderm skeletal elements

Echinoderms exhibit biologically controlled mineralization in which the template for their skeleton is mediated by proteins and proteinaceous structures that the echinoderm produces as a result of genetics (Marin et al., 2013). Our understanding of this mineralization process has been greatly enhanced by documenting gene regulatory networks (GRNs) that govern crystal initialization and growth. Evolutionary processes acting on these networks result in the expression and timing of different genes that control skeletal development at different taxonomic levels (Bottjer, 2017). Echinoderms have extensive GRNs that are just now beginning to be understood (Kohr and Ettensohn, 2017; Morgulis et al., 2019, Thompson, 2022), although early data suggests variation in these GRNs across echinoderm classes which results in subtle differences seen in the stereom microstructure (i.e., echinoid tooth has a laminated structure rather than porous) as well as the chemical composition of these skeletal elements (as seen in work by Weber, 1969, 1973; Kołbuk et al., 2019; Iglikowska et al., 2020; Limbeck et al., 2022).

The control GRNs have over the mineralization process is readily observed in the variety of structures produced in stereom. Ten different types of stereom that have been observed in echinoderms (see Smith, 1980 for descriptions) and individual skeletal elements can have more than one type of stereom present. The kind of stereom present in specific skeletal elements is also related to structure and function of that specific element. For example, spines grow by producing longitudinal microspines that connect through a series of lateral bridges. The bridges thicken as the spine grows to create wedges that thicken the spine overall, giving the spine a wagon wheel structure in cross section

(Albéric et al., 2019). This structure is the related to spines ability to regenerate quickly after breakage (Gilbert and Wilt, 2011; Gorzelak et al., 2013; Albéric et al., 2019). In contrast, the tooth element of echinoids has the porous stereom that is organized into laminated structures (Lowenstam and Weiner, 1989; Ma et al., 2007, Reich and Smith, 2009). The stereom here is organized into primary plates and needle complexes that overlap to create a T shaped tooth (Ma et al., 2007) that is strong enough to scrape food from rocks while continuously growing from the proximal end as the tip becomes worn.

Growth effects on chemical structure

Differences in GRNs among echinoderms along with variation seen in growth and growth rates of echinoderm skeletal elements also has been shown to affect chemical composition of these elements (Weber, 1969, 1973; Kołbuk et al., 2019; Iglikowska et al., 2020; Limbeck et al., 2022). For example, the tooth and other parts of the echinoid Aristotle's lantern (jaw apparatus) along with the ossicles that make up the corona (test) of the echinoid incorporate more Mg than the spines. These skeletal elements (lantern elements and coronal elements) are also more structurally sound as damage to these parts would likely be deadly to the organism. In contrast, the spines are more Ca-rich than the rest of the skeletal elements. This fast growth rate has been hypothesized to be equated with indiscriminate ion incorporation however, data from modern echinoids do not support this. For example, spines and teeth have similarly rapid growth rates, but different chemical composition. Spines are more Ca- rich and are statistically different compositionally from other skeletal elements while teeth are more Mg-rich, but are not

significantly different compositionally from other lantern elements or body plates. This variation in chemical composition among skeletal elements and within individual skeletal elements can be significant and has been deemed “vital effect” (Weiner and Dove, 2013, Kołbuk et al., 2019, Iglikowska et al., 2020). This variation is important to take into consideration when using echinoderms as chemical proxies.

Diagenetic potential in echinoderms

Pores within the stereom microstructure of echinoderms in life are filled with organic tissues that degrade rapidly after death (Brett et al., 1997). The removal of this tissue after death increases the surface area within the skeletal element making it easier for diagenesis and secondary mineralization to occur. Echinoderms readily demonstrate two diagenetic changes: growth of syntaxial cements and loss of Mg. Syntaxial cement nucleates on the surface of the stereom and continues growing in the same optical orientation as the original calcite of the skeletal element. The syntaxial nature of the cement makes it hard to distinguish between the original calcite of the stereom and the secondary mineralization that has infilled the pores of the stereom (Meyers and Lohmann, 1978; Dickson, 2001b; Gorzelak et al., 2016). Additionally, echinoderms transform from high-Mg calcite to low-Mg calcite in a geologically short time span, 7,000–10,000 years (MacQueen and Ghent, 1970). Where this Mg goes after mobilization within the skeletal element and the rate at which this transition occurs is not well understood, though it is well documented. The susceptibility to diagenetic change is important to consider with echinoderms because skeletal elements may be externally,

optically well preserved but when examined internally with petrographic tools, the skeletal element may be completely diagenetically altered.

Ionic composition of seawater

The major ionic composition of seawater has oscillated throughout Earth's history, leading to periods known as calcite and aragonite seas (Stanley and Hardie, 1998; Lowenstein et al., 2001; Ries, 2004; Stanley 2008; Balthasar and Cusack, 2015). These changes are hypothesized to result from hydrothermal fluids released through basaltic crustal weathering during seafloor spreading and dolomitization (Hardie, 1996; Holland and Zimmerman, 2000). Changes in the major ionic composition of seawater affects the predominant calcite polymorph precipitated in the ocean (Wilkinson et al., 1983) and can impact the predominant biomineral phases (Ries, 2004; Stanley and Hardie 1998; Balthasar and Cusack, 2015; Gorzelak et al., 2016). These cycles of seawater composition are recognized using Mg/Ca ratios measured either form fluid inclusions in evaporites (Lowenstein et al., 2001) or fossil organisms that precipitate in equilibrium with seawater (Dickson, 1995, 2002; Ries, 2004; Gorzelak et al., 2016). It has been determined that the Mg/Ca ratio varies between 1.0–5.2 throughout the Phanerozoic and when the ratio is <2 it is characterized as a calcite sea (calcite is the dominant $CaCO_3$ polymorph) and when the ratio is >2 it is characterized as an aragonite sea (aragonite is the dominant $CaCO_3$ polymorph) (Lowenstein et al., 2001; Balthasar and Cusack, 2015; Gorzelak et al., 2016). These relationships are important because different clades of organisms mineralize different $CaCO_3$ polymorphs that can be impacted by different

ocean chemistries during calcite and aragonite sea conditions. Therefore, biomineralization has the potential to inform current and past seawater chemistry (Weber, 1969; Dickson, 1995; Lowenstein et al., 2001; Gorzelak et al., 2016).

Magnesium incorporation into calcite, however, is also a function of temperature and salinity (Carpenter and Lohmann, 1992) and measurements of this ratio have been used to determine paleo seawater temperatures. Based on literature, this proxy appears to work best with foraminifera examining seawater conditions in the Cenozoic (Eggins et al., 2003; Regenberg et al., 2009) although it has been attempted with varying degrees of success with bivalves (Immenhauser et al., 2003). An important caveat to using Mg/Ca ratios for paleo seawater temperatures is that is its commonly used in conjunction with other proxies such as $\boldsymbol{\delta}^{18}O$ and $\boldsymbol{\delta}^{44}CO_2$ to corroborate the resulting temperatures (Immenhauser et al., 2003; Regenberg et al., 2009). This is because other factors, such as the fossilization process and diagenesis can dramatically influence the amount of Mg that is retained in the fossil skeleton (Al-Aasm and Veizer, 1982; Leutloff and Meyers, 1983). That said, Mg/Ca ratios are of importance to researchers because of their utility in understanding past seawater chemistry and the need to understand how changes in ocean chemistry affect skeletal elements of organisms.

Echinoderm skeletal elements as proxies

As previously stated, echinoderm skeletal elements are abundant in sediments throughout the Phanerozoic making them an obvious choice for proxies (Dickson, 1995, 2002, 2004). However, our understanding of how high-Mg calcite producing organisms

interact with changing Mg/Ca ratios of seawater and how Mg incorporation changes based on the Mg/Ca_{SW} is of concern. Dickson (2002, 2004) calculated Mg/Ca_{SW} using $Mg/Ca_{Echinoid}$ and constant D_{Mg} calculated for 20°C, 25°C, and 30°C. Further experiments were conducted on modern echinoid to elucidate how echinoids incorporate Mg and the effects of different water chemistries reflecting various stages of calcite and aragonite sea conditions (Ries, 2004, 2010). The results of these experiments show differences in Mg incorporation between spines and body plates (the only examined skeletal elements in the experiment) and that the echinoids, when exposed to calcite sea conditions, produce low-Mg calcite rather than high-Mg calcite (Ries, 2004). This would suggest that the physiological controls of the organism's genetics are influenced by seawater chemistry (Ries, 2010). However, it is important to note the variability in skeletal element composition (Weber, 1969, 1973; Kołbuk et al., 2019; Iglikowska et al., 2020) recognized in modern echinoderms can be inferred to have been present in fossil echinoderm skeletal elements as well (Leutloff and Meyers, 1983), which may alter interpretations of Mg/Ca ratios from fossil echinoderms. Here we examine fossil echinoid skeletal elements for their utility as proxies using both petrology and geochemical techniques.

Sample selection

Bulk samples of poorly indurated shale were collected from the Pennyrile Parkway locality of the uppermost Middle Mississippian (Chesterian) Glen Dean Formation in Christian County, southwest Kentucky (Atwood and Sumrall, 2012). Rock

samples were placed in water for the initial disaggregation of the shale and washed by boiling in 3% hydrogen peroxide. The samples were sieved, and specimens of echinoid and other echinoderm ossicles were collected by hand from the processed residues. Echinoid skeletal elements were identified as *Archaeocidaris* and *Lepidesthes*. These echinoid species are unknown in this locality as articulated specimens, however, their skeletal elements are abundant in the sediment. Elements representing ambulacral and interambulacral plates, spines, and elements of the Aristotle's lantern (teeth, rotula, epiphysis, and dipyramid) (Figure 3.1) were identified and collected. Other skeletal elements (remaining parts of the Aristotle's lantern, the apical system) were not collected from the bulk sediment sample because there is little consensus of how to recognize these skeletal elements in Paleozoic taxa.

Echinoids from this locality were selected for this study because they are optically well preserved (minimal secondary mineralization was visible on the outer surface of the stereom) (Figure 3.2) and they were initially preserved in shales which can function as aquicludes and slow the movement of pore waters through the skeletal elements. A combination of SEM, SEM-EDS, and CL was used to assess the diagenetic effects within selected specimens and ICP-MS was used on the remaining specimens to gather bulk composition of major and minor elements in fossilized echinoid skeletal elements. Spar drilled from the internal cavity of a blastoid from the same locality was used as a comparison of inorganic calcite precipitated from diagenetic pore fluids.

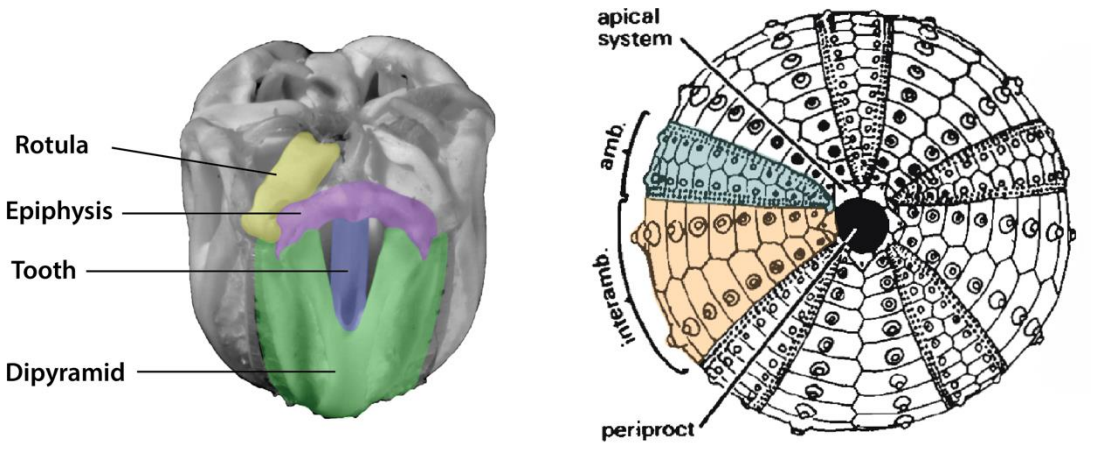

Figure 3.1 Aristotle's lantern and echinoid test with labeled skeletal elements. Left is the Aristotle's lantern, and all pieces were analyzed in this study. Right is the echinoid test and ossicles form the interambulacral and ambulacral columns were analyzed.

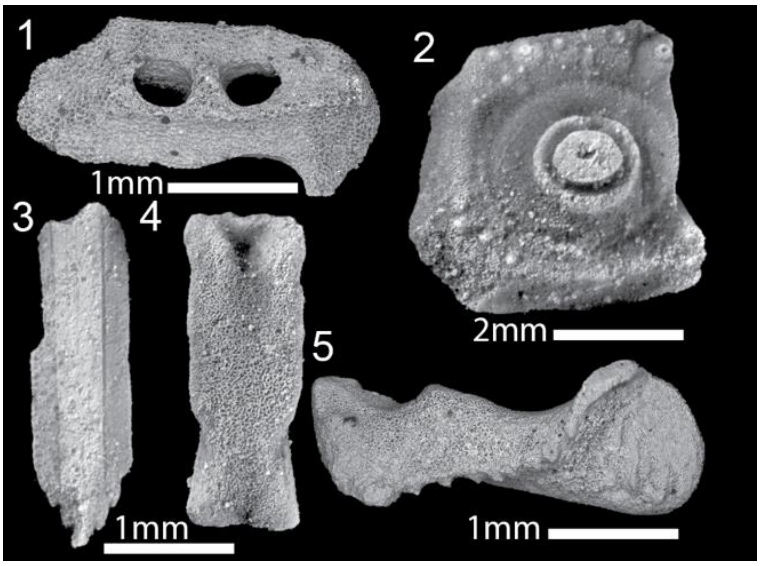

Figure 3.2 SEM images of fossil echinoid skeletal elements. 1 and 2 are *Archaeocidaris* interambulacral and ambulacral plates respectively. 3-5 are elements of the Aristotle's lantern that make up the jaw apparatus. Genus-level designation is not currently possible for lantern elements. These skeletal elements were selected for this study as they are optically well preserved and show minimal secondary mineralization.

Methods

Sample preparation

Skeletal elements were cleaned in a 3% hydrogen peroxide bath for 24 hours to remove additional non-skeletal material (like remaining shale and secondary minerals) adhering to the elements. The skeletal elements were then examined via optical microscopy to select specimens that could easily be cleaned of remaining adhering matrix. These specimens were cleaned individually within an ultrasonic bath, examined under optical microscope, and pieces of non-skeletal material were removed by hand using a pin tip. This process was repeated for each specimen. Many of the skeletal elements, however, still had sparse pyrite on the surface that were unable to be removed. The ossicles that had the least amount of secondary mineralization were selected for bulk geochemical analysis via ICP-MS and the remaining ossicles were examined using SEM-EDS and CL.

SEM and Cathodoluminescence

Fossil echinoderm ossicles that were not used for ICP-MS analysis were imaged using a Phenom XL SEM in backscatter mode. These ossicles were mounted in epoxy and polished for viewing internal structure. Backscatter images were collected to determine regions of interest in the skeletal elements (potential preservation of stereom, boundaries between different preservational textures) for electron backscatter diffraction (EDS). Additional cathodoluminescence (CL) imaging was done on the same skeletal

elements that were examined using SEM and EDS to check the samples for preservational features that were not apparent in either SEM or SEM-EDS.

ICP-MS

Specimens were weighed to confirm 0.5 mg of sample was collected; this was typically the weight of a single ossicle, so no mixing of ossicles was needed. 2% trace metal grade HNO_3 was spiked with an internal standard (GAC-1) prepared by Inorganic Ventures, was added to a Falcon tube with the sample and agitated with a vortex mixer until all carbonate was dissolved. Samples were then centrifuged for three minutes to remove any insoluble residue. This step retrieved small amounts of pyrite. The remaining liquid was transferred to a new ICP tube and additional 2% HNO_3 was added for use in the ICP-MS. Samples were measured for Ca, Mg, Sr, Mn, Fe, Ba, Pb, Mo, Cr, V, Zn, Cu, and Rb on an Agilent 7700 Quadrupole ICP-MS. Results provide certainties of ±5%.

Results

SEM, SEM-EDS, and CL

Although the skeletal elements were collected from the same locality, SEM, SEM-EDS, and CL imaging of the internal structure of Aristotle's Lantern ossicles suggest variation in the geochemical preservation among the different lantern elements. Variation in geochemical preservation of individual ossicles has been recorded in other studies, albeit from different locations, by Dickson (2001b) and Gorzelak et al. (2016). These results show a highly mosaic nature of the preservation within this locality.

Dipyramid: In the dipyramid (Figure 3.3), there is no stereom preserved, large dolomite rhombs are preserved in the dipyramid cavity, there is microdolomite across the dipyramid, and some pyrite framboids. Microdolomite appears in SEM as small rhombs as well as irregularly shaped dark patches and appears as dark pink blotches in SEM-EDS (Figure 3.3C, E, H). There are three different preservational textures examined in the dipyramid, however, only one texture has abundant microdolomite. There is still a homogeneous distribution of Mg across the other textures. Iron and manganese (Figure 3.3D, F, I) are homogeneously distributed across the skeletal element without any regions that are heavily concentrated, with the exception of scattered pyrite framboids. In CL (Figure 3.4D), the dipyramid has an orange luminescence with dark, blotchy quenched regions. In all visualization techniques, there is no evidence of preserved stereom microstructure.

Epiphysis: The epiphysis illustrated in Figure 3.5, has a minor amount of stereom preserved (identified by dark patches arranged in a semi-regular pattern) (Figure 3.5D) within a relatively homogeneous texture. There are no pyrite framboids present on this skeletal element. The stereom is infilled with syntaxial calcite bearing high concentrations of Sr as well as residual Al interpreted to be from the shale (Figure 3.5E). content, the Sr has only infilled pores and there is minimal microdolomite as there is only one spot with a large concentration of Mg. C shows homogeneous Mn distribution with some spots of increased Fe, though Fe is largely homogeneously distributed. D-F is a heavily altered region with homogeneously distributed Mg (E), Mn and Fe (F). G-I is a

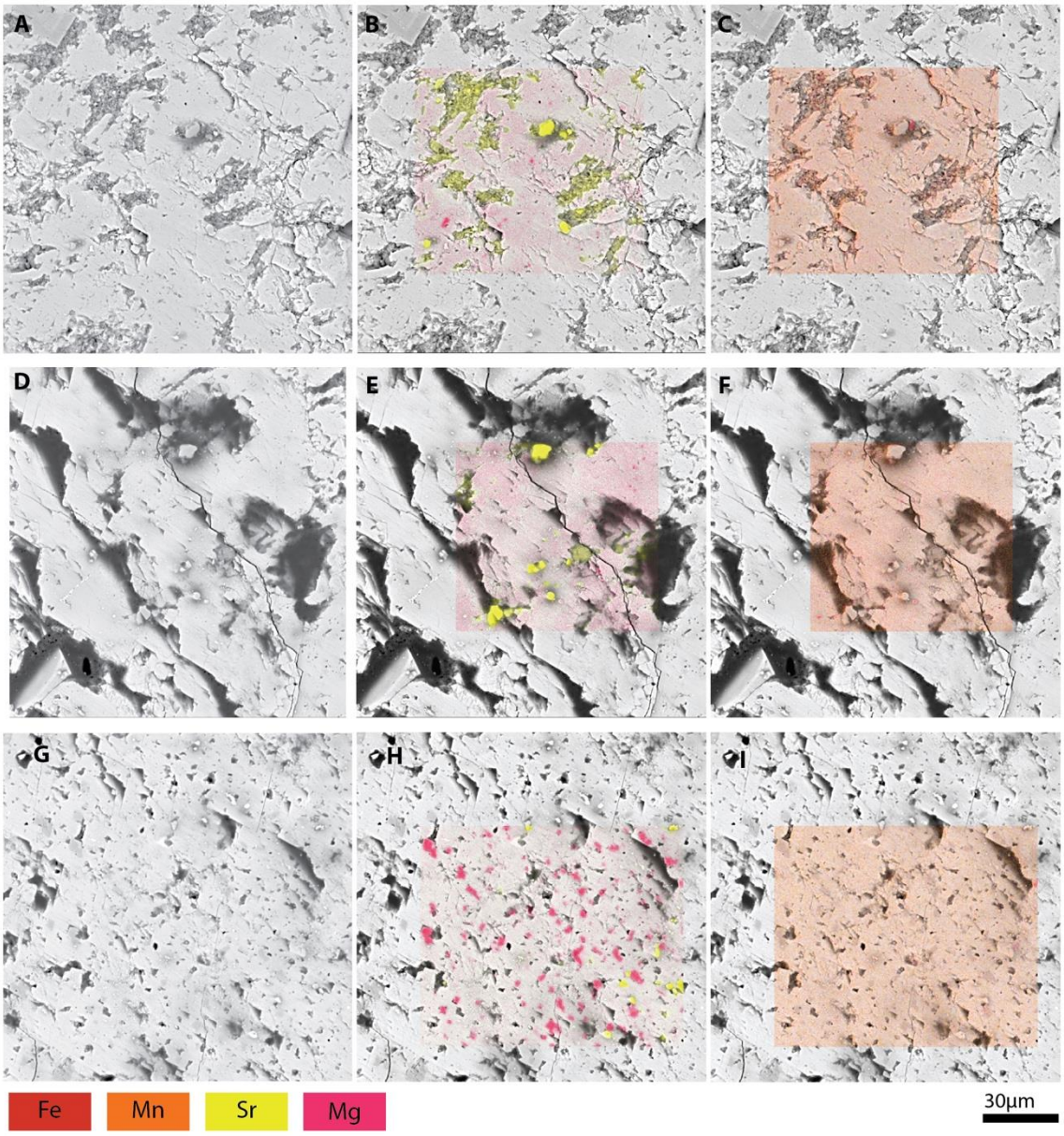

Figure 3.3 SEM and SEM-EDS images of the dipyramid. A-C have a texture representative of stereom that has been secondarily infilled. B shows the Mg and Sr

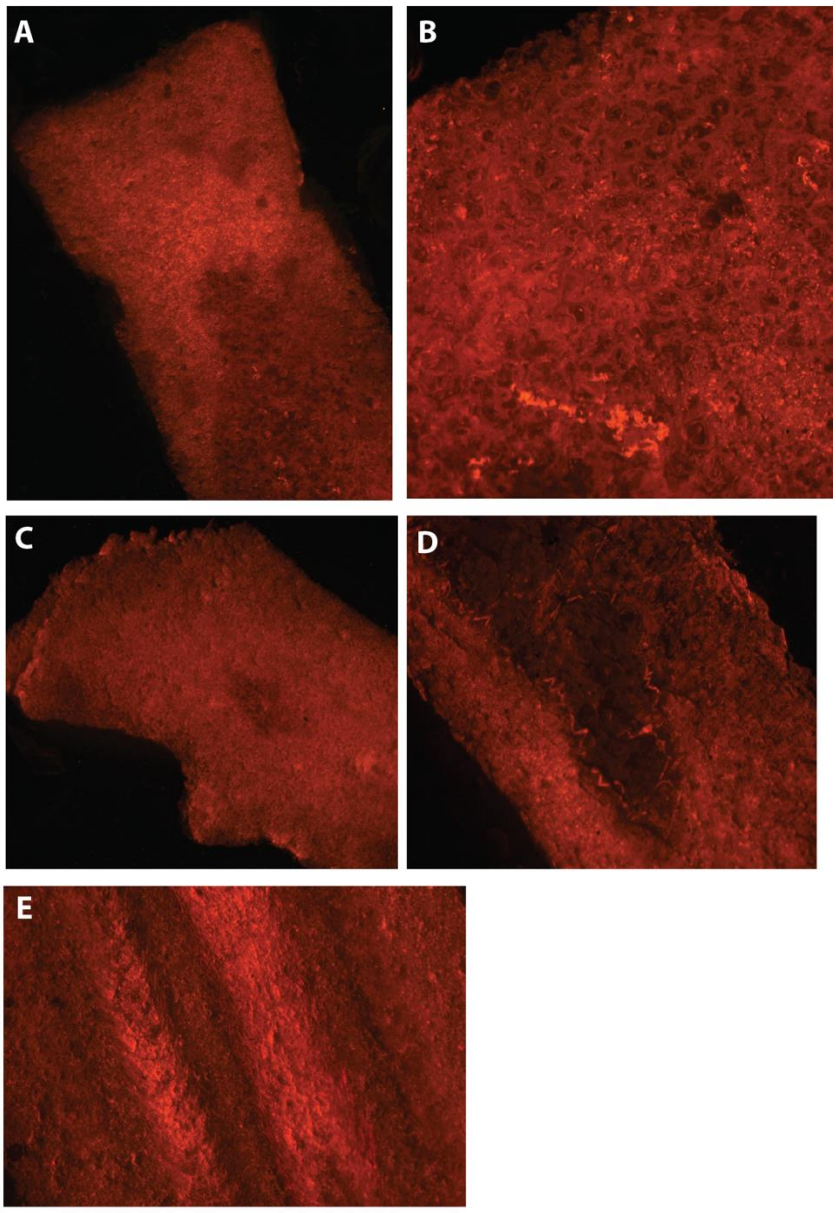

Figure 3.4 Cathodoluminescence of echinoid ossicles. A is the rotula in which there is a brighter orange texture with blotches of dark luminescence. B is zoomed in on the dark luminescence of A in which you can see stereom preservation. C is the epiphysis which is homogeneously dark luminescence with a darker patch that is preserved stereom. D is the dipyramid with blotchy luminescence and a dark center. In SEM (Figure 3) there is no stereom preserved in this darker center. E is the tooth, the ridges seen here are compositional bands (Figure 6).

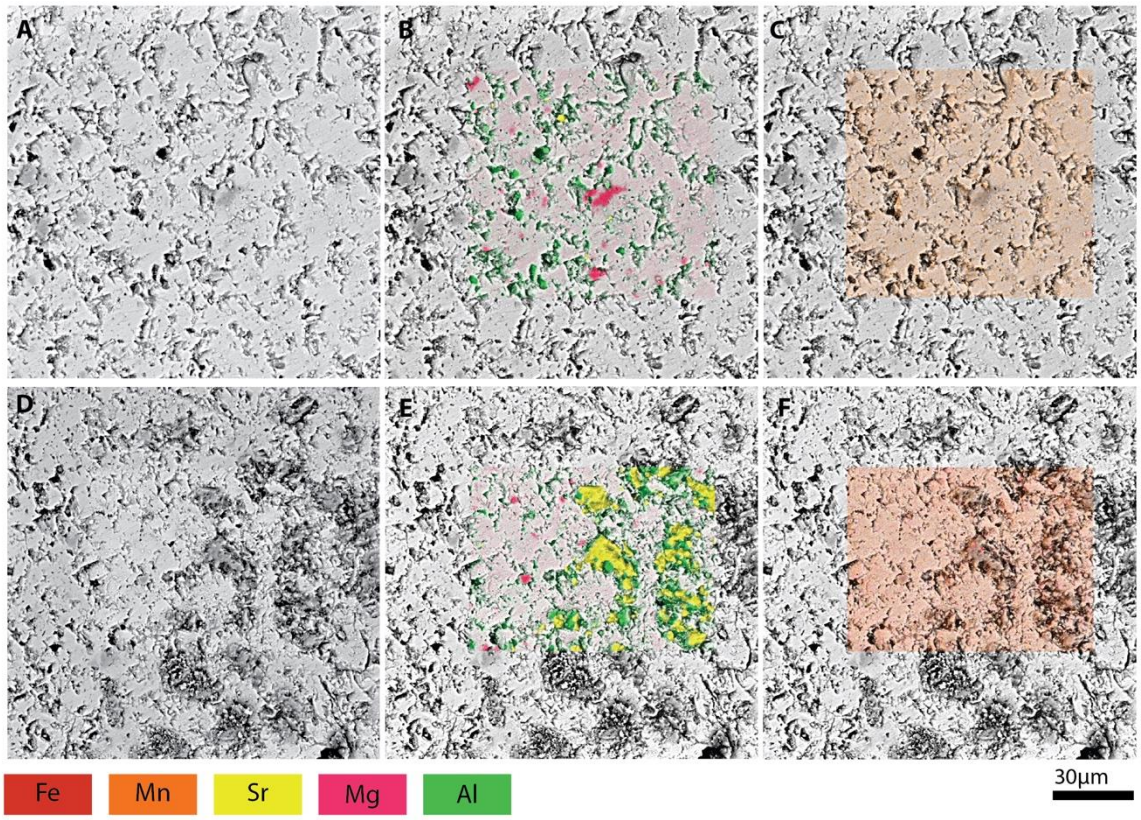

Figure 3.5 SEM and SEM-EDS of the epiphysis. A-C represent completely infilled skeletal elements. A, SEM image, the dark gray patches are microdolomite. B, SEM-EDS in which the dark gray patches of microdolomite are highlighted in pink representing high concentrations of Mg. C shows homogeneous distribution of Fe and Mn. D, SEM images the dark blotches here represent preservation of stereom. E, the stereom is infilled with Sr and Al, there is minor microdolomite. F shows homogeneous distribution of Fe and Mn**.**

less altered region that has a lot of microdolomite present (H) and homogeneously distributed Mn and Fe (I). Surrounding the stereom is minimal amounts of microdolomite. In the regions that do not have stereom present, there is almost no Sr present and there are larger (15µm) rhombs of microdolomite as well as the more typical 1–10µm microdolomite. While there are still pockets of microdolomite, there are no large dolomite rhombs present. Manganese and iron are homogeneously distributed and do not have large concentrations anywhere in the examined regions (Figure 3.5C, F). In CL (Figure 3.4C) the epiphysis has an orange luminescence with dark blotchy regions. When compared with SEM imaging, these dark blotchy regions preserve the stereom microstructure.

Rotula: The rotula illustrated in Figure 3.6, has a band of preserved stereom within a relatively homogeneous texture. Like the epiphysis, the stereom has been infilled with syntaxial calcite bearing Sr and there is residual Al present likely derived from the shale containing the skeletal element (Figure 3.6 B, E). Surrounding the stereom there are a few microdolomite rhombs, but the Mg is largely homogeneously distributed. In the region just below the preserved stereom (Figure 3.6 E) there are still a few scattered stereom pores that have high concentrations of Sr in the calcite infilling but there is very little microdolomite, rather the Mg is homogeneously distributed. This contrasts with the regions of the rotula that do not have stereom preserved, where there is considerable microdolomite present as well as some dolomite rhombs that are 15–20µm across (Figure 3.6 G-I). There is still Mg homogeneously distributed in the background of the skeletal element, but it is concentrated in the dolomite. Manganese and Fe are both

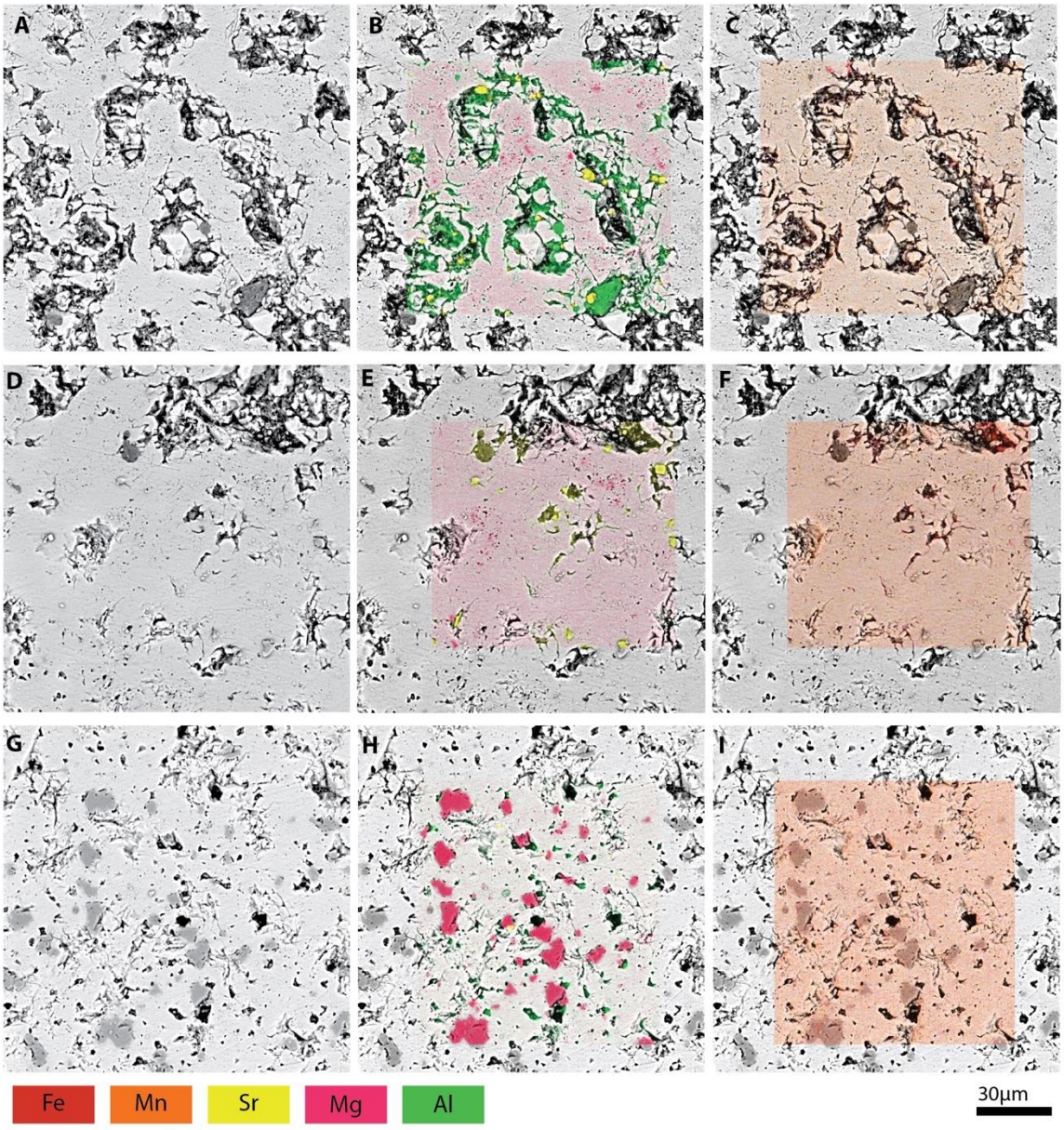

Figure 3.6 SEM and SEM-EDS of the rotula. A-C show stereom preservation. B, there is homogeneous distribution of Mg and there stereom is infilled with Sr and Al. D-F is the region just below where stereom is preserved. E shows homogeneous distribution of Mg as well as Sr infill of the stereom. G-I has no stereom preservation. H shows an increase in microdolomite and there is no Sr and minimal Al in this region. C, F, I all show homogeneous distribution of Fe and Mn in the rotula.

homogeneously distributed in the studied region. Like the epiphysis, in CL (Figure 3.4 A, B), the rotula has an orange luminescence with dark blotchy regions that preserve the stereom microstructure.

Tooth: The tooth illustrated in Figure 3.7, has preserved compositional bands that are typical of echinoid teeth (Lowenstam and Weiner, 1989; Ma et al., 2007; Reich, 2017) and are high in Mg (Figure 3.7D, E). Any laminated structure or perforate stereom that is typical of *Archaeocidaris* teeth is not preserved. Outside of these compositional bands, there is minimal dolomite present, with just a few locations where there is a higher concentration of Mg (Figure 3.7 A, B). Iron and manganese are homogeneously distributed in this ossicle like the others examined (Figure 3.7 C, F). The tooth also has an orange luminescence in CL (Figure 3.4 E), but also has a bright luminescence where the tooth was originally ridged. These areas of bright luminescence correspond to the compositional banding recorded in EDS.

ICP-MS

A total of 32 ossicles (9 identified belonging to *Archaeocidaris*; 7 identified belonging to *Lepidesthes*; the remainder belong to these two genera but are currently unable to be identified and associated with a genus) were measured on ICP-MS and the data are summarized in Table 1, for full dataset and detection limits, see Appendices 1 and 2 at the end of full text. Of the major and minor elements analyzed, only Mg, Sr, Mn, and Fe were able to be compared among all included skeletal elements. Magnesium has a relatively large incorporation range between 4,000–14,000 ppm (1.5–5.7 mol%) into studied ossicles (Figure 3.8) Tooth ossicles have the largest amount of Mg incorporation

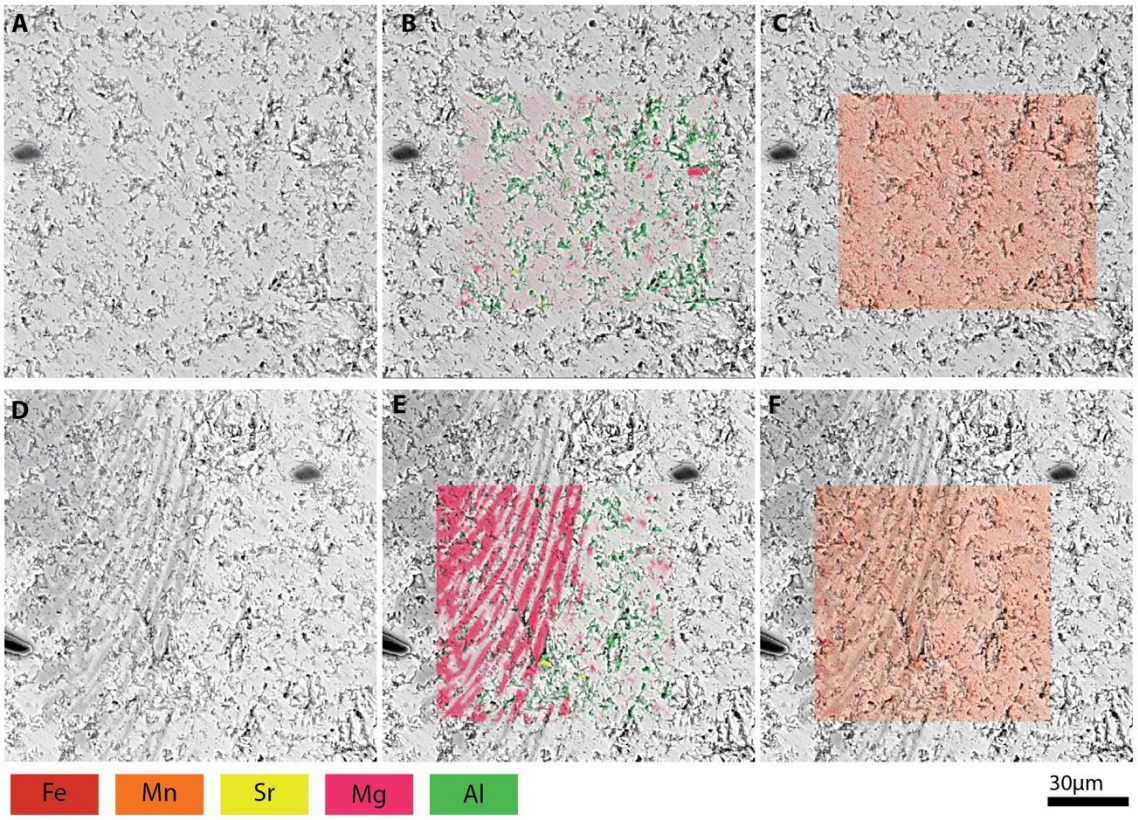

Figure 3.7 SEM and SEM-EDS of the tooth. A-C represent the majority preservational texture of the tooth. B shows homogeneous Mg distribution with little microdolomite and some Al. C shows homogeneous distribution of Fe and Mn. D-F shows the compositional banding seen in CL. E the compositional bands have high concentrations of Mg and there is no Sr present. F shows homogeneous distribution of Fe and Mn across these bands.

(10,000–14,000 ppm) although there are some specimens of rotulae, spines, and ambulacral plates that fall into this range as well. However, all tooth ossicles fall into this higher range of Mg incorporation.

Strontium plotted in a narrow range in all skeletal elements, ranging from ~500–1200 ppm, with no pattern of incorporation in specific ossicle types (Figure 3.8) However, most of the ossicles cluster around concentrations between 700–1200 ppm. The spar from the interior of a blastoid from the same locality, has the lowest amount of Mg and Sr incorporated at 613 ppm and 200 ppm respectively. T-tests were completed to assess significance between spines and other examined skeletal elements. T-tests for Mg, $p = 0.123$, indicating that there is no compositional difference between spines or other skeletal elements. With respect to Sr, $p = 0.04$, indicating some compositional difference between spines and the other skeletal elements.

Manganese and iron content was recorded in all measured ossicles (Figure 3.9). The majority of ossicles clustered around 150–300 ppm Mn incorporation, with a few outliers recording up to 400 ppm Mn incorporation. The spar has the highest amount of Mn incorporation at 1360 ppm. In contrast, Fe incorporation varies widely and ranges from 35–400 ppm. Unlike Mn incorporation, there is not a cluster of data points at a specific range of Fe incorporation (Figure 3.9). There are a few outliers recording higher levels of Fe incorporation between 500–800 ppm. The spar has 352 ppm Fe incorporation, which is at the higher end of the average amount of Fe incorporated into the echinoid ossicles.

Table 3.1 Table of maximum and minimum values for major and minor elements analyzed in each of the ossicle types.

	Elemental Concentration [ppm]							
Ossicle	Magnesium		Strontium		Manganese		Iron	
	Max	Min	Max	Min	Max	Min	Max	Min
Tooth	13916.94	9569.99	1092.45	820.36	198.25	198.25	67.31	35.16
Rotula	12149.97	8352.77	1072.43	848.95	201.26	146.02	155.68	61.16
Epiphysis	7852.59	6831.20	882.12	662.93	345.54	185.86	404.98	70.46
Dipyramid	8094.07	7698.32	977.23	839.64	236.24	183.44	195.59	70.46
Ambulacra	9979.96	7611.38	951.42	748.07	295.75	165.37	517.62	64.51
Interambulacra	9649.78	7151.85	1152.68	747.18	413.59	141.33	594.40	63.50
Spines	13078.17	3635.03	916.17	540.69	415.32	189.96	775.85	142.16
Spar	8493.78		518.31		352.65		195.56	

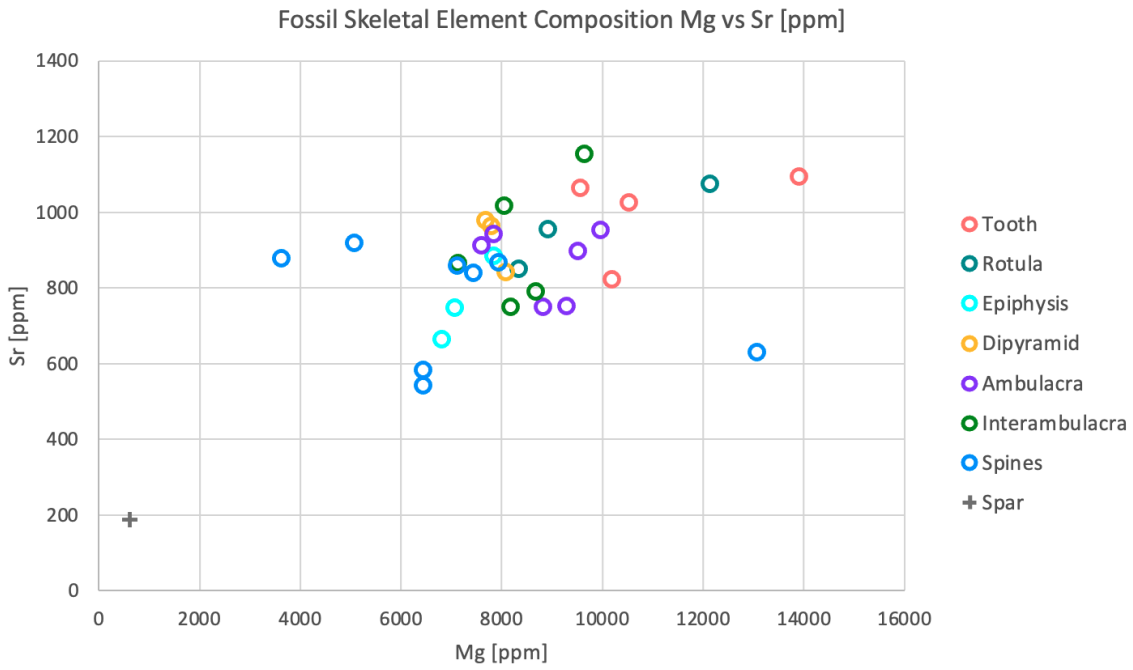

Figure 3.8 Plot of magnesium and strontium incorporation in fossil skeletal elements. There is no distinction among specific ossicles based on magnesium or strontium content. Spar collected from the internal cavity of the blastoid represents abiotic calcite precipitation after death of the organism and has less magnesium and strontium incorporated.

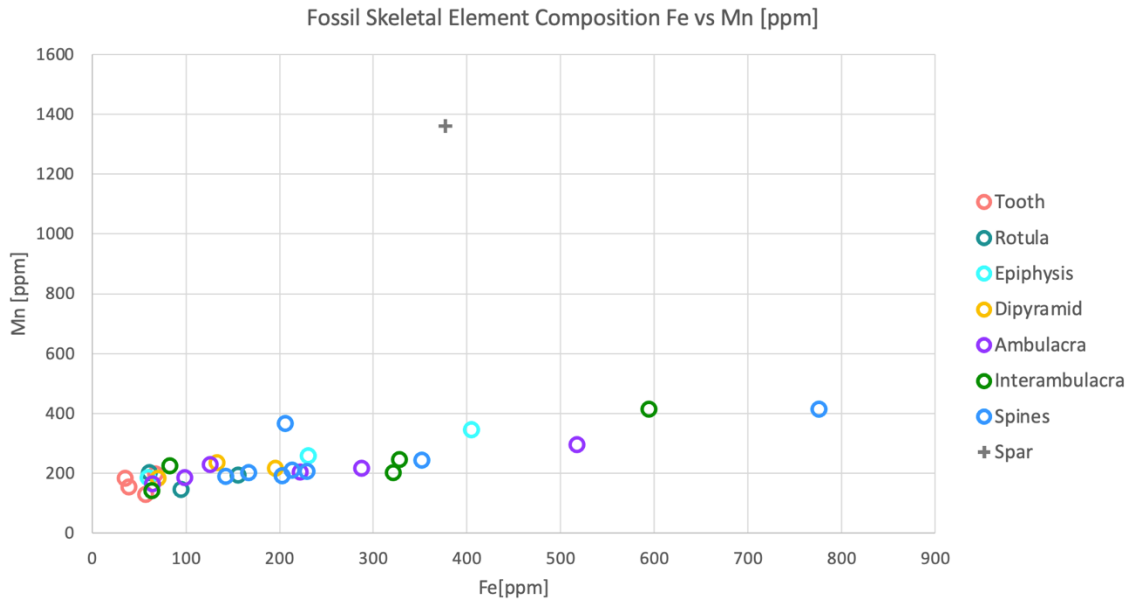

Figure 3.9 Plot of iron and manganese incorporation in fossil skeletal elements. There is no distinction among specific ossicles based on iron or manganese content. Most ossicles have a narrow range of Mn incorporation, though there is a wide range in the amount of Fe incorporated. Again, the spar that was analyzed has very different composition compared to the fossil ossicles.

Discussion

The use of multiple methods to examine preservation style and chemical composition of skeletal elements highlights variability in the preservation and composition within individual ossicles and among ossicles collected from the same locality. These results corroborate the findings of previous work — individual ossicles can have multiple preservation types (Dickson, 2001b; Gorzelak et al., 2016) and trends in chemical composition of fossilized echinoid ossicles reflect the fossilization and diagenetic properties when compared to modern echinoderms (MacQueen and Ghent, 1970; Lohmann and Meyers, 1977; Meyers and Lohmann, 1978; Leutloff and Meyers, 1983; Dickson, 2001b; Gorzelak et al., 2016). This results in lower concentrations of Mg in the ossicles, while Fe and Mn increase when compared to modern echinoderms; these fossilized echinoid ossicles do not preserve their original chemistry.

Elemental composition of modern and fossil skeletal elements

The Mg content in modern echinoids ranges from 4–40 mol% (Gorzelak et al., 2016) with previous work on echinoids from the Gulf of Mexico showing a Mg range of 4.4–18.9 mol%. Spines in multiple taxa (*Eucidaris tribuloides*, *Lytechinus variegatus*, and *Arbacia punctulata*) all have less Mg incorporation than other studied skeletal elements (Figure 3.10).

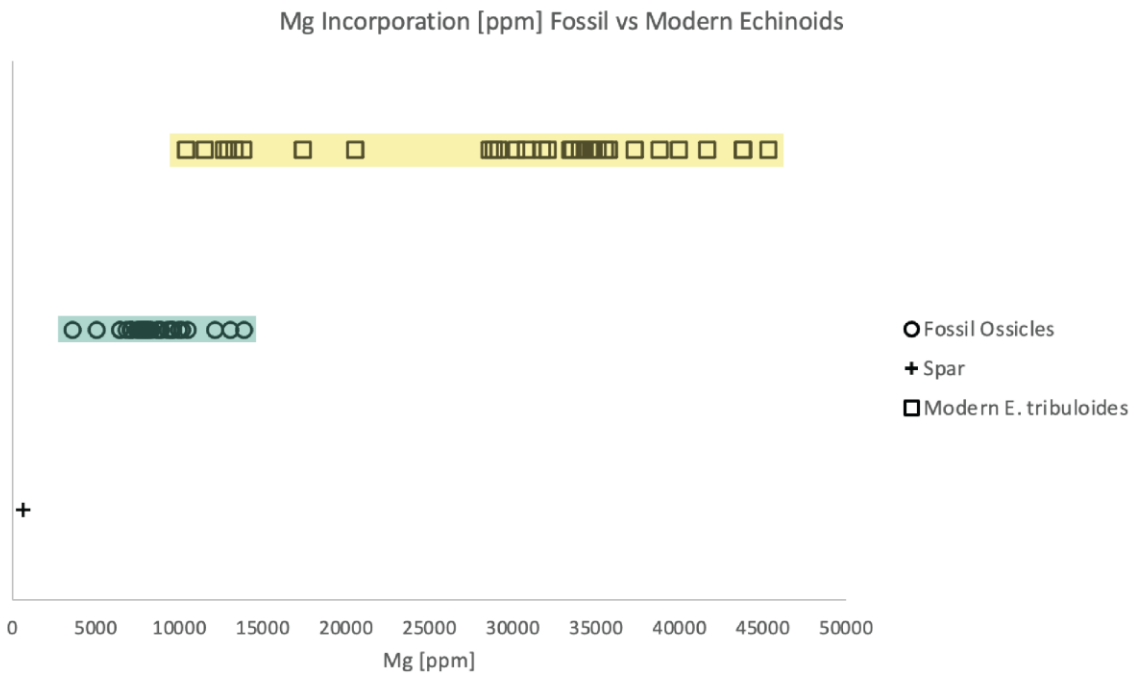

Figure 3.10 Comparison of Mg incorporation in fossil ossicle and modern echinoid ossicles. The modern ossicles compared here are *E. tribuloides*. The *E. tribuloides* ossicles have a large range of Mg incorporation. Based on previous work, the ossicles with the lowest amount of included Mg are spines. In the fossil ossicles, there is no distinction made among the specific ossicles, but the fossils have a narrow range of Mg incorporation representing about a 25% reduction in Mg between modern and fossil ossicles.

Additionally, the incorporation range of Mg does distinguish between genus somewhat as *Clypeaster* and *Arbacia* have restricted ranges of Mg compared to *Lytechinus* and *Eucidaris*. Strontium incorporation in modern echinoids ranges from 0.2–0.35 wt% and there is not a demonstrable difference in Sr incorporation based on ossicle type or genus (Figure 3.11). In comparison, the fossil ossicles range from 1.5–5.7 mol% Mg and 0.05–0.12 wt% Sr, and when graphed, plot in a distinct cluster from the modern ossicles (Figure 3.11). The difference in Mg and Sr content between modern and fossil echinoids is the result of diagenesis and fossilization transforming the metastable high-Mg calcite to stable low-Mg calcite (Leutloff and Meyers, 1983). In experiments on coralline algae using atomic absorption spectroscopy (AAS) Gavish and Friedman (1969) demonstrated that the Mg-calcite of coralline algae rapidly recrystallized to calcite between 2000–10,000 years after burial. If we compare the Mg mol% between the fossilized skeletal elements and skeletal elements from *E. tribuloides* (the modern echinoid most closely related to the echinoids used in this study), the elements from *E. tribuloides* have 12.5 mol% Mg on average and the fossil echinoid elements have 3.5 mol% Mg on average, reflecting a 72% loss of Mg incorporated in skeletal elements. This loss is likely not as drastic as it seems, but rather reflects the dilution of Mg content because of mixing the original biomineralized calcite with the syntaxial calcite abiotically precipitated during diagenesis. Currently, there is not a way to account for the contribution of secondary calcite infilling the echinoid skeletal elements except for the directionality of the mixing. Regardless, the amount of Mg calculated from fossil echinoid skeletal elements is lower than original amount of Mg that was incorporated.

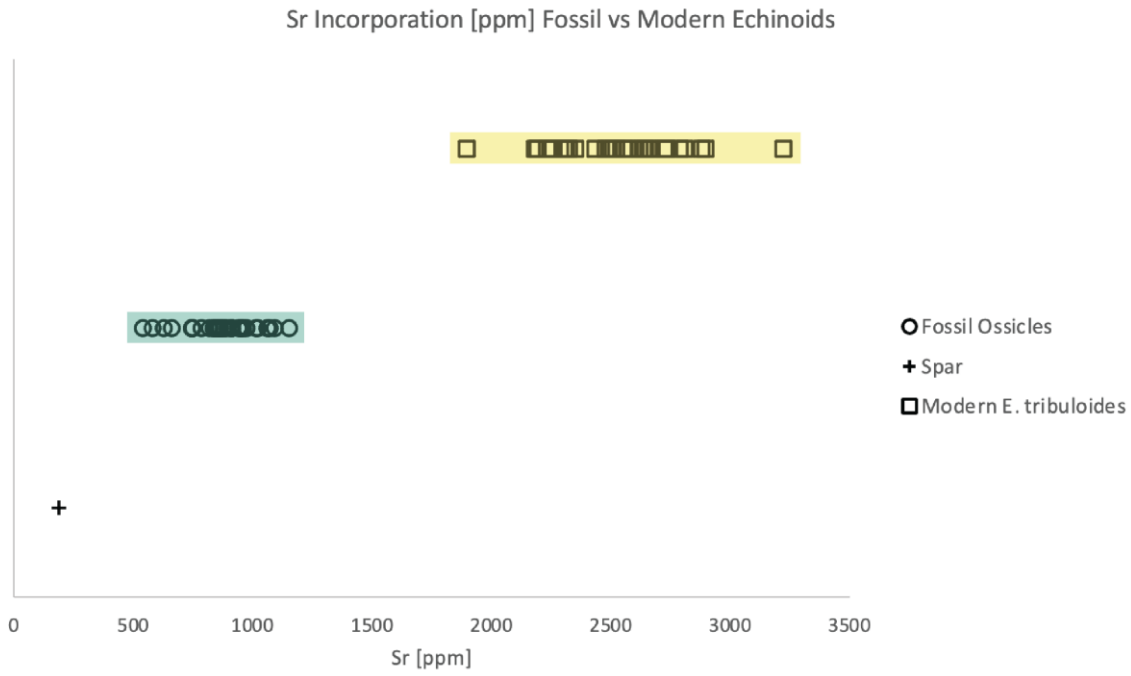

Figure 3.11 Comparison of Sr incorporation in fossil ossicles and modern echinoid ossicles. The modern ossicles compared here are *E. tribuloides*. The *E. tribuloides* ossicles have a greater amount of Sr incorporated in the ossicles than the fossil ossicles.

In contrast to Mg and Sr, fossil ossicles have relatively higher amounts of incorporated Fe and Mn than modern ossicles (Figure 3.12). Iron in the fossil ossicles range from 50–400 ppm, while the modern ossicles range from 5–25 ppm. The increase in Fe content likely reflects the mobilization of Fe in pore fluids present both surficially and internally of each fossilized ossicle. Manganese in the fossil ossicles ranges from 130–400 ppm while the modern ossicles range from 0–80 ppm. Typically, the modern echinoids range from 0–15 ppm and only one species, *Clypeaster chesheri*, ranges from 10–80 ppm. *C. chesheri* is an irregular echinoid that lives semi-infaunal, therefore, has more interaction with pore fluids in the sediment in which Mn is mobile. The changes in Fe and Mn incorporation in fossil ossicles results from the mobilization of these elements in pore fluids that can be included in the calcite lattice during early diagenesis in suboxic and anoxic waters (Tribovillared et al., 2006; Smrzka et al., 2019; Wang et al., 2019).

Geochemical preservation of fossil skeletal elements

The geochemical preservation of echinoderm skeletal elements has been categorized by Dickson (2001b) and Gorzelak et al. (2016) and assigned to preservation types. The original categories, Type 1 and 2 were designated based on SEM images of thin sections of fossil echinoderms (crinoids and *Archaeocidaris*) as well as artificially heat-altered modern echinoids (Dickson, 2001b). Types 1 and 2 were later expanded on and additional types, Type 0 and Type 3 were added (Gorzelak et al., 2016). Type 0 represents skeletal elements that were assumed to be rapidly buried as there is minimal evidence of diagenetic change and the original stereom is preserved. Type 1 retains the

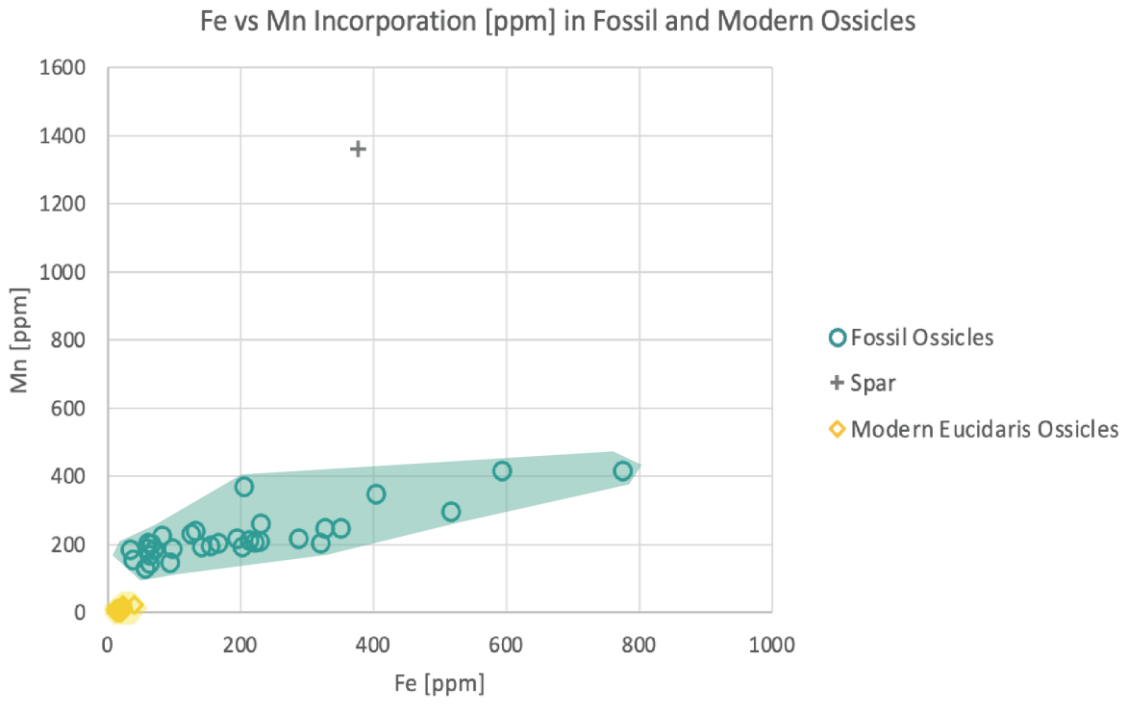

Figure 3.12 Comparison of iron and manganese incorporation between fossil and modern ossicles. The modern ossicles have minor amount of both Fe and Mn incorporated into the ossicles. Fossil ossicles have greater amounts of both elements, though a narrow range of Mn incorporation compared to Fe.

original stereom microstructure and retains the original high-Mg calcite and has minimal dolomitization internally.

Geochemical preservation of fossil skeletal elements

The geochemical preservation of echinoderm skeletal elements has been categorized by Dickson (2001b) and Gorzelak et al. (2016) and assigned to preservation types. The original categories, Type 1 and 2 were designated based on SEM images of thin sections of fossil echinoderms (crinoids and *Archaeocidaris*) as well as artificially heat-altered modern echinoids (Dickson, 2001b). Types 1 and 2 were later expanded on and additional types, Type 0 and Type 3 were added (Gorzelak et al., 2016). Type 0 represents skeletal elements that were assumed to be rapidly buried as there is minimal evidence of diagenetic change and the original stereom is preserved. Type 1 retains the original stereom microstructure and retains the original high-Mg calcite and has minimal dolomitization internally. Type 2 ossicles have lost the stereom microstructure, the ossicle is speckled with dissolution pores, and contains many irregularly shaped internal dolomite crystals. Type 3 ossicles have completed the transition to stable, low-Mg calcite and like type 2, have many dissolution pores and irregularly shaped dolomite crystals (Dickson, 2001b; Gorzelak et al., 2016). Both of these studies recognized that within a singular ossicle multiple types of geochemical preservation can be present.

The ossicles examined with SEM, SEM-EDS, and CL in this study reflect these preservation types to some extent, however, there are regions in these ossicles that do not fit these definitions. The dipyramid (Figure 3.3, 3.4D) is petrographically the most

diagenetically altered. There is no preservation of the stereom microstructure and large dissolution pores (Type 2) but the regions with these dissolution pores have no irregular dolomite crystals that are characteristic of this Type 2 preservation. Both the epiphysis (Figures 3.4C, 3.5) and rotula (Figures 3.4A, B, 3.6) have stereom preserved with minimal dolomitization but do not retain the original high-Mg calcite which would be characteristic of Type 1 preservation. In contrast, the tooth (Figures 3.4E, 3.6) examined retains the high-Mg (protodolomite) core and has minimal dolomitization outside of that core (Lowenstam and Weiner, 1989) though the perforate stereom on the outer lateral zones is not preserved (Reich and Smith, 2009). These preservation types suggested by Dickson (2001b) and Gorzelak et al. (2016) are useful as checkpoints to determine the level of geochemical preservation within ossicles, however, they do not reflect all of the variation seen within all echinoderm ossicles. The ossicles used in this study while surficially optically well preserved are not geochemically well preserved and therefore are not reliable indicators of original composition and are not suited for proxy data.

Magnesium content and transport

Biomineralized calcite from modern echinoids range from 4–40 mol% Mg (Gorzelak et al., 2016) and the fossil ossicles examined in this study range from 1.5–5.7 mol% Mg, representing a change from metastable high-Mg calcite to more stable low-Mg calcite. Because echinoderms make their skeletons of high-Mg calcite, the Mg content of ossicles has been an important source of data in studies using Mg/Ca ratio to reconstruct

paleoseawater conditions as well as understanding the transitions form metastable high-Mg calcite to low-Mg calcite through diagenesis.

There has been some question whether Paleozoic echinoderms have Mg levels comparable to modern echinoderms. Leutloff and Meyers (1983) suggested that there is an approximate 25% Mg loss in crinoids, interpreted from the average mol% Mg in modern crinoid ossicles compared to the average mol% Mg in fossil crinoids. This interpretation assumes that mineralization occurred in the same way during the Mississippian as it is in the modern which is now supported by paleogenomics (Bottjer, 2017; Thompson, 2022), and that water temperature at the same latitudes would be similar between the Mississippian and the modern (Leutloff and Meyers, 1983). Additionally, the upper Carboniferous records a period of changing seawater chemistry with a shift from a calcite sea to aragonite sea conditions (Lowenstein et al., 2001; Balthasar and Cusack, 2015; Gorzelak et al., 2016). Currently the ocean reflects aragonite seas, allowing the possibility that both upper Carboniferous crinoids and echinoids would have Mg incorporation levels similar to today. However, when we compare our dataset of fossil echinoid skeletal elements to modern *E. tribuloides* skeletal elements, the difference in mol% Mg lost is greater than 25%. Given that seawater chemistry was similar during the upper Carboniferous as it is today and that the GRNs that control mineralization have been in place in echinoderms since the Cambrian, we infer that this loss in Mg is real, though greater than that inferred by Luetloff and Meyers (1983).

The transport of Mg within skeletal elements as fossilization and diagenesis occurs is still unknown and is of great interest and importance to our understanding of the

utility of echinoderms as chemical archives in geochemical studies. Some ossicles, like teeth, retain a high-Mg calcite composition and have sparse microdolomite present. In contrast, other ossicles do transform to low-Mg calcite but have an uneven distribution of microdolomite within an individual ossicle. Within our samples, there is not a clear pattern that would suggest a diagenetic front in these particular ossicles (Figures 3.3-7) that would result in a pooling of microdolomite rhombs. Future work addressing the transport of Mg within skeletal elements includes 1) detailed transect analysis using SEM-EDS or EMPA to see how Mg is concentrated in different preservational textures (i.e., stereom vs secondarily infilled stereom) 2) examination of sub-fossil skeletal elements to examine the rate of Mg loss.

Echinoid utility as Mg/Ca proxies

There have been several studies that utilize fossil echinoderms to calculate Mg/Ca ratios for seawater with the application of understanding paleo seawater temperatures and determining calcite or aragonite sea conditions (Dickson, 2002, 2004; Ries, 2004). The main challenge to this proxy is variation in Mg incorporation in echinoderm skeletal elements of both modern and fossil echinoderms. For example, Mg has been measured to range in modern echinoderms between 4.4–21 mol% Mg (Dickson, 2002, 2004; Gorzelak et al., 2016). Magnesium content also varies within a single skeletal element (Dickson, 2004). The differences in Mg concentration all reflect high-Mg calcite composition (>4 mol% Mg) of skeletal elements. This variation is inferred to have been present in fossil echinoderms as well as the GRNs that control biomineralization have been in place since the Cambrian (Bottjer, 2017; Thompson, 2022).

An average of 3.5 mol% Mg for fossil echinoderm skeletal elements was determined by Dickson (2004) and is corroborated by this dataset (Table 3.1) for fossil echinoderm skeletal elements. In using fossil skeletal elements for Mg/Ca_{sw} it has been proposed that using a set temperature for the distribution coefficient only adds an error of ±0.4 to the ratio (Dickson, 2002). Using the equation:

$$Mg/Ca_{sw} = (Mg/Ca_{sample})/D_{Mg}$$

with D_{Mg} constants calculated for 20°C, 25°C, and 30°C (Dickson, 2002, 2004), the Mg/Ca_{sw} from this dataset (Table 2) is <2 and indicates calcite sea conditions. This is contradictory to other studies that calculate Mg/Ca_{sw} for the late Mississippian to be >2, indicating aragonite sea conditions (Dickson, 2002, 2004; Ries, 2004).

It is important to note, that studies of live, modern taxa to calculate magnesium distribution coefficients for high-Mg calcite show that different skeletal elements (spines and interambulacral plates) have different magnesium distribution coefficients (Ries, 2004). This indicates the importance of using the correct magnesium distribution coefficient for the skeletal elements being examined (Ries, 2004, 2010). It is well known that Mg is not homogeneously distributed in echinoderm skeletal elements and varies within an individual (Weber, 1969, 1973; Hermans et al., 2010) and the Mg pathway in biomineralization is not well understood (Hermans et al., 2010).

Additionally, the geochemical preservation of echinoderm ossicles is variable and complicates our ability to determine which regions in skeletal elements represent original high-Mg calcite. As demonstrated in the petrographic analysis of echinoid ossicles (Figures 3.3, 3.4, 3.5, 3.6) there is great variability in Mg concentrations ossicle to ossicle

Table 3.2 Table of calculated Mg/Ca_{SW} based on Mg/Ca_{sample} calculations and $D^{C}Mg$ based on Dickson (2002, 2004) for 20°C, 25°C, and 30°C.

		Calculated Mg/Ca_{SW}		
	Mg/Ca_{sample}	$D^{C}Mg$ 20°C = 0.02635	$D^{C}Mg$ 25 °C = 0.03757	$D^{C}Mg$ 30°C = 0.05137
Average	0.0218305	0.828481009	0.581061341	0.424965438
Maximum	0.0364239	1.382310973	0.969494121	0.709049915
Minimum	0.0092129	0.349635465	0.245219444	0.179343868

and even within the same ossicle depending on the level of structural preservation that is retained. Even in ossicles that have stereom preserved, which are consistent with being "well-preserved," the amount of Mg varies. These well-preserved ossicles still represent a transition to more stable low-Mg calcite; some ossicles may still have >4 mol% Mg, however, it is inferred that as other ossicles from the same locality are low-Mg calcite, these ossicles with higher mol% Mg likely don't represent original amounts of incorporated Mg.

Echinoderms do represent a rich source of understanding changes in paleo seawater composition; however, their utility currently comes with many challenges. Skeletal elements in question must be examined petrographically (SEM, SEM-EDS, CL) prior to use to gauge the quality of their geochemical preservation. Additionally, regions for analysis should be original stereom material, though it is challenging to understand where the original material is due to syntaxial cement growth. Small spot analyses, EMPA or LA-ICP-MS, is preferable to bulk analysis like ICP-MS, to ensure that the overall composition being recorded is not clouded by regions that have undergone greater diagenetic changes. Finally, more research is needed to understand Mg distribution coefficients in high-Mg calcite versus low-Mg calcite, as well as how the distribution coefficients vary among different skeletal elements.

Conclusions

Fossil echinoid skeletal elements can inform the geochemical and diagenetic conditions at a specific location; however, petrographic and chemical analyses should be used in conjunction to make these determinations. In this case, a combination of SEM,

SEM-EDS, CL, and ICP-MS were used to examine fossil echinoid ossicles. The results of these analyses show that original geochemical trends are not preserved, and the fossilization process results in a transformation from the original high-Mg calcite to low-Mg calcite, redistribution of Mg in the skeletal elements, an increase in Fe and Mn due to a reducing environment, all while maintaining a high level of variation ossicle to ossicle.

The level of variation recorded in all analyses demonstrates the difficulty in utilizing fossil echinoids as geochemical proxies. A joint approach of petrographic imaging as well as geochemical analysis is needed to understand the diagenetic history and level of preservation of the original microstructure in the echinoderm skeletal element in question. More work is needed with respect to understanding the original composition of the fossil ossicles and understanding the movement of Mg within the skeletal elements and how that affects the quantification of the original Mg content. Regardless of method, given that the majority of echinoderm skeletal elements exhibit varied geochemical preservation with extensive alteration, the use of echinoderms as geochemical proxies should be done with caution.

ACKNOWLEDGMENTS

We are grateful to Julie Bartley and Jeff La Frenierre at Gustavus Adolphus College for the use of lab space and materials, ICP-MS facilities, and assistance in collecting the geochemical data for this study. We would like to thank Jesse Scholpp and Allan Patchen for instruction and trouble-shooting the SEM and SEM-EDS. Thanks to Jacob Gann for sample selection and preparation. This work was supported by grants awarded to MRL from The Geological Society of America.

REFERENCES

Al-Aasm, I.S. and Veizer, J., 1982, Chemical stabilization of low-Mg calcite: An example of brachiopods. Journal of Sedimentary Petrology, **52**, 1101–1109.

Alberic, M., Stifler, C.A., Zou, A., Sun, C., Killian, C.E., Valencia, S., Mawass, M., Bertinetti, L., Gilbert, P.U.P.A., Politi, Y., 2019, Growth and regrowth of adult sea urchin spines involve hydrated and anhydrous amorphous calcium carbonate precursors. Journal of Structural Biology: X, **1**, 1–9.

Asnaghi, V., Mangialajo, L., Gattuso, J.P., Francour, P., Privitera, D., Chiantore, M., 2014, Effects of ocean acidification and diet on thickness and carbonate elemental composition of the test of juvenile sea urchins. Marine Environmental Research, **93**, 78–84.

Atwood, J.W. and Sumrall, C.D., 2012, Morphometric investigation of the *Pentremites* fauna from the Glen Dean Formation, Kentucky. Journal of Paleontology, **86**, 813–828.

Balthsar, U., and Cusack, M., 2015, Aragonite-calcite seas—Quantifying the gray area. Geology, **43**, 99–102.

Brett, C.E., Moffat, H.A., Taylor, W.L., 1997, Echinoderm taphonomy, taphofacies, and Lagerstätten. The Paleontological Society Papers, **3**, 147–190.

Bottjer, D.J., 2017, Geobiology and palaeogenomics. Earth-Science Reviews, **164**, 182–192.

Carpenter, S.J. and Lohmann, K.C., 1992, Sr/Mg ratios of modern marine calcite: Empirical indicators of ocean chemistry and precipitation rate. Geochimica et Cosmochimica Acta, **56**, 1837–1849.

Dickson, J.A.D., 1995, Paleozoic Mg calcite preserved: Implications for the Carboniferous ocean. Geology, **23**, 535–538.

Dickson, J.A.D., 2001a, Diagenesis and crystal caskets: Echinoderm Mg calcite transformation, Dry Canyon, New Mexico, USA. Journal of Sedimentary Research, **71**, 764–777.

Dickson, J.A.D., 2002, Fossil echinoderms as monitor of the Mg/Ca ratio of Phanerozoic Oceans. Science, **298**, 1222–1224.

Dickson, J.A.D., 2004, Echinoderm skeletal preservation: Calcite-Aragonite seas and the Mg/Ca ratio of Phanerozoic oceans. Journal of Sedimentary Research, **74**, 355–365.

Durham, J.W., Fell, H.B., Fischer, A.G., Kier, P.M., Melville, R.V., Pawson, D.L., Wagner, C.D., 1967, Echinoids. *In* Moore, R.C. (ed.) *Treatise on Invertebrate Paleontology, Part U, Echinodermata 3*. Geological Society of America, & University of Kansas.

Eggins, S., Deckker, P.D., Marshall, J., 2003, Mg/Ca variation in planktonic foraminifera tests: implications for reconstructing palaeo-seawater temperature and habitat migration. Earth and Planetary Science Letters, **212**, 291–306.

Gavish, E. and Friedman, G.M., 1969, Progressive diagenesis in Quaternary to Late Tertiary carbonate sediments: Sequence and time scale. Journal of Sedimentary Petrology, **39**, 980–1006.

Gilbert, P.U.P.A. and Wilt, F.H., 2011, Molecular aspects of biomineralization of the echinoderm endoskeleton. *In* Müller, W.E.G. (ed.) *Molecular Biomineralization*. Progress in Molecular and Subcellular Biology **52**, 199–223.

Gorzelak, P., Stolarski, J., Dery, A., Dubois, P., Escrig, S., Meibom, A., 2014, Ultrascale and microscale growth dynamics of the cidaroid spine of *Phyllacanthus imperialis* revealed by ^{26}Mg labeling and NanoSIMS isotopic imaging. Journal of Morphology, **275**, 788–796.

Gorzelak, P., Kryzkawski, T., Stolarksi, J., 2016, Diagenesis of echinoderm skeletons: Constraints on paleoseawater Mg/Ca reconstructions. Global and Planetary Change, **144**, 142–157.

Hardie, L.A., 1996, Secular variation in seawater chemistry: An explanation for the coupled secular variation in the mineralogies of marine limestones and potash evaporites over the past 600 m.y. Geology, **24**, 279–283.

Hermans, J., Borremans, C., Willenz, P., André, L., Dubois, P., 2010, Temperature, salinity and growth rate dependences of Mg/Ca and Sr/Ca ratios of the skeleton of the sea

urchin *Paracentrotus lividus* (Lamarck): an experimental approach. Marine Biology, **157**, 1293–1300.

Holland, H. D. and Zimmermann, 2000, The dolomite problem revisited. International Geology Review, **42**, 481–490.

Iglikowska, A., Humphreys-Williams, E., Przytarska, J., Chełchowski, M., Kukliński, P., 2020, Minor and trace elements in skeletons of Arctic echinoderms. Marine Pollution Bulletin, **158**, 1–12.

Immenhauser, A., Porta, G.D., Kenter, J.A.M., Bahamonde, J.R., 2003, An alternative model for positive shifts in shallow-marine carbonate $\delta^{13}C$ and $\delta^{18}O$. Sedimentology, **50**, 953–959.

Khor, J.M. and Ettensohn, C.A., 2020, Transcription factors of the Alx family: Evolutionarily conserved regulators of deuterostome skeletogenesis. Frontiers in Genetics, **11**, 1–15.

Kołbuk, D., Dubois, P., Stolarski, J., Gorzelak, P., 2019, Effects of seawater chemistry (Mg^{2+}/Ca^{2+} ratio) and diet on the skeletal Mg/Ca ratio in the common sea urchin *Paracentrotus lividus*. Marine Environmental Research, **145**, 22–26.

Leutloff A.H. and Meyers, W.J., 1984, Regional distribution of microdolomite inclusions in Mississippian echinoderms from southwestern New Mexico. Journal of Sedimentary Petrology, **54**, 0432–0446.

Limbeck, M.R., Bartley, J., Kah, L.C., Sumrall, C.D., 2022, Minor element distribution in skeletal elements of modern echinoid (Echinodermata) genera. Geological Society of America Abstracts with Programs, **54**.

Lohmann, K.C. and Meyers, W.J., 1977, Microdolomite inclusions in cloudy prismatic calcites: A proposed criterion for former high-magnesium calcites. Journal of Sedimentary Petrology, **47**, 1078–1088.

Lowenstam, H.A. and Weiner, S., 1989, Echinodermata. *In* On biomineralization, Oxford University Press on Demand, 123–134.

Lowenstein, T.K., Timofeeff, M.N., Brennan, S.T., Hardie, L.A., Demicco, R.V., 2001, Oscillations in Phanerozoic seawater chemistry: Evidence from fluid inclusions. Science, **294**, 1086–1088.

Ma, Y.R., Weiner, S., Addadi, L., 2007, Mineral deposition and crystal growth in the continuously forming teeth of sea urchins. Advanced Functional Materials, **17**(15), 2693–2700.

MacQueen, R.W. and Ghent, E.D., 1970, Electron microprobe study of magnesium distribution in some Mississippian echinoderm limestones from western Canada. Canadian Journal of Earth Sciences, **7**, 1308–1316.

Marin, F., Marie, B., Hamada, S.B., Silva, P., LeRoy, N., Guichard, N., Wolf, S., Montgnani, C., Joubert, C., Piquemal, D., Saulnier, D., Gueguen, Y., 2013, “Shellome”:

Proteins involved in mollusc shell biomineralization—diversity, functions. Recent Advances in Pearl Research, **149**, 1–18.

Meyers, W.J. and Lohmann, K.C., 1978, Microdolomite-rich syntaxial cements: Proposed meteoric-marine mixing zone phreatic cements from the Mississippian limestones, New Mexico. Journal of Sedimentary Petrology, **48**, 475–488.

Morgulis, M., Gildor, T., Roopin, M., Sher, N., Malik, A., Lalzar, M., Dines, M., de-Leon, S.B., Khalaily, L., de-Leon, S.B., 2019, Possible cooption of a VEGF-driven tubulogenesis program for biomineralization in echinoderms. PNAS, **116**(25), 12353–12362.

Regenberg, M., Steph, S., Nürnberg, D., Tiedemann, R., Garbe-Schönberg, D., 2009, Calibrating Mg/Ca ratios of multiple planktonic foraminiferal species with δ^{18}O-calcification temperatures: Paleothermometry for the upper water column. Earth and Planetary Sciences Letters, **278**, 324–336.

Reich, M. and Smith, A.B., 2009, Origins and biomechanical evolution of teeth in echinoids and their relatives. Palaeontology, **52**, 1149–1168.

Ries, J.B., 2004, Effect of ambient Mg/Ca ratio on Mg fractionation in calcareous marine invertebrates: A record of the oceanic Mg/Ca ratio over the Phanerozoic. Geology, **32**, 981–984.

Ries, J.B., 2010, Review: geological and experimental evidence for secular variation in seawater Mg/Ca (calcite-aragonite seas) and its effects on marine biological calcification. Biogeosciences, **7**, 2795–2849.

Smith, A.B., 1980, Stereom microstructure of the echinoid test. Paleontology, **25**, 1–81.

Smrzka, D., Zwicker, J., Bach, W., Feng, D., Himmler, T., Chen, D., Peckmann, J., 2019, The behavior of trace elements in seawater, sedimentary pore water, and their incorporation into carbonate minerals: a review. Facies, **2019**, 1–47.

Stanley, S.M., 2008, Effects of global seawater chemistry on biomineralization: Past, present, and future. Chemical Reviews, **108**, 4483–4498.

Stanley, S. M. and Hardie, L.A., 1998, Secular oscillations in the carbonate mineralogy of reef-building and sediment-producing organisms driven by tectonically forced shifts in seawater chemistry. Palaeogeography, Palaeoclimatology, Palaeoecology, **144**, 3–19.

Sumrall, C.D., 1997. The role of fossils in the phylogenetic reconstruction of Echinodermata.
Paleontological Society Papers, **3**, 267–288.

Thompson, J.R., 2022, Molecular paleobiology of the echinoderm skeleton. *In* Sumrall, C.D. (ed.), Elements of Paleontology, 1–70.

Tribovillard, N., Algeo, T.J., Lyons, T., Riboulleau, A., 2006, Trace metals as paleoredox and paleoproductivity proxies: An update. Chemical geology, **232**, 12–32.

Wang, Q., Li, J., Wang, F., Sakanakura, H., Tabelin, C.B., 2022, Effective immobilization of geogenic As and Pb in excavated marine sedimentary material by magnesia under wet-dry cycle, freeze-thaw cycle, and anaerobic exposure scenarios. Science of the Total Encironment, **848**, 1–11.

Weber, D.M., 1959, Crystallography of Echinoid Calcite. The Journal of Geology, **67**, 661–674.

Weber, J.N., 1969, The incorporation of magnesium into the skeletal calcites of echinoderms. American Journal of Science, **267**, 537–566.

Weber, J.N., 1973, Temperature dependence of magnesium in Echinoid and Asteroid skeletal calcite: A reinterpretation of its significance. Journal of Geology, **81**, 543–556.

Weiner, S. and Dove, P.M., 2003, An overview of biomineralization processes and the problem of the vital effect. Reviews in mineralogy and geochemistry, **54**(1), 1–29.

Wilkinson, B.H., Buczynski, C., Owen, R.M., 1984, Chemical control of carbonate phases: Implications from Upper Pennsylvanian calcite-aragonite ooids of Southeastern Kansas. Journal of Sedimentary Petrology, **54**, 0932–0947.

APPENDIX 1

Sample Name	24 Mg [He] Conc. [ppm]	43 Ca [He] Conc. [ppm]	88 Sr [He] Conc. [ppm]	55 Mn [He] Conc. [ppm]	56 Fe [He] Conc. [ppm]
PRT1	13916.93748	382082.6359	1092.454266	183.9157331	35.16285797
PRT2	9569.994492	387410.1215	1061.988884	198.2538922	67.31106263
PRT4	10539.04942	386340.3323	1023.606176	128.557191	57.23431605
PRT5	10209.28059	386957.6559	820.356372	153.7764342	38.80469336
PRR1	8352.767873	389133.5557	848.9480223	201.2631413	61.1561022
PRR3	12149.96509	384098.5366	1072.434973	194.1847433	155.6782391
PRR4	8933.428278	388310.8848	954.2619278	146.0208312	94.94475346
PRE3	6831.197099	390876.5785	662.9344228	258.8300262	230.4538897
PRE4	7852.594022	389728.264	882.1154788	185.8552881	59.54298992
PRE5	7076.082847	390298.3172	746.4729218	345.5355951	404.9805914
PRD1	8094.06667	389468.5731	839.6446717	183.4428968	70.46317212
PRD2	7698.31603	389693.0526	977.2339709	236.2444878	132.9382433
PRD3	7812.714485	389527.1548	961.0173102	215.7731037	195.5897204
PRAA1	9979.964524	386989.9643	951.4226936	186.1455205	98.53248964
PRAA2	8832.592202	388551.6555	748.0686122	229.3034642	125.8440618
PRAA3	9530.218286	387374.2383	894.7054751	216.5468653	287.4947132
PRA1	7611.376524	390002.9439	911.1578804	165.3669959	64.5070191

Sample Name	24 Mg [He] Conc. [ppm]	43 Ca [He] Conc. [ppm]	88 Sr [He] Conc. [ppm]	55 Mn [He] Conc. [ppm]	56 Fe [He] Conc. [ppm]
PRA2	7857.759867	389459.1427	940.73788	204.1980076	221.9672175
PRA3	9308.446075	387485.4972	750.4969044	295.74955	517.6199047
PRIAA1	8193.291409	388433.9333	747.1838101	413.5949255	594.3995847
PRIAA2	8055.940845	389376.9074	1014.507017	141.3289519	63.49571299
PRIAA3	8695.73904	388681.3826	787.7476069	224.4838456	83.06828436
PRIA1	7151.847801	390254.4772	864.5281036	245.0027761	328.2025674
PRIA2	9649.776913	386945.0225	1152.681529	202.7148672	321.5933184
PRSARCH1	7945.147625	389425.556	865.9698236	206.207942	229.4353866
PRSARCH2	7125.942944	390485.1598	856.3618423	191.7316277	202.7715055
PRSARCH3	7459.446689	390070.8457	838.6108884	210.1748174	213.3571129
PRST1	6455.603938	391391.8687	581.4176344	244.6747543	351.6132343
PRST2	13078.16756	382607.1488	627.9340677	415.3162707	775.8546978
PRSS1	5086.983796	392946.9984	916.1749446	202.9213814	166.9394034
PRSS2	6450.327667	391704.3273	540.6905081	189.963414	142.1453327
PRSS3	3635.034825	394559.4761	876.7409776	367.2707096	206.2288459
PRSPAR	613.2502387	397764.5522	187.8527526	1360.284883	377.2795258

CONCLUSION

Echinoderms are marine organisms that are abundant in both the fossil record and in the modern and they show great utility as study organisms for a variety of lines of inquiry. However, they need to be placed in context to understand how their interactions with biological, physical, and chemical environments affect their utility as indicators of the past. This study investigates both phylogenetics/disparity and geochemistry to understand this context. These results further improve our understanding of echinoderms and provide a clearer picture of how they can be used to address broader questions about Earth's past.

There are many unusual groups of Paleozoic echinoderms that previously have been challenging to include in phylogenetic analyses because their unusual morphologies are hard to reconcile with features of other more plesiomorphic taxa. One such group is Paracrinoidea. Paracrinoids exhibit highly aberrant morphologies, especially in the ambulacral system that make their morphologies difficult to compare to other echinoderms. This study represents the first quantitatively rigorous phylogenetic analysis for this group. The inclusion of paracrinoids into a phylogenetic hypothesis allows for their placement into a phylomorphospace analysis to understand the evolution of traits like respiratory structures and their inclusion in studies of echinoderm biogeographic patterns.

Echinoderms have also been used as geochemical proxies for seawater chemistry in the geologic past and modern, however, they are known to show considerable variation in how they incorporate major and minor elements into their skeletons. This variability

needs to be characterized better in order to effectively use fossil echinoderms to better understand chemical changes in seawater through the Phanerozoic. The work done in this study corroborates the variability in metal incorporation, but also highlights that chemical trends appear to be independent of skeletal element growth rate, unlike what has previously been reported. The echinoids used in this study provide a foundation of understanding of echinoid geochemistry for four genera of echinoids from the Gulf of Mexico.

The final study examined the preservation of geochemical trends in echinoids after fossilization and diagenesis. Echinoderm skeletal elements are frequently suggested for use in studies using Mg/Ca ratio to reconstruct paleo seawater temperatures. However, this study suggests that Mg is lost during diagenesis and measured amounts represent the minimum Mg that would have originally been present in the skeletal element. Additionally, this study highlights the importance of petrography prior to geochemical analysis as the amount of diagenesis varies even in skeletal elements collected from the same locality.

These three studies provide a foundation for 1) understanding the evolutionary history of aberrant fossil clades and 2) understanding the variability in geochemical information stored in echinoderm skeletal elements and how that affects their utility in understanding changes in seawater chemistry through the Phanerozoic. Additionally, these studies all demonstrate the importance of using combined approaches (i.e. phylogenetics and phylomorphospace or petrographic imaging and geochemistry) to

better understand fossil groups. These three studies provide further insight to echinoderms and biotic changes through the Phanerozoic.

APPENDIX 1

See attachment titled All Data.xlsx for all ICP-MS data collected for both chapters 2 and 3. This document has several sheets separated into raw data, processed data, and data converted to ppm. The top of each sheet contains relevant information with respect to the equipment used, standards used, and calculations used to process the data.

APPENDIX 2

See attachment titled Detection Limits.xlsx for the calculation of detection limits for each element examined in both chapters 2 and 3. This document has several sheets organized based on standard and elements examined with that particular standard. The top of the first sheet describes the methods used to calculate detection limits.

VITA

Maggie Limbeck was born and raised in Victor, New York. She attended Victor Central High School and graduated in 2012. She attended Allegheny College and graduated with a B.S. in Geology in 2016. Maggie completed her senior thesis as a member of Dr. Lisa Whitenack's lab investigating the effects of ocean acidification on the taphonomy of echinoids. Following graduation, Maggie moved to Knoxville, TN to pursue a M.S. in Geosciences working with Dr. Colin Sumrall. She switched the Ph.D. Program in spring of 2018 and continued working with Dr. Sumrall. Her dissertation combined many aspects of echinoderm paleobiology. While pursuing her Ph.D., Maggie has been a teaching assistant for several undergraduate courses, given guest and invited lectures, coordinated several outreach events with the McClung Museum, been president of Darwin Day, president of GeoClub, developed an educational board game on climate change, presented at conferences nationally and internationally, and co-chaired several sessions at the Geological Society of America Southeastern section meetings. Her research has been supported by numerous external grants.